Potential Applications of *Eucalyptus camaldulensis* in Food Preservation and Biofilm Inhibition on Food Contact Surfaces

Nwabor Ozioma Forstinus

A Thesis Submitted in Fulfillment of the Requirements for the Degree of

Doctor of Philosophy in Microbiology (International Program)

Prince of Songkla University

2020

Potential Applications of *Eucalyptus camaldulensis* in Food Preservation and Biofilm Inhibition on Food Contact Surfaces

Nwabor Ozioma Forstinus

A Thesis Submitted in Fulfillment of the Requirements for the Degree of

Doctor of Philosophy in Microbiology (International Program)

Prince of Songkla University

2020

Thesis Title Potential Applications of *Eucalyptus camaldulensis* in Food Preservation and Biofilm Inhibition on Food Contact Surfaces

Author Mr. Nwabor Ozioma Forstinus

Major Program Microbiology

Major Advisor

…….....
(Prof. Dr Supayang Voravuthikunchai)

Co-advisor

…….....
(Asst. Prof. Dr Kitiya Vongkamjan)

Examining Committee:

…….....Chairperson
(Assoc. Prof. Dr M. Lertcanawanichhkul)

…….....Committee
(Prof. Dr Supayang Voravuthikunchai)

…….....Committee
(Asst. Prof. Dr Kitiya Vongkamjan)

.....Committee
(Prof. Dr Duangporn Kantachote)

.....Committee
(Asst. Prof. Dr Pimonsri Mittraparp-arthorn)

The Graduate School, Prince of Songkla University, has approved this thesis as fulfillment of the requirements for the Degree of Doctor of Philosophy in Microbiology (International Program)

……...
(Prof. Dr Damrongsak Faroongsarng)
Dean of Graduate School

This is to certify that the work here submitted is the result of the candidate's own investigations. Due acknowledgement has been made of any assistance received.

……..... Signature

(Prof. Dr. Supayang Voravuthikunchai)

Major Advisor

……..... Signature

(Mr. Ozioma Forstinus Nwabor)

Candidate

I hereby certify that this work has not been accepted in substance for any degree and is not being currently submitted in candidature for any degree.

……..... Signature
(Mr. Ozioma Forstinus Nwabor)
Candidate

Thesis Title Potential Applications of *Eucalyptus camaldulensis* in Food Preservation and Biofilm Inhibition on Food Contact Surfaces

Author Mr. Ozioma Forstinus Nwabor

Major Program Microbiology

Academic Year 2020

ABSTRACT

Plants are excellent source of bioactive compounds that could be applied in medicine, food, and cosmetics. In this study, the applications of *Eucalyptus camaldulensis* ethanolic extract in food production were explored. The minimum inhibitory concentration (MIC) and minimum bactericidal concentration (MBC) of the extract against the foodborne pathogen *Listeria monocytogenes* were 64 to 128 µg/mL and 256 to 512 µg/mL, respectively. Time-kill assay revealed growth inhibitory effects after 4 h treatment of the bacteria with the extract. A reduction of ~2 to 3 log CFU/mL was observed against the tested food and environmental isolates after challenging the pathogens with the extract at MIC for 6 h. Sub-MICs of the extract significantly inhibited listerial attachment to food contact surface materials, motility and listeriolysin O production up to 80%, with a 60% inhibition of biofilm formation ($p<0.05$). Antioxidant assay revealed free radical scavenging activity with IC_{50} of 57.07 µg/mL for 2,2-diphenyl-1-picrylhydrazyl (DPPH) and 29.01 µg/mL for 2,2'-azino-bis (3-ethylbenzothiazoline-6-sulfonic acid) (ABTS) assay. Ferric Reducing Antioxidant Power (FRAP) assay further showed a total antioxidant power equivalent to 92.93 µM ascorbic acid equivalent/mg extract. Encapsulation of the extract in sodium alginate – sodium CMC matrix revealed an irregular shaped microparticles with mean diameter ranging from 6.7 to 26.6 µm. Zeta potential and polydispersity index ranged from

-17.01 to 2.23 mV and 0.344 to 0.489, respectively. Percentage yield and encapsulation efficiency ranged between 70.4 to 81.5 and 74.2±0.011 to 82.43±0.772%, respectively. In addition, the microcapsules exhibited high swelling index with poor solubility. DPPH and ABTS assays revealed that the radical scavenging activities varied directly with the concentration of the extract. Minimum inhibitory and minimum bactericidal concentrations of the microcapsules against Gram-positive foodborne pathogens ranged from 0.19 to 3.12 mg/mL and 0.19 to 12.25 mg/mL, respectively. Moreover, the microcapsules at concentration of 1 mg/mL did not show cytotoxic effects on human colon cell Caco-2. In addition, synthesis of silver nanoparticles with the extract as reducing and capping agent yielded spherical nano-sized particle with mean diameters of 13.11 nm, zeta potential of –35.85 mV, and effective diameter of 138.6 nm. MIC and MBC of synthesized silver nanoparticles on pathogenic foodborne bacteria ranged from 0.99 to 1.99 µg/mL and 3.98 to 15.91 µg/mL, respectively. Fabricated active PVA-Chitosan nanocomposite packaging functionalized by incorporation of the synthesized silver nanoparticles showed good physical and mechanical properties without significant alterations when compared with control PVA-Chitosan packaging ($p<0.05$). Antimicrobial activity of PVA–CH/silver nanoparticles (1:1) films showed bactericidal effects against important foodborne pathogenic bacteria (*Escherichia coli* O157:H7, *L. monocytogenes*, *Staphylococcus aureus*, and *Bacillus cereus*), with greater than 99.9% reduction. Antioxidant activities suggested a concentration–dependent free radical scavenging activity. In addition, PVA–CH/silver nanoparticles showed first order release with fickian diffusion and were non-toxic to Caco-2 cells at 1 mg/mL. Similarly, UV–vis spectra of silver nanoparticles functionalize packaging nanocomposite fabricated from recycled waste papers presented a peak at 427 nm, indicating the

surface plasmon resonance band of silver in the paper. SEM and EDS analysis showed uniform distribution of silver nanoparticles, whereas EDS and ICP-OES results indicated Ag concentration of 0.1 %Wt and 0.0112 µg/cm^2, respectively. Antimicrobial efficacy of the paper, tested against selected important foodborne pathogens, demonstrated a bactericidal effect against *B. cereus* and *E. coli* O157:H7 with > 3log reduction in CFU/mL after 3 h of treatment and a bacteriostatic effect against *L. monocytogenes* and *S. aureus.* Cytotoxicity against HEK293T and Caco-2 cells revealed >80% cell viability. The results of the study suggested that *E. camaldulensis* leaf could be a source of bio-friendly antimicrobial agent that could be used in food as antimicrobial and antioxidant preservative and/or antimicrobial food-grade sanitizer for the inhibition of microbial attachment and biofilm formation on food contact surfaces. The results also revealed that encapsulation of the extract could be employed to preserve its stability and activity in food system. Moreover, the results further showed that the extract could be used in the synthesis of silver nanoparticles for the fabrication of active nanocomposite packaging material.

ACKNOWLEDGEMENTS

I wish to express my sincere gratitude to my supervisor, Prof. Dr Supayang Piyawan Voravuthikunchai, for accepting me as a PhD candidate and for the numerous support and privilege to work without restrictions. I also wish to express my appreciation to my co-supervisor, Asst. Prof. Dr. Kitiya Vongkamjan for her friendly disposition, suggestions and advice when I needed them most.

Special thanks to the Department of Microbiology and all its Professors, Doctors and Staffs for the convivial treatment, advice and encouragement during my challenging days as a fresh PhD student.

My deepest appreciations to my thesis examination committee members for the thorough scrutiny and corrections.

I am grateful to the Graduate School, the Prince of Songkla University, the Thailand education Hub and the Kingdom of Thailand for the full funding provided throughout my PhD. To the Staffs, Doctors and Professors that contributed to the successful completion of my research work, I say thank you.

My path to a PhD would have been slippery and gloomy if you my friends were not there. I love you all.

To all members of the Natural Products Research Center of Excellence and all MSc and PhD colleagues you all made me better person. Thank you for the love, the care, the tolerance and above all your assistance when I needed it.

To my family, what more can I say? I love you all.

Finally, to all who believed in me, all who saw the light at the end of the tunnel when I could see, all who encouraged and assured me of a successful ending, all who stood by me when I needed it most. I owe you and cannot pay in full. You are special.

To him my source of hope and an ever-present friend. In the loneliness and darkness of my journey, I have called many times and you never failed to show up. I worship you.

Ozioma Forstinus Nwabor

TABLE OF CONTENT

LIST OF TABLES

LIST OF FIGURES

LIST OF APPREVIATIONS AND SYMBOLS

ABTS	2,2'-azino-bis (3-ethylbenzothiazoline-6-sulfonic acid)
AgNPs	Silver Nanoparticles
ASTM	American Society for Testing and Materials
ATCC	American Type Culture collection
BATH	Bacterial Attachment to Hydrocarbon
BHI	Brain Heart Infusion
CFS	Cell Free Supernatant
CFU	Colony Forming Unit
CH	Chitosan
CLSI	Clinical and Laboratory Standard Institute
CMC	Carboxymethyl Cellulose
CV	Crystal violet
DLS	Dynamic Light Scattering
DMEM	Dulbecco's Modified Eagle Media
DMSO	Dimethyl sulfoxide
DNA	Deoxyribonucleic acid
DPPH	2,2-diphenyl-1-picrylhydrazyl
DSC	Differential scanning calorimetry
EAB	Elongation at Break
EDS	Energy Dispersive Spectroscopy
FBS	Fetal Bovine Serum
Fmax	Maximum Force
FRAP	Ferric Reducing Antioxidant Power
FTIR	Fourier Transformed Infrared Spectroscopy
GAE	Garlic Acid Equivalent
GRAS	Generally Recognized as Safe

IC_{50}	50% Inhibitory Concentration
ICP-OES	Inductively Coupled Plasma-Optical Emission Spectrometry
InlA	Internalin A
InlB	Internalin B
ISO	International Organization for Standards
KV	Kitiya Vongkamjan
LLO	Listeriolysin O
LOD	Loss on Drying
MBC	Minimum Bactericidal Concentration
MC	Moisture Content
MHA	Mueller-Hinton Agar
MHB	Mueller-Hinton Broth
MIC	Minimum Inhibitory Concentration
MTT	3-[4,5-dimethylthiazole-2-yl]-2,5-diphenyltetrazolium bromide
OD	Optical Density
PBS	Phosphate Buffered Solution
PDI	Polydispersity Index
PSU	Prince of Songkla University
PVA	Polyvinyl Alcohol
QE	Quercetin Equivalent
RBC	Red Blood Cell
rpm	Revolutions Per Minute
SEM	Scanning Electron Microscopy
SFP	Staphylococcal Food Poisoning
TEM	Transmission Electron Microscopy
TFC	Total Flavonoid Content
Tg	Glass Transition
TGA	Thermogravimetric Analysis

Tm	Melting Temperature
TPC	Total Phenolic Content
TPTZ	2,4,6-Tri(2-pyridyl)-s-triazine
TS	Tensile Strength
TSA	Trypticase Soy Agar
TSB	Trypticase Soy Broth
TSBYE	Trypticase Soy Broth-Yeast Extract
UV	Ultraviolet
Wt	Weight
WVP	Water Vapor Permeability
XRD	X-Ray Diffraction
λmax	Maximum Wavelenght

LIST OF PUBLICATIONS

Nwabor OF, Vongkamjan K, and Voravuthikunchai SP (2019). Antioxidant properties and antibacterial effects of *Eucalyptus camaldulensis* ethanolic leaf extract on biofilm formation, motility, haemolysin production, and cell membrane of the foodborne pathogen *Listeria monocytogenes. Foodborne Pathogens and Diseases,* 16*:*581–589.

Nwabor OF, Singh S, Paosen S, Vongkamjan K, and Voravuthikunchai SP (2020). Enhancement of food shelf life with polyvinyl alcohol-chitosan nanocomposite film from bioactive eucalyptus leaf extracts. *Food Bioscience,* 36:100609.

Nwabor OF, Singh S, Marlina D, and Voravuthikunchai SP (2020). Chemical characterization, release, and bioactivity of *Eucalyptus camaldulensis* polyphenols from freeze dried sodium alginate and sodium carboxymethyl cellulose matrix. *Food Quality and Safety,* FQS-2020-014 (Accepted).

Nwabor OF, Singh S, Ontong JC, Vongkamjan K, and Voravuthikunchai SP (2020). Valorization of wastepaper through antimicrobial functionalization with biogenic silver nanoparticles, a sustainable packaging composite. WAVE-D-20-00427 (Submitted).

Nwabor OF, Bioactive phytochemicals in *Eucalyptus calmadulensis* inhibit important foodborne pathogens, reduce listeriolysin O-induced haemolysis, and ameliorate hydrogen peroxide-induced oxidative stress on human embryonic colon cells.

Nwabor OF, Facile in situ deposition of biogenic silver nanoparticles on porous alumina disc, an antibacterial, antibiofilm and antifouling strategy for food contact surfaces.

Nwabor OF, Ethanolic leaf extracts of *Eucalyptus camaldulensis* inhibits *Listeria monocytogenes* attachment and biofilm formation on food contact surfaces and modifies cell hydrophobicity.

REPRINTS WERE MADE WITH PERMISSION FROM THE PUBLISHERS

CHAPTER 1

INTRODUCTION

1. Background

Microbial food contamination is a global safety issue that results from poor hygiene, improper sanitation and handling of food, non-compliance to standards by food producers, poor manufacturing practices as well as preservative failures. Microbial contamination of food is one of the leading causes of foodborne disease outbreaks and food spoilage. According to the Food Standards Organization of Australia and New Zealand, besides the contamination of food products by undeclared allergens, microbial contamination was the highest cause of food recall between January 2008 and December 2017. Microorganisms associated with food recall included bacteria, viruses, and other parasitic organisms. However, bacteria contamination of food showed the highest prevalence in food recall with the Gram positive pathogen *Listeria monocytogenes* topping the chart, followed by the Gram negatives, *Salmonella* spp. and *Escherichia coli* (FSANZ, 2018). On the other hand, Microbial food spoilage results from the proliferation of microorganisms in food, with accumulation of malodorous by-products that alter the organoleptic, nutritional, and sensory qualities of the food product, making them distasteful to consumers.

To address the menace of microbial food contamination, the addition of antimicrobial and antioxidant agents in food as preservatives is intended to preserve sensory, organoleptic, nutritional and compositional qualities by inhibiting the proliferation of both spoilage mediating and foodborne pathogenic microorganisms in food and in addition, inhibit natural enzymatic oxidative processes that leads to spoilage of food.

However, as consumers awareness on the adverse health effects associated with the consumption of most age long preservatives hightens and the demand for green consumerism increases, the use of conventional synthetic preservatives is becoming obsolete and unacceptable. The search for alternative efficient, cost effective and bio-friendly agents has created a surge in natural products research, with various plants phytochemicals and bioactive compounds isolated and used for various applications. Various plants has shown promising results as alternative source of bioactive healthy ingredients that could be used in food production. Thus, this work focuses on exploring the possible applications of active phytochemical rich extracts of *E. camaldulensis* in food productions as antimicrobial and antioxidant preservatives.

2. Foodborne Pathogens

2.1. *Listeria monocytogenes*

Listeria monocytogenes is a facultative, rod-shaped, Gram-positive foodborne bacterium, that is motile by means of flagella at 25 ˚C to 30 ˚C. The specie monocytogenes consists of 13 serotypes, including 1/2a, 1/2b, 1/2c, 3a, 3b, 3c, 4a, 4ab, 4b, 4c, 4d, 4e, and 7. Serotypes 1/2a, 1/2b, and 4b have been associated with foodborne infections. *L. monocytogenes* is a ubiquitous environment bacterium found in the soil, sewage, decaying vegetation, and moist environments. It is a recalcitrant foodborne pathogen that can adapt to various extreme environments, including high salt content and temperatures below 1°C. Tolerance to storage temperature and resistance to food grade antimicrobial sanitizers and preservatives are responsible for the persistence of *L. monocytogenes* in food-manufacturing environments.

L. monocytogenes is among the leading causes of foodborne mortality, with about 255 deaths annually in the U.S. and a case-fatality rate of 15% to 30%. In the case of listeria

meningitis, the case-fatality rate may be as high as 70%; from septicemia, 50%, and in perinatal/neonatal infections, more than 80% (FDA, 2012). Listeriosis presents a self-limiting infection with mild or no symptoms in healthy individuals. However, in immunocompromised, aged, and pregnant victims, it is characterized with fever, muscle aches, nausea, and vomiting, and, occasionally, diarrhea. Severe cases might spread to the nervous system with symptoms including headache, stiff neck, confusion, loss of balance, convulsions, and death.

2.1.1. Virulence of *L. monocytogenes*

L. monocytogenes is a foodborne pathogen that is often transmitted via the fecal-oral route. Upon ingestion, the bacteria colonize the small intestine and invade cells lining the gastrointestinal tract through the "zipper-mechanism" using invasion molecules such as InlA and InlB to disrupt the cell membrane (Pizarro-Cerdá, Kühbacher, & Cossart, 2012). Phagocytic macrophages often engulf the bacterium in a vacuole creating phagolysosome, following the secretion of lysosome to digest the bacterium. However, the low pH of the phagolysosome compartment triggers the production listeriolysin O, phospholipase A, phospholipase B and phospholipase C, listeria exotoxin and virulence factors that destroys the phagolysosome's membrane leading to escape of the pathogen. The bacterium then multiplies within the cytoplasm and using the thin actin filaments of cell as a tail, it propels towards the membrane. *L monocytogenes* then exit from the cell using pseudopods and invades neighboring cell. Using the same virulence factors, the pathogen spread from cell to cell repeating the life cycle and evades the immune system.

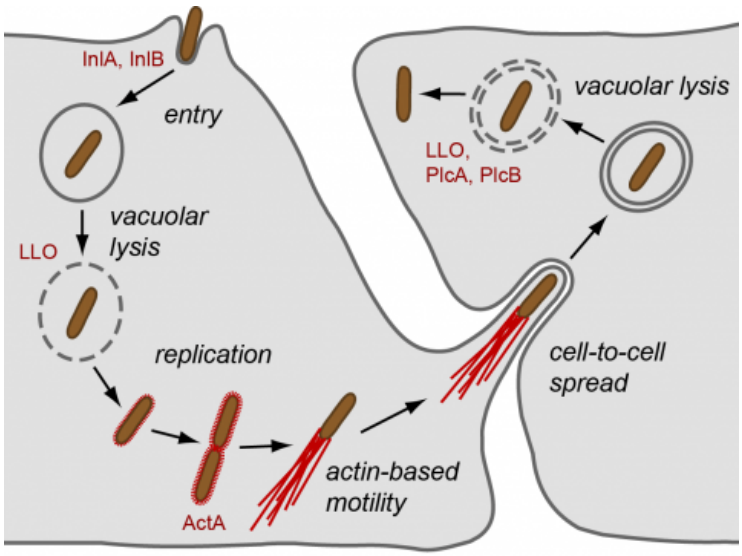

Figure 3. Virulence and infection cycle of *Listeria monocytogenes*

Source: Pasteur institute

2.2. *Escherichia coli*

Escherichia coli is a commensal Gram-negative, rod-shaped bacterium commonly found in the gut of humans and warm-blooded animals. Most *E. coli* are considered harmless to humans. However, certain pathogenic strains can infect the gut area and cause severe illness. Infection by pathogenic strains occurs through consumption of contaminated food such as raw or undercooked ground meat products, raw milk, and contaminated raw vegetables and sprouts, or ingestion of contaminated water (Yang, Lin, Aljuffali, & Fang, 2017). Pathogenic *E. coli* infection usually causes severe diarrhea. Annually, *E. coli* accounts for 63,158 (STEC O157), and 112,752 (STEC-non O157) cases of foodborne illnesses in the United States. Amounting to 2138 and 271 cases of hospitalizations respectively and a total of 20 death. Thus, *E. coli* accounts for approximately 1.9% of all foodborne illnesses, with a 4.3% hospitalization incidence and 1.5% foodborne death, translating into an annual economic loss of $34,619,998 and $14,277,961 for *E. coli* O157 and non-O157, respectively. Thus,

foodborne *E. coli* accounts for 65% of all the economic burdens arising from foodborne diseases (Hoffmann, Maculloch, & Batz, 2015).

2.3 *Staphylococcus aureus*

Staphylococcus aureus is a common normal flora bacterium found on the skin and in the nasal passages of up to 25% of healthy people and animals. They are responsible for variety of diseases ranging from uncomplicated skin and soft tissue infections such as styes, abscesses, boils, carbuncles, and impetigo to life-threatening diseases such as septicemia. In addition, they mediate toxin-related diseases such as toxic shock syndrome, staphylococcal scalded skin syndrome, and staphylococcal food poisoning (SFP). Enterotoxigenic *S. aureus* is a major cause of mild food poisoning resulting from the production toxins that act within the intestine to damage the mucosal endothelium making the mucosae more permeable to ions and water leading to vomiting and diarrhea. *S. aureus* enterotoxins are stable at 100 °C. Staphylococcal food poisoning is a gastroenteritis is caused by ingesting foods contaminated with staphylococcal toxins. The most common way for the transmission of Staphylococcal in food is through contact with asymptomatic food workers and handlers or through contaminated milk and cheeses.

S. aureus is salt tolerant and can grow in salty foods, however growth of this pathogen is inhibited at freezing temperatures. Staphylococcal toxins are heat stable and cannot be destroyed by cooking. Examples of foods that have been linked to this type of food poisoning include meat and meat products, poultry and egg products, salads, tuna, chicken, potato, and macaroni. Bakery products such as cream-filled pastries, cream pies, and chocolate éclairs; sandwich fillings; and milk and dairy products have also been implicated in the transmission of Staphylococcal infections.

2.4. *Bacillus spp*.

Bacillus species are Gram positive, aerobic, ubiquitous bacteria, characterized by their ability to form resistant spore coats. The genus *Bacillus* consists of about 48 known species, however, only *B. anthracis* and *B. cereus* have been linked to human disease. Species of *Bacillus* are mesophilic, growing at temperatures between 10 °C to 48 °C, with optimal temperature of 28 °C to 35 °C (Labbé & García, 2013). *Bacillus anthracis* is known to cause diseases in animal and man via direct contact or inhalation of endospores, however in rare cases, consumption of contaminated food like meats has led to *B. anthracis* associated foodborne illnesses.

Amongst the species of *Bacillus*, *B. cereus* is a well-recognized cause of food poisoning. A number of the other species have also been implicated in episodes of similar types of disease (Griffiths & Schraft, 2017). *B. cereus* is ubiquitous in the environment and can be found in the soil, water, on plants, sediments, and dust. Thus, it is frequently found on farm produce and frequently contaminates vegetables, spices, milk, and herbs. *B. cereus* like other *Bacillus* spp. Produces spores that are highly resistant to adverse environmental conditions like heat, dehydration, acidity, radiation, disinfectants and cleaning agents (Labbé & García, 2013). Production of large variety of extracellular virulent substances, and toxicity ranges from strains used as probiotics for humans to highly toxic strains are responsible for *B. cereus* foodborne fatalities. Foodborne intoxication associated with *B. cereus* contamination is characterized by the production of two types of symptom. The diarrheal type illness results from the production of heat labile enterotoxins during growth of vegetative cells in the small intestine of the host (Logan, 2012). Once in the small intestine, the bacteria produce

heat labile enterotoxins within 8–16 h incubation time. Symptoms associated with the syndrome includes abdominal pain, watery diarrhea, and occasional nausea. This form of illness results in mild to profuse watery diarrhea that is self-limiting, and often disappears after 12–24 h. Meat products, soups, milk and milk products, puddings, sauces and vegetables are some of the frequently implicated foods (Griffiths & Schraft, 2017). A more severe and acute form of *B. cereus* food poisoning is the emetic syndrome. This form of food poisoning is characterized by nausea, vomiting and abdominal cramps. The toxin responsible for this syndrome is a small cyclic heat-stable peptide that causes vomiting after 0.5 to 6 h (Tewari & Abdullah, 2015). Unlike the diarrhea syndrome, the emetic *B. cereus* poisoning is caused by the ingestion of a pre-formed toxin in the food. The foods involved are usually heat-treated, with surviving spores being the source of the food poisoning. In addition to food poisoning, *B. cereus* has been implicated in several opportunistic systemic and local infections such as endophthalmitis and septicemia. The risk population of *B. cereus* non-gastrointestinal infections are; neonates, intravenous drug abusers, patients sustaining traumatic or surgical wounds and patients with indwelling catheters (Labbé & García, 2013).

3. Microbial Food Spoilage

Microbial food spoilage is primarily a natural phenomenon mediate by food autochthonous microflora referred to as food specific spoilage organisms (SSO). Microbial food spoilage is a product of inherent microbial metabolism that results in the accumulation of malodorous by-products. Such metabolites alter the organoleptic, nutritional, and sensory qualities of the food product, making them distasteful to consumers. Annually, economic losses resulting from microbial mediated food spoilage accounts for millions of dollars in monetary terms, with millions of tons worth of

products wasted. The United Nations Food and Agricultural Organization estimated that 1.3 billion tons of food products is lost annually to spoilage (Cichello, 2015). Microbial spoilage contributes significantly to this lose, resulting in final products with an inadequate physical properties (Bevilacqua et al., 2016). It has been estimated that about 25% of all foods produced globally are lost due to microbial spoilage (Bondi et al., 2014).

Spoilage and deterioration have undoubtedly remained a global challenge. Efforts at containing this menace have significantly succeeded at extending products shelf life while concurrently reducing the prevalence of foodborne infections and intoxications. However, consumers craving for minimal processed food with little or no preservative is a challenge to available preservation techniques. To effective design and implementation of a reliable preservation regime, basic understanding of the microbial metabolism and ecology is required. Unfortunately, most preservative technologies neglect this basic understanding of food from a natural perspective, vis-à-vis its ecosystem and ecology as well as ecological influence on food spoilage and deteriorative process.

4. Biofilm Formation

Biofilm formation on food contact surfaces and food processing environment is a critical food safety concern. Bacterial attachment and biofilm formation contribute significantly to the burden of food industries and researchers. Biofilm formation on food contact surfaces is a major route of food contamination, especially of finished and processed food products. Formation of biofilm on food contact surface results to impaired heat transfer and contamination of finished products resulting in a

compromise of food quality. In addition, microbial influenced corrosion resulting in pitting of stainless-steel amounts to huge economic lost to food processing scientist and technicians. Exo-polymer matrix associated with matured biofilm on food contact surfaces limits the diffusion and migration of antimicrobial sanitizers and cleaning agents. In addition, depositions of multi-layers biofilm structure results in formation of crevice resulting in the impairment of fluid flow and dynamics in food processing environments and makes cleaning of food surfaces a difficult task.

5. Natural Products Antimicrobial and Antioxidants in Food

Nature is a warehouse of myriads of useful compounds that can be used to the benefits of mankind. From ancient time, man has used natural products in folk medicine, preservation and as flavours and spices for various products. The application of bioactive compounds of plant and microbial origin as antimicrobial and antioxidant food preservatives is well documented. However, despite the excellent qualities and prospects associated with natural products and their health promoting properties, synthetic chemical preservatives have dominated the science of preservation for so long a time. In recent times, heightened awareness on the adverse health effects of these chemical preservatives have resulted in a renewed search for bioactive compounds of natural sources that can be used in food production as preservatives, additives, enhancers, stabilizers and flavouring agents. Plant antimicrobial peptides, phytochemicals, essential oils, and bioactive agents of microbial origin such as nisin, pediocin, plantaricin, and reuterin have shown promising efficacy as possible alternatives.

6. *Eucalyptus camaldulensis*

Eucalyptus is an economic plant genus, belonging to the family Myrtaceae. It is widely exploited for its rich medicinal essential oil. Leaf of the specie *globulus* is approved for food application and is generally regarded as safe (GRAS). The species *camaldulensis* is grown for pulping in paper industries and is a rich source of essential oil with the terpenoid 1,8-cinole (eucalyptol) as the major bioactive volatile compound (Ashraf, Sarfraz, Mahmood, & ud Din, 2015; Sebei, Sakouhi, Herchi, Khouja, & Boukhchina, 2015). The leaf extracts contain various bioactive phytochemicals including flavonoids, sterols, alkaloids, glycosides, tannins, and phenols. An acyl phloroglucinol derivatives has been identified as a major antimicrobial constituent present in the leaf extract (Singab et al., 2011). Phytochemical-rich leaf extracts of the plant demonstrated good antimicrobial and antioxidant ethanolic leaf extracts of *Eucalyptus camaldulensis* (Alghamdi & Ababutain, 2019; Nasr, Saleem Khan, & Zhu, 2019; Nwabor, Vongkamjan, & Voravuthikunchai, 2019).

Table 1. Bioactivity of *Eucalyptus camaldulensis*

Part	Bioactivity	Reference
Leaf extracts	Antimicrobial and schistosomicidal	(Ghareeb, Habib, Mossalem, & Abdel-Aziz, 2018)
Leaf extracts	Antibacterial, antifungal and antioxidant	(Elansary, Salem, Ashmawy, Yessoufou, & El-Settawy, 2017)
Leaf	Antioxidant	(Singab et al., 2011)
Leaf, bud, capsule, and seed crude extracts	Antimicrobial activity	(Nasr, Zhou, et al., 2019)
Essential oils	Antimicrobial	(Knezevic et al., 2016)
Essential oil	Antifungal	(Gakuubi, Maina, & Wagacha, 2017)
Essential oil	Antimicrobial and Antioxidant	(Ghaffar et al., 2015)
Essential oil	Antioxidant	(Siramon & Ohtani, 2007)
Leaf	Gastroprotective and antimicrobial	(Adeniyi, Lawal, & Olaleye, 2006)
Leaf	Antibacterial	(Ghalem & Mohamed, 2008)
Essential oil	Antibacterial	(Akin, Aktumsek, & Nostro, 2010)
Leaf	Anti-dermatophyte	(Falahati, Omidi Tabrizib, & Jahaniani, 2005)
Essential oil	Larvicidal	(Medhi et al., 2010)
Essential oil	Antioxidant and antidiabetics	(Basak & Candan, 2010)
Essential oil	Beta-lactamase activity	(Chaves et al., 2018)
Essential oil	Insecticidal	(Rezaei, Khaghani, & Moharramipour, 2019)
Leaf	Antimicrobial	(Ishag et al., 2018)
Essential oil	Pesticidal	(Üstüner, Kordali, Bozhüyük, & Kesdek, 2018)

7. Encapsulation of Bioactive Compounds

Encapsulation is a widely employed method, applicable in both medical, pharmaceutical, food, agricultural and cosmetics industries. Encapsulation of inert active compounds shields from direct contact with processing environment, and thus prevent destructive interaction that might result in the loss of activity (Saikia, Mahnot, & Mahanta, 2015). In addition, encapsulation preserves the core through regulated release for delivery at the site of activity and ensures the masking of unpleasant properties (Rezende, Nogueira, & Narain, 2018). Researchers have developed various methods of encapsulation, using single wall material or a combination. Previous studies suggest that spray drying, and freeze drying are the most commonly used methods, however methods such as coacervation, co-crystallization, entrapment, emulsion, extrusion, and liposome are also alternative techniques with practical applications in food and pharmaceutical industries.

A major limitation to the incorporation of natural products into food and industrial system is the inert nature of such products, which makes it, unfit for processing. In addition, solubility of natural products in complex food matrix also poses a limitation to its use (Soković, Glamočlija, Marin, Brkić, & van Griensven, 2010). To overcome this impending factor, numerous methods of incorporating these products in food are been tried. Depending on the nature of the food product, direct incorporation of natural products has been employed through various ways, such as sprinkling, spraying, dipping, or coating. However, direct incorporation often leads to loss of activity and alteration of food sensory or organoleptic qualities, (Del Nobile, Lucera, Costa, & Conte, 2012). Encapsulation/entrapment of natural products in carrier molecules such as polymers has demonstrated reproducible bioactive effects, with a controlled release

and prolonged stability in food system (Del Nobile et al., 2012; Hintz, Matthews, & Di, 2015).

Table 2. Methods of encapsulation

Methods	**Principles**
Freeze drying	Entrapment occurs by dehydration through sublimation under pressure.
Emulsification	Core material is dissolved into polymerization solution. The monomers are polymerized to form capsules in an aqueous solution
Spray drying	Dispersion of the core material in an entrapment material, followed by atomization and spraying of the mixture in a hot air desiccant into a chamber
Coacervation	The entrapment occurs due to phase separation of one or many hydrocolloids from the initial solution and the subsequent deposition of the newly formed coacervate phase around the active ingredient suspended or emulsified in the same reaction media
Inclusion complexation	Molecular inclusion is generally achieved by using cyclodextrins (CDs) as the encapsulating materials. Apolar molecules are entrapped through a hydrophobic interaction inside cyclodextrins cavity replacing water molecules
Supercritical fluid technology	Create a dispersion of active and dissolved or swollen shell material in supercritical fluid. Release the fluid to precipitate the shell onto the active
Electrospraying	Electrospraying also known as electro-hydrodynamic atomization is a new nanoencapsulation technique similar to electrospinning. Unlike electrospinning, NPs are generated by this means instead of ultrathin fibers. High voltages are responsible for the atomization of liquids into fine droplets.
Electrospinning	Novel method for the continuous fabrication of nonwoven nano-fibers with diameters of nearly a few nanometers that could be employed in the delivery of bioactive food components. involves

	injecting polymer/biopolymer solution from a spinneret toward a prepared collector.
Co-crystallisation	crystalline structure of sucrose is modified from a perfect to an irregular agglomerated crystal, to provide a porous matrix in which a second active ingredient can be incorporated
Liposome entrapment	Phospholipids are dispersed in an aqueous phase spontaneously formation a liposome. A core material is entrapment into a liposome
Emulsion Phase Separation	The core material is added in the polar or apolar layer of an oil-in-water emulsion -O/W or water-in-oil -W/O emulsion. The emulsions are prepared using a surfactant
Extrusion	Forcing a core material in a molten wall material mass through a die (laboratory scale) or a series of dies of a desired cross section into a bath of desiccant liquid. The coating material hardens on contacting liquids, entrapping the active substances
Ionic gelation	Coating material with dissolved core material is extruded as drops within an ionic solution. The capsules are formed by ionic interaction

8. Active and Intelligent Food Packaging

Food packaging is an essential part of the food production chain. Conventional food packaging involves the use of passive inactive container that enable efficient transportation of food and protection from mechanical and physical mutilations. However, with the emergences of innovative technologies in food sciences, packaging materials are now designed to play active roles in enhancing and maintaining the shelf life of food products.

Active packaging is an innovative approach aimed at prolonging the shelf-life of food products while preserving their quality, safety, and integrity. According to the European commission regulation No 450/2009, active packaging comprises packaging systems

that interact with the food in such a way as to “deliberately incorporate components that would release or absorb substances into or from the packaged food or the environment surrounding the food” (European Commission, 2009). In recent times, numerous food packaging related research have centered on the functionalization of packaging materials with antimicrobial and antioxidant compounds. Natural products such as plant extracts and derivative compounds (Alehosseini, Gómez-Mascaraque, Martínez-Sanz, & López-Rubio, 2019; Oudjedi, Manso, Nerin, Hassissen, & Zaidi, 2019), microbial metabolites such as bacteriocin (Salvucci et al., 2019), and metal-based nanoparticles (Biswas, Tiimob, Abdela, Jeelani, & Rangari, 2019; Dairi, Ferfera-Harrar, Ramos, & Garrigós, 2019; Yu, Wang, Kong, Lin, & Mustapha, 2019) are frequently employed in most research works for the functionalization of packaging materials. Bioactive components released from these packaging materials diffuse into the food matrix and inhibits the growth of food spoilage bacteria or serve as radical scavenging agents for oxidation mediators generated in the food. The incorporation of sensors and signaling agents into food packaging material is a recent advancement in food packaging design. Unlike active packings, intelligent packaging material do not necessarily play an active role in ensuring the stability of the food. However, they serve as a source of useful information on the state of the food product. Intelligent packaging is a broad approach that involves the incorporation of quality and freshness indicators such as temperature indicators, pH indicators, time-temperature integrators, and gas-level controls that monitors the quality state of the food. It improves the product quality, enhance food safety, and guarantees the confidence of consumers. Like in active packaging, natural products and metal-based nanoparticles have been utilized in the design of intelligent food packaging material (Jayakumar et al., 2019; Jung et al., 2019; C. Wu et al., 2020).

9. Nanotechnology in Food Packaging

Nanotechnology is an emerging science with applications in various areas including engineering, environmental, pharmaceuticals, medicals, food, agriculture, and textile. In the food sector, nanotechnology has been used in the design of active and intelligent packaging as antimicrobial or signaling agents for the extension of food shelf life. Various materials, including polymers and metals salts are used in the synthesis of nanoparticles with excellent activities as microbial inhibitors or sensors. Silver nanoparticles is the most extensively used nanomaterial, due to its excellent qualities and antimicrobial activities. Biogenic synthesis of nanoparticles using natural products is an ecofriendly method that has received extensive research attention. Plant extracts, phenolics, and flavonoids (Marrez, Abdelhamid, & Darwesh, 2019; Vishnuvarthanan & Rajeswari, 2019) and microbial metabolites and cultures (Adebayo-Tayo, Inem, & Olaniyi, 2019; Momin, Rahman, Jha, & Annapure, 2019) are used as reducing and capping agents for the synthesis of nanoparticles. Introduction of nano-sized materials into food packaging improves mechanical strength, barrier properties, and can serve as antimicrobial and sensing for pathogen detection for enhancing food safety (Singh et al., 2017). Since spoilage initiates at the surface of the food matrix, contact of food product with the packaging material helps inhibit the growth of microorganisms. However, release of nanoparticles and migration into the food matrix have raised questions on the safety of nanoparticles in food packaging.

10. Antimicrobial Mechanism of Nanoparticles

Nanoparticles have shown excellent activities as antimicrobial agents in food packaging materials and other applications. However, the antimicrobial mechanism of nanoparticles is still not fully understood. Factors such as the nano-size of the particles

is believed to influence the activity due to increased surface area of interaction with the bacterial cell (Bardhan et al., 2019; Jeong, Lim, & Choi, 2014). In addition, the positively charged nanoparticles surface is believed to establish an electrostatic bounding with the negatively charged bacterial surface, insulting in increased and firm interaction and adherence that makes for effective antimicrobial activity (Abbaszadegan et al., 2015; Katas, Lim, Azlan, Buang, & Busra, 2019; Qiao, Yao, Song, Yin, & Luo, 2019). Various research works focused on the antimicrobial mechanism of silver nanoparticles reports the disruption of cell membrane as a probable antimicrobial target (Bondarenko et al., 2018; M. Singh, Mallick, Banerjee, & Kumar, 2016). Silver nanoparticles induce cell membrane damage leading to a loss of membrane functionality and hence influx and efflux of molecules across the membrane. The antimicrobial effects of silver nanoparticles have been reported to relate to induction of oxidative stress (Liao et al., 2019; Mao, Chen, Wang, & Yan, 2018; Song, Wu, Wang, & Han, 2019; Yan et al., 2018; Zhang, Wu, Si, & Shu, 2018). Alterations of redox hemostasis was reported in multi-drug resistant *Pseudomonas aeruginosa* treated with silver nanoparticles, resulting in the over expression of proteins involved in reactive oxygen metabolism, oxidative stress, and REDOX while the proteins involved in synthesis of macromolecules and metabolic processes were under expressed (Liao et al., 2019). Moreover, the internalization of silver nanoparticles is believed to interfere with cellular metabolism and synthesis, resulting in the aggregation of proteins and damage of DNA.

CHAPTER 2

MATERIAL AND METHODS

Part I. Antimicrobial and Antioxidant Activities of *Eucalyptus camaldulensis* Ethanolic Extract and Effects on *Listeria monocytogenes* Virulence, Attachment, and Biofilm Formation

1. Plant Extraction

Classified reference voucher specimen of *E. camaldulensis* was deposited at the Herbarium of Faculty of Pharmaceutical Sciences, Prince of Songkla University, Thailand. The leaves were extracted as described in previous works from our laboratory (Hiranrat, Chitbankluoi, Mahabusarakam, Limsuwan, & Voravuthikunchai, 2012; Limsuwan et al., 2009). Dried leaves were macerated in 95% ethanol for seven days. The extract was completely dried and dissolved in 1% dimethylsulfoxide (DMSO, Merck, Germany) before use.

2. Bacteria and Culture Conditions

Twenty isolates of *L. monocytogenes* were used in this study. A reference strain F2365 was obtained from Nightingale *et al*. (2007). Other 19 isolates were previously isolated from ready-to-eat food and food processing environment and kept in a culture collection at the Department of Food Technology, Prince of Songkla University, Thailand (Vongkamjan, Fuangpaiboon, Jirachotrapee, & Turner, 2015). All the bacterial cultures were stored in Tryptic Soy Broth (TSB; Difco, Le Port de claix, France) supplemented with 40% glycerol and kept at -80^{o}C. Isolates were subcultured on Tryptic Soy Agar (TSA; Difco Le Port de claix, France) at 37^{o}C for 18 to 24 h (overnight culture) prior to the study.

3. Antimicrobial Activity of *E. camaldulensis*

Disc diffusion technique was used to evaluate the antimicrobial activity (CLSI, 2006). Colonies of *L. monocytogenes* from overnight culture were transferred into TSB and incubated at 37ºC for 4 h to early log phase. The bacterial suspensions were adjusted to 0.5 McFarland standard (1.5×10^8 CFU/mL) before use. Hundred microliters (100 µL) of 10^6 CFU/mL bacterial suspensions were spread plated on solidified Mueller-Hinton agar (MHA; Difco Le Port de claix, France) and seeded with disc containing 2.5 mg/mL of the test extract. Disc impregnated with 1% DMSO solution were used as negative control. Experiments were performed in triplicate and means zones of inhibition ± SD were calculated.

4. Determination of Minimum Inhibitory and Minimum Bactericidal Concentrations

Minimum inhibitory concentrations of ethanolic extract of *E. camaldulensis* was determined using standard broth microdilution method (CLSI, 2015). Stock solution of the extract were serially diluted (2-fold) to concentrations of 0.016 to 1.024 mg/mL in a 96-well polystyrene microtiter plate. The wells were then seeded with 100 µL of 10^6 CFU/mL bacterial suspension in MHB and incubated for 18 to 24 h at 37ºC. Sodium nitrite and sodium benzoate (4 to 128 mg/mL) were used as reference preservatives. MIC values were recorded as the lowest concentration that completely inhibited the bacterial growth. The minimum bactericidal concentrations were determined using the spot plate technique by seeding 10 µL aliquots from wells without growth on TSA. The plates were incubated at 37ºC for 24 h. The MBC values were recorded as the lowest concentrations that showed no growth on TSA plates. All experiments were set up in triplicate for two independent studies.

5. Time kill Assay

Bacteria inactivation kinetics of the extract was determined using the time kill assay (Mitsuwan *et al*., 2017). Colonies of *L. monocytogenes* isolates PSU-KV-032, PSU-KV-120 and reference strain F2365 from an overnight culture were sub-cultured into freshly prepared TSB and incubated to early log phase. The bacterial suspensions were adjusted to a 0.5 McFarland standard and 100 µL of 10^6 CFU/mL bacterial suspensions was added to 100 µL of TSB supplemented with 4MIC, 2MIC, MIC, and 1/2MIC in 96-well polyester microtiter plate. The cultures were incubated statically at 37 ˚C. Hundred (100 µL) was withdrawn from individual concentrations at 0, 4, 8, 12, 16, and 24 h. The samples were serially diluted and 10 µL of respective dilution were plated on TSA. Viable bacteria cells were counted, and results were recorded as log CFU/mL. Negative controls with media supplement with 1% DMSO were also included in the assay. The experiments were performed in triplicate and recorded as Mean ± SD.

6. Sub-Inhibitory Concentrations Assay

The SICs (concentrations not inhibiting growth) of the extract against the test *L. monocytogenes* isolates and strain F2365 were determined as previously described (Miao et al., 2019) with slight modifications. Overnight bacterial culture was diluted to 10^6 CFU/mL in TSB and treated with MIC, 1/2MIC, 1/4MIC and 1/8MIC of extract and incubated at 37 °C. At time intervals (0, 2, 4, 6, 8, 10, 12, 18, and 24), 200 µL of the bacterial suspension were transferred to 96-well plate, and the bacterial cell density at 600 nm was measured using a multi-mode plate reader (PerkinElmer, Waltham, USA).

7. Attachment Assay

The inhibitory effects of *E. camaldulensis* crude ethanolic extracts on *L. monocytogenes* attachment to food contact surfaces (Glass, stainless and plastics) was evaluated as described (Vazquez-Armenta et al., 2018). Contact surface coupons (1.0 cm x 1.0 cm) were cleaned by washing and soaked overnight in absolute ethanol. The glass and stainless slides were then sterilized by autoclaving and allowed to dry overnight at 70 ˚C while the plastics were UV-sterilized. Overnight BHI *L. monocytogenes* cultures were adjusted to 0.5 McFarland standard (1.5×10^8 CFU/mL). The clean contact surface materials were aseptically transferred to individual wells of a sterile 24-well plate. One milliliter 1 mL of the adjusted bacterial culture was then added to each of the well and the plates were incubated at 37ºC. At 2, 4 and 6 hours, the attached cells on the contact materials were enumerated. Briefly, the contact materials were withdrawn from the culture, gently washed with PBS (pH 7.4) and transferred to a sterile tube containing 1 mL PBS. Attached cells were detached by vortexing and ultrasonication. Cells were counted on TSA incubated overnight at 37 ˚C and recorded as CFU/cm^2.

8. Biofilm Formation on Food Contact Materials

The effects of the extract on *L. monocytogenes* biofilm formation was evaluated using crystal violet assay. Clean, grease free contact materials were aseptically transferred into 24 well plates. Overnight cultures were adjusted to 10^6 CFU/mL and 1 mL of the culture was added to the 24-well plate containing the surface material. After 24 hours incubation at 37 ˚C, the culture media were carefully discarded, and the contact material were gently washed with PBS, transferred to new clean 24 well plates and

fixed with 95% ethanol. Dried slides were stained with 0.1% crystal violet for 30 min. The stained contact surface materials were washed with distilled water to remove the excess dye, transferred to fresh 24-well plates and destained with DMSO. Optical densities were read at 570 nm and the biofilm inhibitory effects were recorded.

9. Effect of the Extract on Biofilm Bacterial Population

The inhibitory activity of the extract on biofilm formation was investigated on the contact surfaces as previously described (Kim, Chung, Kim, & Rhee, 2019), with slight modifications. The contact materials were washed clean, dried under the laminar and aseptically transferred into 24 well plates. Bacterial culture adjusted to 10^6 CFU/mL was then added into each well and incubated for 24 h, at 37 °C. Afterwards, the contact materials were carefully withdrawn from the culture, washed gently with PBS and the cells were detached by 2 min vortexing, followed by ultrasonication. The bacterial population was enumerated by drop plate technique and recorded as CFU/mL.

10. Effects of the Extract on Established Biofilm

To evaluate the effects of the extract on established *L. monocytogenes* biofilm, the surface materials were cleaned as previously described and were aseptically transferred into wells of the 24 well plate. Adjusted overnight cultures 10^6 CFU/mL were then added to respective wells and incubated at 37 ˚C. After incubation for 48 h, the spent media were discarded, the wells were rinsed, and fresh media were added and incubated further for an additional 48 h. After the incubation period, the wells containing the contact materials were rinsed twice with PBS and air dried. 0.5 mL of a freshly prepared BHI broth supplemented with MIC to 16MIC of the extract was added to each sample and incubated for 24 h at 37 ˚C. The contact materials were carefully

withdrawn from the wells, rinsed repeatedly with PBS, and transferred to a clean tube containing 1 mL of PBS. Attached cells were enumerated as described previously.

11. Scanning Electron Microscopy

The time-course development of *L. monocytogenes* biofilm on stainless steel, glass and plastic surface material was monitored using a scanning electron microscope. The contact materials were cleaned and incubated with 10^6 CFU/mL of bacterial culture. At 6, 24, 48, 72, and 96 h, coupons were carefully removed, washed to remove non-attached cells, air dried and analyzed using SEM.

12. Affinity of *L. monocytogenes* to Solvents

The affinity of strong biofilm forming isolates and strain F2365 were determined using the BATH assay as previously described (Lamari, Khouadja, & Rtimi, 2018). Briefly, 24 and 72 h cultures were harvested at $4000 \times g$ for 5 min and washed twice with normal saline solution. The cell suspension was then adjusted to an absorbance of 0.4 ± 0.020 at 400 nm. Briefly, 0.5 mL of solvents (Toluene, Hexane, Petroleum ether and Chloroform) were introduced into 3 mL of the bacterial suspensions in a tube. The mixture was then vortexed vigorously for 2 min and allowed to stand for 10 min to ensure complete phase separation. Afterwards, 1 mL of the aqueous phase was carefully withdrawn, and absorbance was read at 400 nm. The percentage affinity of the cells to solvents were calculated following the formula:

$$\% \text{ affinity} = \left(1 - \frac{A_a}{A_i}\right) \times 100$$

Where A_a is the absorbance of the cell suspension after mixing with the solvent, and A_i is the initial absorbance before mixing.

13. Effect of *E. camaldulensis* on the Hydrophobicity of *L. monocytogenes*

The effect of the extract of the cell surface hydrophobicity of the test strain F2365 and isolate PSU-KV-148 was determined as described (Mordmuang *et al.*, 2015) with slight modifications. Stationary phase culture was supplemented with MIC, 1/2MIC, 1/4MIC and 1/8MIC of the extract and incubated with mild shaking at 37 ˚C for 5 h. After incubation, the bacterial cells were harvested at 4000 ×g for 5 min and washed twice with sterile saline solution. The cell suspension was then adjusted to 0.4 ± 0.020 at 400 nm (OD initial). The bacterial cells incubated without the extract were used as a control. Briefly, 0.5 mL of toluene was introduced into 3 mL of the cell suspensions in a tube. The mixtures were vortexed vigorously for 2 min and allowed to stand for 10 min until phases were completely separated. OD of the aqueous phase was then read at 400 nm. The hydrophobicity index of the cells was calculated following the formula:

$$\text{Hydrophobicity index} = \left(1 - \frac{A_a}{A_i}\right) \times 100$$

Where *Aa* is the absorbance value of the aqueous phase after addition with toluene and *Ai* is the initial absorbance value of the adjusted culture.

14. Motility Assay

All 19 isolates and strain F2365 were evaluated for motility at 30ºC and 37ºC according to the method previously described in Borges, Saavedra, & Simões, 2012; Vazquez-Armenta et al. (2018) with slight modifications. The effect of the extract on the motility of highly motile isolates (PSU-KV-108, PSU-KV-116, PSU-KV-122) and strain F2365 were evaluated at 30ºC. Motility was tested on 0.3% agar in TSB supplemented with MIC and sub-inhibitory concentrations of extract. The plates were

seeded with 10 µL of 10^6 CFU/mL bacterial suspension and incubated at test temperatures for 24 h. Motility medium supplemented with 1% DMSO was maintained as negative control. Triplicate values of two independent trials and recorded as Mean diameter of motility ± SD.

15. Listeriolysin O Inhibition Assay

Haemolytic activity of *L. monocytogenes* was investigated following a method described previously (Sansano, Rivas, Pina-Pérez, Martinez, & Rodrigo, 2017) with slight modifications. Fresh overnight cultures grown in TSB at 37°C were harvested at (8000 rpm, 10 min), and washed three times with TSB. Pelleted cells were re-suspended in TSB to a final concentration of 10^6 CFU/mL. The cultures were incubated for 12 to18 h. Stationary phase cultures (12–18 h) were centrifuged at 13,500 rpm for 10 min, and the cell free supernatant (CFS) were collected for haemolysis assay. To determine the effect of *E. camaldulensis* on listeriolysin O activities, freshly prepared TSB were supplemented with sub-inhibitory concentrations (1/2MIC, 1/4MIC, 1/8MIC, and 1/16MIC) of the extract before incubation. Human red blood cells (RBC) obtained following the methods of Upadhyay *et al*. (2012) were suspended into PBS to obtain a 3% RBC (approx. 7.4 x 10^7 cells/mL). Haemolysis assay was conducted in micro-dilution plates by adding 100µl of CFS, 100 µL of PBS and 100 µL of 3% RBC and incubating for 30 min. A positive control (100% haemolysis) 100 µL of 1% Triton X-100, 100 µL of PBS, and 100 µL of 3% RBC and negative control (0% haemolysis) 100 µL fresh TSB, 100 µL PBS and 100 µL 3% RBC were included in the assay. Absorbance at 600 nm were read using a microplate reader (EnSpire Multimode Plate Reader - PerkinElmer) and values were recorded as mean ± SD of triplicate values.

Percentage haemolysis was calculated using the formula (Du, Zhou, Liu, Chen, & Li, 2018).

$$\% \text{ Haemolysis} = (OD_s - OD_n) \div (OD_p - OD_n) \times 100$$

where OD_s, OD_n and OD_p are absorbance values for sample, negative control, and positive control.

16. Effects of *E. camaldulensis* on *L. monocytogenes* Biofilm Formation

Effect of the extract on biofilm formation was determined as described by (Du *et al*., 2018), with slight modifications. In brief, 1 mL of overnight cultures in TSB + 0.6% yeast extract were adjusted to 10^6 CFU/mL. Hundred milliliter (100 µL) portions of adjusted cultures (10^6 CFU/mL) were transferred into wells containing 100 µL of trypticase soy broth yeast extract media supplemented with sub-inhibitory concentrations of the extract (MIC, 1/2MIC, and 1/4MIC). The plates were incubated at 37°C for 24 h. The effects of the extract on biofilm formation was determined by staining with 0.1% crystal violet. Wells containing culture and TSBYE were used as negative control. Absorbance were read at 570 nm and values were recorded as mean ± SD of triplicate values.

17. Membrane Permeability Assay

The effects of *E. camaldulensis* extract on membrane integrity of *L. monocytogenes* strain F2365 was determined following the method described by Devi, Nisha, Sakthivel, & Pandian, (2010) with slight modifications. Overnight cultures of *L. monocytogenes* were harvested, washed, and re-suspended in TSB supplemented with 2MIC, MIC, and 1/2MIC of extract to a final concentration of 1.5 x 10^8 CFU/mL. The bacterial suspensions were incubated for 30 min at 37 ˚C. Cells were harvested at 11,500 rpm for 5 min and pellet were resuspended in PBS containing 10 µg/mL of crystal violet

and incubated statically at 37 ˚C for 10 min. Cell suspensions were centrifuged at 14,000 rpm for 15 min, and the supernatant were collected and measured at OD_{590}. Cultures treated with 1% DMSO were used as negative control. Experiments were performed in triplicate for two independent trials and the crystal violet uptake was calculated as:

$$\% \text{ CV uptake} = (OD_{\text{crystal violet}} - OD_{\text{test}}) \div (OD_{\text{crystal violet}}) \times 100$$

18. DPPH assay

Stock solution (0.076 mM) of 2,2-diphenyl-1-picrylhydrazyl (DPPH) was prepared by dissolving 0.003 g crystalline powder in 100 mL of 95% methanol. Standard solution of trolox and ascorbic acid was also prepared by dissolving 1 mg of crystalline trolox and 1 mg ascorbic acid powder in 1 mL 95% methanol. The antioxidant activities of *Eucalyptus camaldulensis* ethanolic extract was evaluated using DPPH free radical scavenging activity assays following the modified method of (Kharat & Mendhulkar, 2016). Aliquot (20 µL) portion of varying concentrations of extract (7.8 to 125.0 µg/mL), Trolox and ascorbic acid (7.8-62.5 µg/mL) following a 2-fold serial dilution were tested against 180 µL of stock DPPH solution in a 96 well plate. Experimental blanks containing 20 µL of samples or standard with 180 µL of 95% methanol and a negative control (20 µL of methanol and 180 µL of DPPH) were included in the assay. Absorbance at 517 nm were read and the free radical scavenging ability of the test sample and standards were calculated using the formula

$$\% \text{ Inhibition} = (AB_{control} - AB_{test}) \div AB_{control} \times 100$$

Where $AB_{control}$ is the absorbance of the negative control, AB_{test} is the difference of the absorbance of samples and corresponding blanks. The concentrations of samples required to scavenge 50% of the DPPH free radicals (IC_{50}), were calculated from a

regression line of percentage inhibition against concentrations. The experiment was conducted in triplicate for two independent trials.

19. ABTS Radical Scavenging Activity

The 2, 2´-azino-bis (3-ethylbenzthiazoline-6-sulphonic acid) was performed as described by (Li et al., 2012), with some modifications. The ABTS solution was prepared by reacting equal volumes of 1.8 mg/mL aqueous ABTS and 0.66 mg/mL potassium persulfate ($K_2S_2O_8$), and then storing in the dark for 12 h at room temperature. Then ABTS solutions (200 µL) were added to 20 µL samples of different concentrations (7.8 to 250 µg/mL). The mixture was then incubated in the dark at room temperature for 30 min. The absorbance of the resulting solutions was measured at 734 nm. Different concentrations of Trolox and ascorbic acid solutions were used to prepare the standard curve. The ABTS radical concentration (µg/mL) in the reaction medium was calculated from the following calibration curve, determined by linear regression. A blank consisting of 20 µL of Trolox or sample in 200 PBS µL PBS was maintained alongside control of ABTS OD (0.7 ± 0.02) at 734 nm

$$\text{Scavenging activity (\%)} = (A_{control} - A_{sample}) \div A_{control} \times 100$$

The antioxidant capacity of test samples was expressed as IC_{50} (anti-radical activity), the concentration necessary for 50% reduction of ABTS.

20. Ferric Reducing Antioxidant Power (FRAP) Assay

The ability of the test extracts to reduce ferric ions was measured using the FRAP assay as described by (Benzie & Strain, 1999). Freshly prepared FRAP reagent produced by mixing 300 mM sodium acetate buffer (pH 3.6), 10.0 mM TPTZ (tripyridyl triazine) solution and 20.0 mM $FeCl_3$.6H2O solution in a ratio of 10:1:1 in

volume were used for the assay. Briefly, 30 µL of varying concentrations of the extract (9.375 to 300 µg/ mL) were added to 270 µL of FRAP reagent in a 96 well plate and the reaction mixture was incubated at 37 °C for 30 min in the dark. Absorbance at 593 nm was measured. Standard curve was prepared using different concentrations of ascorbic acid. All solutions were used on the day of preparation. The results were expressed as µM ascorbic acid equivalent/ mg extract. Analyses were performed in triplicate on each extract.

21. Folin-Ciocalteu Assay

The total phenolic content of the extracts were determined using the Folin–Ciocalteu method (Kaur & Kapoor, 2002) with modifications. The extracts were serially diluted to obtain concentrations 9.375 to 300 µg/ mL. Briefly, 20 µl of the sample were added to 100 µL of Folin-Ciocalteu reagent (diluted 1:10 in distilled water). Afterwards, 80 µL of a 0.2 g/mL Na_2CO_3 solution was added and the plates were incubated for 90 min in the dark. Absorbance at 700 nm were then read from a microplate reader. A double fold serially diluted 1 mg/mL solutions of gallic acid in 1% DMSO was used as standard. The calibration curve was constructed by plotting the absorbance against concentration. Total phenolic content was expressed as milligrams of garlic acid equivalent (GAE) per mg of extract. Measurement were in triplicate and values recorded as Mean ± SD.

22. Total Flavonoid

The total flavonoid content of the extracts were determined using aluminum chloride calorimetric method as previously described (Tohidi, Rahimmalek, & Arzani, 2017) with some changes. The extract was diluted to concentrations 9.375 to 300 µg/mL. A volume of 20 µL of respective extract concentrations were added to 80 µL

of distilled water and 6 µL a 5% $NaNO_2$ solution. The blend was incubated in the dark for 5 min, and 6 µL of a 10% $AlCl_3$ solution was added and incubated for 5 min. Afterwards, 40 µL of a 4% NaOH solution and 48 µL of distilled water were added. The mixtures were left standing in the dark for 15 min, and the absorbance was measured at 510 nm. The total flavonoid content (TFC) was presented in mg of quercetin equivalents (QE) per mg of the extract.

Part II. Microencapsulation of *Eucalyptus camaldulensis* Crude Ethanolic Extract by Freeze Drying Technique, Using Sodium Alginate and Sodium Carboxymethyl Cellulose as Wall Materials

1. Materials and Chemicals

Sodium alginate and sodium carboxymethyl cellulose (Na-CMC) were purchased from sigma Aldrich, Singapore. Tetrazolium Bromide (3-(4,5-dimethyl-2-thiazolyl)-2,5-diphenyl-2H, MTT), and trypsin were obtained from Merck (Darmstadt, Germany), Dulbecco's modified eagle medium (DMEM) and fetal bovine serum were purchased from Gibco, UK. Bacteriological media were purchased from Thermo Fisher Scientific (Loughborough, Leicestershire, UK).

2. Formation of Alginate-CMC Microcapsules

Alginate-CMC microcapsules were formulated using the freeze drying method. A 2% solution of sodium alginate solution was mixed with 1% CMC solution in a 1:1 ratio. One milliliter of varying concentrations 0 mg (Blank = F0) 250mg (F1), 500mg (F2) and 1000mg (F5) of ethanolic leaf extract of *E. camaldulensis* was then added to the alginate-CMC mixture and allowed to stir for 20 min. The mixture was then added dropwise into a 3% $CaCl_2.2H_2O$ solution using a precision needle at a flow rate of 1 mL/10 min under high speed homogenization at 15,000 rpm. After-which the microcapsule mixture was left to further homogenize for 60 min. The mixture was then centrifuged at 10,000 rpm for 30 min. Pelleted microcapsules were then freeze dried and pulverized into powder.

3. Encapsulation Yield

The encapsulation yield was calculated using the following equation:

$$\% \text{ Encapsulation yield} = \frac{W1}{W2} \times 100$$

where W1 is the total mass of microcapsules after being freeze-dried; W2 is the mass of Na alginate, CMC, and *E. camaldulensis* extract that were fed in the encapsulation process.

4. Encapsulation Efficiency

Encapsulation efficiency was estimated calorimetrically using the indirect method. The extract was serially diluted and a linear regression of concentrations against OD was obtained at a λ_{max} of 400 nm. The supernatant obtained from the microencapsulation process was then collected and the OD at 400 nm was read. The percentage encapsulation was calculated using the formula:

$$\frac{A_{initial} - A_{supernatant}}{A_{initial}} \times 100$$

where $A_{initial}$ is the OD of the microcapsule mixture before centrifugation and $A_{supernatant}$ is the OD of the supernatant after centrifugation.

5. Particle Size Analyzer

The particle size of the microcapsules was determined using a laser scattering particle size distribution analyzer (Horiba LA-300, Japan). Particle size distribution curve was obtained using software and mean of particle size diameter readings were recorded. The measurements were made in triplicate.

6. Fourier Transform Infrared Spectroscopy

The changes in *E. camaldulensis* extract, encapsulated microparticle and blank alginate-CMC particles were characterized by FTIR analysis. IR spectra were obtained

with a Spectrum 100 series FTIR spectrometer (Perkin Elmer) using a transformation of 20 scans with a spectral resolution of 4 cm^{-1}. FTIR spectra were collected in the mid-infrared region between 4000 and 650 cm^{-1}.

7. Micromeritic Properties of Microcapsules

The microcapsules were evaluated for various micromeritic properties including angle of repose, bulk density, tapped density, carr's index and hausner's ratio. All the tests were performed following USP 42–NF 37 procedure. The angle of repose was determined by fixed funnel method using the below Eqn.

$$\text{Tan } \theta = \frac{h}{r}$$

Where h, is height of the microcapsules pile, and r is radius of the microcapsules pile.

For the determination of bulk and tapped density, microcapsules were tapped using USP tapped density tester (Electrolab, model ETD–1020) for 250 taps and the change in volume was measured. Carr's index and Hausner's ratio were calculated using the Equation

$$compressibility\ index\ = \frac{100 \times (Vo - Vf)}{Vo}$$

$$\text{Hausner ratio } = \frac{\text{V}o}{\text{V}f}$$

Where Vo is the initial volume, and Vf is the tapped volume.

8. Determination of Moisture (Loss on Drying)

LOD was determined by drying 1 g of microcapsules in an oven at 100-105 °C for 3 h then sample was kept in desiccator for 24 h and reweighed. The difference in weights were recorded and loss on drying was calculated by the equation

$$\% \text{ LOD } = \frac{(W2 - W3)}{(W2 - W1)} \times 100$$

Where W_1 = Weight of empty weighing bottle, W_2 = Weight of weighing bottle with sample, W_3 = Weight of weighing bottle with dried sample

9. Determination of Swelling Index

The swelling index was determined following previously described method (Surini, Nursatyani, & Ramadon, 2018) with modifications. Briefly, microcapsules (500 mg), was introduced into Petri-dish and 10 mL of distilled water was added and the mixtures were left to stand at 37 °C with constant shaking. After 60 min, the microcapsules were centrifuged at 4500 rpm for 10 min and the supernatant were carefully discarded. The swelling index was then calculated using the equation

$$\text{Swelling index } = \frac{W2 - W1}{W1}$$

Where W_1 = weight of microcapsules swelling, W_2 = weight of microcapsules after swelling.

10. Solubility

The solubility of the formulated microcapsules were measured as described by (Hussain et al., 2018), with slight modifications. Sample's weighing 1.0 g were dispersed in 10 mL distilled water in beaker and stirred for 30 min. The mixture was then centrifugation at 3000×g for10 min. The supernatant was transferred to a pre-weighted petri dish and oven dried at 105 °C for 4.0 h. The solubility was measured on the bases of weight difference and demonstrated in the term of percentage (%)

11. *In vitro* Release of Polyphenols from Microparticles

Release of encapsulated extract was estimated by quantifying the phenolic content released from the microcapsules using Folin-Ciocalteau method (Arriola, de Medeiros, Prudencio, Müller, & Amboni, 2016). In brief, 200 mg of extract was suspended in 5 mL of distilled water at 4 °C and 37 °C with constant stirring at 150 rpm. At interval, aliquot of the supernatant was withdrawn with replacements and the phenolic content was quantified. Obtained results were expressed in mg GAE/mg dry microparticles. Experiments were recorded in triplicate. Released polyphenol content was calculated using the equation,

$$\text{Polyphenols released (\%)} = \frac{TPt}{TP\infty} \times 100$$

Where TP_t is the phenolic content released at time t and TP_∞ is the total phenolic content of the microcapsules.

Values obtained were fitted into various kinetic models including zero-order, first order, Higuchi, and Korsmeyer-Peppa's, equation and coefficient of correlation (r) values were calculated for linear curves by regression analysis of the plots.

12. Colour Measurements

Colour of the microcapsules was determined using colorimeter (ColorFlex, Hunter Lab Reston, VA, USA), and recorded in terms of L*, a*, b*. Where L* indicates the lightness, a* redness and greenness, and b* yellowness and blueness. The manufacturer's standard white plate was used for the calibration (L* = 92.84; a* = -1.29; b* = 0.55). The parameters L*, a* and b* were used to calculate Chroma, Hue

angle, ΔE (total colour change) and browning index (BI) according to the equations stated by (Rigon & Noreña, 2016; Yeşilsu & Özyurt, 2019):

$$\text{Chroma} = \sqrt{(a^{*2} + b^{*2})}$$

$$\text{Hue} = \tan^{-1}(b^{*}/ a^{*})$$

$$\Delta E = \sqrt{(\Delta L^{*2} + \Delta a^{*2} + \Delta b^{*2})}$$

$$\text{BI} = [100(x - 0.31)]/0.17$$

$$\text{Where, } X = (a^{*} + 1.75L^{*}) \div (5.645L^{*} + a^{*} - 3.012b^{*})$$

13. Scanning Electron Microscopy (SEM)

The morphology of the microcapsules was studied using scanning electron microscopy at 20 kV with a magnification of x100. Samples were mounted on copper stopper and gold coated before imaging

14. Determination of Total Phenolic and Flavonoid Contents of Microcapsules

Microcapsules were suspended in sodium citrate solution to a final concentration of 20 mg/mL. The mixture was centrifuged at 4000 g for 20 min, and the supernatant were analyzed for total flavonoid content using $AlCl_3$, and the total phenolic content was evaluated using Folin-Ciocalteu.

15. Antioxidant Activities of Microcapsules

The antioxidant activity of the formulated microcapsules was evaluated using the DPPH and ABTS radical scavenging assays. A 0.076 mM solution of DPPH was prepared by dissolving 0.003 g DPPH powder in 100 mL of methanol. The microcapsules and standard ascorbic acid were then double-fold serially diluted. One hundred microlitre (100 µL) of each dilution was then mixed with 100 µL of the DPPH

solution and incubated for 30 min. Absorbance was measured at 517 nm and the free radical scavenging activity was calculated and recorded as percentage inhibition.

The 2, 2´-azino-bis (3-ethylbenzthiazoline-6-sulphonic acid) was performed as previously described. Stable overnight ABTS solutions were adjusted using PBS pH 7.0 to an OD of (0.7 ± 1.0) at 734 nm. One hundred microliter of dilutions of extract and standard ascorbic acid solutions were then reacted with 100 µL of adjusted ABTS solution and allowed to stand in the dark for 10 min. The absorbance of the resulting solutions was measured at 734 nm. The free radical scavenging activity was calculated using the equation:

$$\%\text{Inhibition} = \frac{A_{cont} - A_{test}}{A_{cont}} \times 100$$

where A_{cont} is the absorbance of the negative control, A_{test} is the difference of the absorbance of samples and corresponding blank. The IC_{50} values were calculated from the regression line of percentage inhibition against concentrations.

16. Antimicrobial Activities of Microcapsules

The antimicrobial activities of encapsulated *E. camaldulensis* extracts were determined using the standard broth micro-dilution method. Bacterial culture (*B. cereus*, *L. monocytogenes*, and *S. aureus*) in the log phase were adjusted to 10^6 CFU/mL in MHB, and 100 µL was seeded into wells containing serially diluted microcapsules. The 96-well micro-titer plates were then incubated for 18 h at 37°C. Minimum inhibitory concentrations were recorded as the lowest concentration that completely inhibited the bacteria growth. The minimum bactericidal concentrations were determined using the spot plate technique by seeding 10 µL aliquots from wells without

growth on TSA. The plates were incubated at 37 ˚C for 24 h. The MBC values were recorded as the lowest concentrations that showed no growth on TSA plates. All experiments were set up in triplicates.

17. Cell Culture and Cytotoxicity

Human embryonic colon cells Caco-2 were cultured in high glucose DMEM supplemented with 10 % heat inactivated fetal bovine serum and 1 % Penicillin-Streptomycin. The cells were incubated at 37 ºC with 5% CO_2. Spent media was replaced after every 3 days until a confluent monolayer of cell was formed. Cells 1 x 10^4 cells/well was then transferred into 96-well micro titer plates and incubated overnight.

Toxicity of the microcapsules were evaluated on Caco-2 cells. Briefly, 10 mg of sterilized microcapsules were suspended in 10 mL of DMEM and incubated at 37 ºC. At time intervals (6, 12, 24, 48 and 72 h), 1 mL of eluent was withdrawn from each sample. Cells were then treated with 200 µL of eluent and incubated at 37 ºC with 5% CO_2. After 24 h incubation, cytotoxicity of the microcapsules was evaluated using MTT. Formazan crystals were dissolved with DMSO and OD was recorded at 570 nm. Cell viability was calculated as,

$$\% \text{ Cell viability } = \frac{\text{OD } Treatment}{\text{OD } Control} \times 100$$

Part III. Synthesis, Characterization, and Antibacterial Activities of Biogenic Silver Nanoparticles Using Ethanolic Extract of *Eucalyptus Camaldulensis* as Reducing and Capping Agent

1. Synthesis of Ag Nanoparticles

Leaves of *E. camaldulensis* were obtained as waste from paper industry and extracted by maceration with 95% ethanol. The extract was used for the synthesis of Ag nanoparticles as described previously (Mohammed, 2015). Briefly, 20 mg of the extract was mixed with 0.0216 mg of $AgNO_3$ in a conical flask containing 120 mL of deionized water. The mixture was left to stir for 40 min until the formation of a deep brown coloration. The Ag nanoparticles colloidal solution was then centrifuged and resuspended in equal volume of deionized water. The concentration of the Ag in the film forming solution was then measured using Inductively coupled plasma–optical emission spectrometry (ICP–OES), Avio500, Perkin Elmer, Waltham, MA, USA.

2. Characterization of Silver Nanoparticles

Preliminary confirmation of Silver nanoparticles synthesis was detected using UV–visible spectroscopy at a wavelength of 300–800 nm. TEM was performed to determine the morphology and size of synthesized Silver nanoparticles using transmission scanning microscopy, Hitachi, Tokyo, Japan. Zeta potential and particle sizes were also obtained using PALS–zeta potential analyzer by dynamic light scattering (DLS). Elemental composition of Silver nanoparticles was determined by energy dispersive X–ray spectroscopy (EDS)

3. Fourier Transform Infrared (FTIR)

Fourier transformed infrared spectroscopy (VERTEX 70, Bruker, Germany) was used to determine the interaction between functional groups during the synthesis.

4. Antimicrobial activities of Silver Nanoparticles

The antibacterial effects of the green synthesized Silver nanoparticles was determined using the standard broth microdilution method (CLSI, 2018). The MIC values were recorded as the lowest concentration that completely inhibited the bacteria growth, and the minimum bactericidal concentration (MBC) values as the lowest concentrations that showed no growth on tryptic soy agar (TSA) plates after incubation for 24 h. All the experiments were set up in triplicate for two independent studies. *E. coli* O157:H7, *L. monocytogenes* F2365, *S. aureus* ATCC 25923 and an isolate of *B. cereus* were used in the assay.

5. Evaluation of Potassium Ions Leakage from Bacterial Isolates

The membrane disruption activities of the biogenic silver nanoparticles were estimated by measuring the potassium ion concentration released from the bacterial pathogens into the surrounding medium. Exponential phase bacterial cultures were harvested at 4500 rpm for 5 min and resuspended into PBS (pH 7.4). The bacterial suspensions were treated with bactericidal concentrations of Silver nanoparticles and incubated for 4 h. Untreated bacterial suspensions were used as negative control. The bacterial suspensions were centrifuged at 8000 rpm for 10 min and the supernatant collected. The leakage of K+ ions from the cells was measured using inductively coupled plasma-optical emission spectroscopy (ICP-OES, Optima 8000, Perkin Elmer, MA, USA).

6. Effects of Silver Nanoparticles of Cell Membrane of Foodborne Pathogens

The effects of the Silver nanoparticles on the cell membrane of foodborne pathogenic bacterial isolates was investigated by scanning electron microscopy. Overnight bacterial cultures were harvested at 4500 rpm for 5 min and adjusted using a spectrophotometer to optical density of 0.2 at 600 nm. The cultures were treated with 4MIC of Silver nanoparticles and incubated at 37 °C for 2 h. The cells were washed with normal saline and aliquot spotted on a 1 cm^2 glass slide. Dried cells on glass slide were fixed in 3% (v/v) glutaraldehyde for 2 h and serially dehydrated using 20, 40, 60, 80, and 100% ethanol for 15 min each. Morphology of the bacterial cells was examined under a scanning electron microscope (Quanta 400 FEI, Oregon, USA).

Part IV. Fabrication of Antibacterial Chitosan-PVA Based Nanocomposite Food Packaging Functionalized with Biogenic Silver Nanoparticles

1. Materials

Low molecular weight (mol wt 50,000–190,000 Da based-on viscosity) 75–85% degree of deacetylation chitosan, $AgNO_3$ Reagentplus®, ≥ 99.0% (titration) and Poly (vinyl alcohol) were purchased from Sigma-Aldrich, Steinheim, Germany. Ethanol, acetic acid, ethylene tetrazolium bromide (3-(4,5-dimethyl-2-thiazolyl)-2,5-diphenyl-2H, MTT), and trypsin were obtained from Merck, Darmstadt, Germany, dulbecco's modified eagle medium (DMEM) and fetal bovine serum were purchased from Gibco, Paisley, UK, while glycerol was purchased from Thermo Fisher Scientific, Loughborough, UK. Gram–positive foodborne pathogenic bacteria including *S. aureus* ATCC 25923, *L. monocytogenes* F2365, and an isolate of *B. cereus* obtained from the culture collection at the Department of Microbiology, Prince of Songkla University as well as Gram–negative foodborne bacterium *E. coli* O157:H7 were used in the study.

2. Fabrication of PVA–Chitosan Film

The PVA–CH films were prepared following a previously reported method (Yaowen Liu, Wang, & Lan, 2018). Briefly, a 1% chitosan solution was prepared in 0.5% acetic acid. The solution was stirred at 1400 rpm at 60 ºC until the chitosan was completely dissolved. A 5% solution of PVA was then prepared in ultra–pure water at 90 ºC and 400 rpm. PVA–CH copolymer film was formed by mixing the chitosan and PVA solutions in a ratio of 3:1 (v/v). The films were produced by casting on a Teflon plate (11.5 ×11.5 cm) using 0.75% glycerol as a plasticizer. PVA–CH/Ag nanoparticles films were synthesized by mixing PVA–CH solution and colloidal Ag nanoparticles solution at different ratios 1:1, 1.5:0.5, and 1.75:0.25.

3. Characterization of Films

The green synthesized Ag nanoparticles, PVA–CH, and PVA–CH/Ag nanoparticles film forming solution were analyzed using the UV visible spectroscopy to detect the presence of Ag nanoparticles. The mixtures were scanned at wavelengths of 300–800 nm using a Multi–mode plate reader, Perkin Elmer.

4. ATR Fourier Transform Infrared Spectroscopy

Chemical structures of the PVA–CH and PVA–CH/Ag nanoparticles composite films were analyzed by attenuated total reflectance Fourier-transform infrared (ATR–FTIR) spectrometry with resolution of 4 cm^{-1}, aperture setting of 6 mm, scanner velocity of 2.2 kHz, background scan time of 32 s, sample scan time of 32 s, and 100 total scans per sample. The spectral were obtained in a Fourier transform infrared spectrometer, VERTEX 70, Bruker, Ettlingen, Germany.

5. X–ray Diffraction

XRD pattern of the films were obtained using an X–ray diffractometer WI–RES–XRD EMPYREAN–001 (Empyrean, PANalytical, Almelo, Netherlands) with a reference target of Cu Kα radiation (the weighted average $\lambda = 0.15406$ nm) voltage of 40 kV, current of 30 mA. The films were measured at an angle from 1.5° to 90° (2θ) with steps of 0.026° (2θ)/min at 70.125 sec/step.

6. Thermal Analysis

The thermal stability of the films was monitored using a thermogravimetric analyzer, differential scanning calorimetry and differential thermal analyzer. The film samples (10 mg) were heated in 100 μL ceramic pans from ambient temperature to 900 ºC under a nitrogen atmosphere at a rate of 10 ºC/min using TGA7, Perkin Elmer.

Differential scanning calorimeter DSC 7, Perkin Elmer, was also used to obtain the glass transition (Tg), melting temperatures (Tm) and the enthalpy (ΔHm) of the films, between 25–220 ºC with 10 ºC/min heating. The analysis was done in triplicate for all samples. Furthermore, the films were subjected to DTA using DTA 7 Analyzer, Perkin Elmer. The samples were scanned at heat range of 50–400 ºC at 10 ºC/min in a nitrogen environment.

7. Mechanical and Physical Properties of Film

The thickness of films was measured in 5 replicates with a digital micrometer (0.01 mm) (Mitutoyo Manufacturing Co. Ltd., Tokyo, Japan), and average values were calculated. elongation at break (EAB) were measured according to ASTM D412 (Khalaf, El Nashar, Helaly, & Soliman, 2018) using a tensile testing machine (Zwick GmbH & Co. KG, Ulm, Baden-Württemberg, Germany),with measurement range of 0.002–20 mm. Five dumbbell shaped samples of 115 mm length and 20 mm width were analysed for each film. Films were mounted on the film extension grip at an initial grip distance of 50 mm and crosshead speed was 50 mm/min. Tensile strength, elongation at break, and Young's modulus were obtained from the testXpert® II software version 3.31.

8. Transmittance and Transparency

The transmittance of the samples was measured at 600 nm, using UV-vis spectroscopy (F300s Ultraviolet lamp, Shimadu, Tokyo, Japan), and transparency was calculated (Roy, Shankar, & Rhim, 2019).

$$\text{Transparency} = \log(\frac{T_{600}}{t})$$

where T_{600} is the transmission at 600 nm, and t is the film thickness in (mm).

True density was determined using the gas displacement method with a true density analyser, AccuPyc II 1340, Micromeritics, Norcross, GA, USA. Four measurements were taken for each film and the mean values ± SD were obtained.

The viscosity of the film forming solutions were measured using a digital viscometer, model LVDV–I Prime, Brookfield, Middleboro, MA, USA. Spindle number S00 was used for the determination at a speed of 12 rpm for PVA–CH and PVA–CH/Ag nanoparticles (1.75:0.25), 20 rpm for PVA–CH/Ag nanoparticles (1.5:0.5), and 30 rpm for PVA–CH/Ag nanoparticles (1:1).

9. Water Vapour Permeability

Water vapour permeability of the films was measured as previously reported (Nilsuwan, Benjakul, & Prodpran, 2018), with slight modifications. Briefly, aluminium permeation cup of diameter (5 cm) containing 20 g of dried silica gel (0% RH) were used for the analysis. The cups were placed in an environmental chamber at 25 ± 0.5 °C and 50 ± 5% RH. The cups were weighed at 1 h interval using an analytical balance (Mettler Toledo ME403), and experiment proceeded for 48 h. WVP of the film was calculated as follows:

$$WVP = wdA^{-1}t^{-1}(\Delta P)^{-1}$$

where w is the weight gain of the cup (g); d is the average film thickness (m); A is the exposed area of film (m^2); t is the time of gain (s); P_2–P_1 is the vapor pressure difference across the film in mmHg.

10. Moisture Content and Swelling Degree

Moisture content (MC) of the films were measured as described previously (Hanani, Yee, & Nor-Khaizura, 2019) and calculated following the equation;

$$\mathrm{MC}(\%) = 100 \times (\mathrm{M_{initial}} - \mathrm{M_{final}})/\mathrm{M_{initial}}$$

where $M_{initial}$ is the initial film weight (g) and M_{final} is the final weight of films dried at 105 ºC (g). Samples were measured in triplicate.

The degree of water uptake by the films was measured using the immersion assay. Samples of known weight were submerged in deionized water (pH 7.0) for 24 h at ambient temperature. The films were removed and blotted with a filter paper to remove the excess liquid and was weighted immediately. The percentage of a water adsorption (WSW) was calculated from the equation:

$$DS = [(W_s - W_d)/W_d] \times 100$$

Where DS is the degree of swelling, W_s is the weight of swollen film, and W_d is the initial weight of dried film.

11. Contact Angle Measurement

The contact angles and surface energy of the samples were measured by the sessile drop method using a contact angle meter, OCA 15 EC, GmbH, Raiffeisenstraße, Filderstadt, Germany. Deionized water, ethylene glycol, Fisher scientific, and formamide, Polysciences, Warrington, US were used as probe liquid. Four measurements were taken, and the values were obtained as mean ± SD.

12. Atomic Force Microscopy (AFM)

The surface of films was analyzed using AFM (Atomic Force Microscopy, Solver next, NT-MDT, Moscow, Russia). Two and three-dimensional images of the film surface area (50 × 50 μm) were obtained in each test. The roughness parameters were measured as mean roughness (Ra) and root–mean–square roughness (Rq).

13. Antimicrobial Activity of Films

The samples were tested for antibacterial activities against Gram–positive and Gram–negative foodborne pathogenic bacteria including *L. monocytogenes* F2365, *S. aureus* ATCC 25923, an isolate of *B. cereus* and *E. coli* O157:H7. The bacteria cultures were incubated at 37 ºC for 12 h in Muller hinton broth (MHB) Difco, Le pont de claix, France and adjusted to 10^6 CFU/mL before use. The method of (López de Dicastillo et al., 2011) was adopted in a 24 well plate with slight modifications using 0.05 g of films (2 × 2 cm to 3.5 × 3.5 cm) in 1.5 mL of bacterial suspension. The plates were incubated statically at 37 ºC, and aliquot of samples were withdrawn at 2, 6, 12, and 24 h and bacterial growth was measured.

14. Antioxidant Activity of PVA–CH and PVA–CH/Ag Nanoparticles Films

The antioxidant activity of the samples were measured using the DPPH and ABTS assays as previously described (Kaya et al., 2018; J. Wu et al., 2018). Samples weighing 0.05 g were placed in a tube, and 1 mL of a 0.15 mM solution of DPPH, Sigma Aldrich was added to each tube. The tubes were vortexed for 1 min and incubated at ambient temperature in the dark for 30 min. Two hundred microlitre (200 µL) of the resultant solution was then transferred to a 96–well plate and the OD measured at 517 nm.

For the ABTS assay, 0.05 g piece of respective films was placed in a tube and 1 mL of the adjusted $ABTS^+$ solution (Sigma Aldrich) was added to the tubes. The tubes were then vortexed and allowed to stand for 6 min. The absorbance of the resultant solution were measured spectrophotometrically at 734 nm.

The experiments were done in triplicate and the percentage inhibition I(%) for both assays were obtained using the formula

$$I(\%) = \frac{A_{control} - A_{sample}}{A_{control}} \times 100$$

where $A_{control}$ is the absorbance of the DPPH or ABTS solution and A_{sample} is the absorbance of the reduced free radical solution.

The scavenging activities of the $DPPH^{\bullet}$ and $ABTS^{\bullet+}$ radicals were expressed as ascorbic acid concentration, using a calibrated curve of ascorbic acid concentration versus I (%) (López de Dicastillo et al., 2011).

15. Effects of Films on The Shelf–Life of Chicken Sausage

The shelf life extension effects of the films were monitored on sausage slice as described (Fasihi et al., 2019). Commercial sausage was purchased from a local supermarket in Hat Yai, Thailand and were de–filmed. The sausage was cut into pieces of 2 g and aseptically wrapped with films previously sterilized under a UV. All the packaged slices of sausage were incubated at 20 ºC and studied on days 3, 7, and 15 for visual signs of spoilage. For each sample, three replications were prepared. The control sample consisted of sausage packed in PVA–CH films without Ag nanoparticles and unwrapped sausage.

16. *In vitro* Ag release assay

The release of Ag nanoparticles from the films was evaluated. Briefly, 100 mg of sample was dispersed in 20 mL buffer solution and incubated at 25 °C with continuous shaking. At time interval, 2 mL of sample was withdrawn and replaced with same volume of fresh buffer. The Ag nanoparticles content was measured by inductively coupling plasma optical emission spectrometer (ICP-OES). The total Ag

nanoparticles concentration in the film samples was also determined by digesting 100 mg of samples in 20 mL of solvent. *In vitro* release data were fitted into various kinetic models like zero-order, first order, Higuchi, and Korsmeyer-Peppa's, equation and coefficient of correlation (r) values were calculated for linear curves by regression analysis of the plots.

17. Toxicity of Ag nanoparticles composite films

Toxicity of the PVA–CH/Ag nanoparticles composite films was evaluated on human colon cell Caco-2. The cells were cultured in high glucose Dulbecco's Modified Eagle Medium (DMEM) supplemented with 10% fetal bovine serum and 1% penicillin−streptomycin solution, Gibco. Approximately, 4×10^4 cells/mL of Caco-2 was seeded in 24–well plates and incubated at 37 °C with 5% CO_2 atmosphere for 48 h. The cells were then treated with 1 mL of eluent from 1 and 5 mg/mL of samples released in DMEM and incubated for 24 h. The viability of cells after treatment was analyzed using MTT assay and the OD was measured at 570 nm.

$$\% \text{ Cell viability } = \frac{OD\ Treatment}{OD\ Control} \times 100$$

Part V. Fabrication of Nanocomposite Food Packaging from Recycled Wastepaper and Functionalization with Biogenic Silver Nanoparticles

1. Wastepaper Recycling and Nanocomposite Paper Fabrication

Waste papers of weight 4.45–5.00 g, were sterilized under UV. The paper was then blended into pulp in 500 mL of distilled water using an Electrolux blender Model No. ESTM54175, China with 0.4% starch Sigma Aldrich, Singapore added as binder. The nanocomposite paper was fabricated by blending in 400 mL of distilled water and 100 mL of colloidal Silver nanoparticles solution. The mixtures were heated in a microwave for 5 min at a temperature of 80–90 ºC. Afterwards, 250 mL portion of each mixture was casted on a tray covered with muslin cloth in a 19.5 × 28 cm frame. The casted pulp was left to drain water and was then transferred to an oven (70 ºC) to dry for 6 h.

The fabricated nano composite paper and blank were characterized for physicochemical, mechanical, structural, and functional properties using various techniques as described below.

2. Fourier Transformed Infrared Spectroscopy (FTIR)

Chemical structures of the recycled nanocomposite paper and blank control paper were analyzed by attenuated total reflectance Fourier-transform infrared (ATR–FTIR) spectrometry with resolution of 4 cm^{-1}, aperture setting of 6 mm and scanner velocity of 2.2 kHz. The spectral were acquired at 4000–500 cm^{-1} by Bruker 66 spectrometer (Germany).

3. X–ray Diffraction (XRD)

The X–Ray diffraction pattern of the samples were obtained with a reference target of Cu Kα radiation (the weighted average λ = 0.15406 nm) voltage of 40 kV, current of 30 mA. The samples were measured at an angle of 2θ with steps of 0.026º (2θ)/min at time 70.125 sec/step using (Empyrean, PANalytical, Netherlands).

4. Scanning Electron Microscope (SEM) and Energy Dispersive X–ray (EDS)

The morphology of synthesized Silver nanoparticles paper and blank recycled paper were examined by Field emission scanning electron microscopy (SEM, Quanta 250 SEM–FEI, FEI/Thermo Fisher Scientific, USA). Piece of sample was mounted on an aluminum stub and sputter–coated with gold. The elemental compositions of the samples were also obtained by EDS analysis (EDS, JEOL, JSM-6010LA). In addition, mapping for the distribution of elemental components was done using EDS technique.

5. Thickness and Tensile Strength

Nano composite paper thickness was measured by a digital micrometer (Mitutoyo Manufacturing Co. Ltd., Tokyo, Japan) and recorded as mean value in micrometer (mm) ± SD. The tensile strength (TS), and percentage elongation at break (EAB) were evaluated using tensile testing machine, Zwick Roell Germany (Z010). Five samples were analyzed for each film. Tensile strength, elongation at break, and Young's modulus were obtained from the testXpert® II software version 3.31

6. Grammage and Bulk Density Analysis

Synthesized Silver nanoparticles and blank recycled paper were cut into 10 cm x 10 cm and weighed using an analytical balance to give the response in g/m^2. The bulk

density of the samples were calculated according to ISO 534 from the ratio between the grammage and thickness (Battisti et al., 2017).

7. Water Absorption

Water absorption capacity of the recycled silver nanoparticles paper and blank control was determined after 24 h immersion in water using 2×2 cm^2 piece of each sample. The initial dry weight (M_{dry}) of the samples was recorded, afterward the samples were placed in a petri dish containing 10 mL of distilled water. After 24 h, the excessive water was wiped off with blotting paper. The wet dry weight (M_{wet}) of the samples were measured and the water absorption capacity was calculated and recoded in (g/m^2).

$$WA\ (\%)\ = \frac{[Mwet - Mdry]}{Mwet} \times 100$$

8. UV-Visible Spectroscopy

The nano composite and blank control paper were characterized by UV-visible spectroscopy analysis. The absorbance and percentage reflectance from synthesized Silver nanoparticles papers and blank were measured for wavelengths between 200–1800 nm using a UV–vis spectroscopy (F300s Ultraviolet lamp, Shimadu, Tokyo).

9. Silver Release and Migration in Food

To study the migration of silver from synthesized Silver nanoparticles paper into the meat, the papers were cut into circles of diameter 5 cm. Then, 5 g of minced meat was weighed into a petri-dish of diameter (5 cm) and flattened to form a bed with uniform surface. Synthesized silver nanoparticles paper was placed on the surface of the meat such that the entire surface was in contact with the meat. The paper surface was damped with 500 µL of distilled water to act as a mobilizer and plates were stored

at refrigerator temperature 4–7 °C. At 0, 12, 24, and 48 paper samples were carefully removed from the meat surface and analyzed for silver content using Inductively coupled plasma–optical emission spectrometry (ICP–OES). The concentration of silver that has migrated into the meat was calculated as the difference between the paper silver content at a given time and the silver content at time 0 h.

10. Mathematical Models

To further study the pattern of Ag release from the recycle silver nanoparticles paper, the *In vitro* release data were fitted into various kinetic models like zero-order, first order, Higuchi, and Korsmeyer-Peppa's, equation and coefficient of correlation (r) values were calculated for linear curves by regression analysis of the plots.

11. *In vitro* Antimicrobial Activities of Active Paper

The nanocomposite paper and blank were tested for antibacterial activities against important Gram-positive and Gram-negative foodborne pathogenic bacteria including *L. monocytogenes* F2365, *S. aureus* ATCC 25923, an isolate of *B. cereus* and *E. coli* O157.H7. The bacterial cultures were incubated at 37 ºC overnight in Muller Hinton broth (MHB). The culture was harvested and adjusted to 10^6 CFU/mL before use. The method of (López de Dicastillo et al., 2011) was adopted in a 24 well plate with slight modifications using piece of paper (3 cm^2) in 1.5 mL of bacterial suspension. The plates were incubated statically at 37 ºC, and aliquot of samples were withdrawn, plated out on TSA and counted at 3, 6, 12, and 24 h. Samples were also prepared for OD measurement at each of the test time. OD values were recorded at 600 nm and change in bacterial population as ΔCFU/mL.

12. Antibacterial Testing (ISO 20743)

The survival of bacterial isolates in contact with synthesized Silver nanoparticles packaging paper was evaluated using a modified method from ISO 20743. The test bacterial isolates and strain were maintained in tryptic soy broth to exponential growth phase and used for the testing. Briefly, the cultures were diluted in TSB to 1.5 x 10^8 CFU/mL. Then 50 µL of the diluted bacterial suspension was loaded onto synthesized Silver nanoparticles paper and blank control. The test papers were left damp and then incubated in a humid condition for 24 h. Afterwards, the surviving bacterial on the papers were enumerated in 1 mL of neutralizer solution and serial dilution using saline solution. Aliquot (10 µL) of the dilutions were spot plated on TSA and incubated overnight at 37 °C. Bacterial colonies were then counted and recorded as CFU/mL.

13. Cytotoxicity of Silver Nanoparticles Packaging Paper

Synthesized Silver nanoparticles paper was evaluated for toxicity using HEK293T and Caco–2 human cell lines as described (Jiang et al., 2018) with modifications. The cells were collected from the Department of Physiology, Prince of Songkla University and cultured in high glucose Dulbecco's Modified Eagle Medium (DMEM) (Gibco, Thermo Fisher Scientific, China) supplemented with 10% fetal bovine serum (FBS) and 1% penicillin−streptomycin solution. Approximately 1 × 10^4 cells were seeded in 96–well plates (100 µL/well) and incubated at 37 °C in an incubator humidified with 5% CO_2 atmosphere for 24 h. The medium was removed, and the cells were washed twice with phosphate buffer solution. The cells were exposed to 100 µL of medium containing Silver nanoparticles released from the packaging material at different time intervals (12, 24, and 48 h). Release media from blank paper and fresh

media were used as control. The cells were then incubated for 24 h in a CO_2 incubator at 37 °C. Cell viability after exposure to treatment, blank and control was analyzed using MTT assay Briefly, 10 µL of 5 mg/mL MTT solution in PBS buffer and 100 µL of DMEM was added to each well and incubated in the dark for 4 h. The absorbance (optical density) value of the wells was measured at a wavelength of 570 nm using a multi-mode plate reader Enspire. The percentage cell viability was then calculated as

$$\frac{\text{OD } Treatment}{\text{OD } Control} \times 100$$

CHAPTER 3

RESULTS AND DISCUSSION

Part I. Antimicrobial and Antioxidant Activities of *Eucalyptus camaldulensis* Ethanolic Extract and Effects on *Listeria monocytogenes* Virulence, Attachment, and Biofilm Formation.

1. Antibacterial Effects of *Eucalyptus camaldulensis* on *Listeria monocytogenes*

This study presents the antibacterial effects of *E. camaldulensis* leaf extract on recalcitrant foodborne pathogenic *L. monocytogenes*. The results revealed good antilisterial effects with MIC ranging from 64 to 128 µg/mL and MBC of 256 to 512 µg/mL for all the tested isolates (Table 3). In contrast, the antilisterial activities of sodium nitrite and sodium benzoate used commercially as food preservatives were relatively high, with MIC values of 8 to 32 mg/mL and 32 to 64 mg/mL, respectively, with MBC higher than 128 mg/mL. The antibacterial activity of these plants reflects the abundance of active phytochemicals such as polyphenols (Ishnava, Chauhan, & Barad, 2013). Microbial growth during food storage is a major cause of food spoilage (Petruzzi, Corbo, Sinigaglia, & Bevilacqua, 2017). Thus, application of antimicrobial extracts of *E. camaldulensis* as a natural preservative agent will retard spoilage, extend shelf-life, and improve food quality and safety. Plants from the family Myrtaceae, such as *Rhodomyrtus tomentosa* (Odedina *et al.,* 2015), *Myrtus communis* (Amensour *et al.*, 2010), and *Psidium guajava* (Olatunde *et al.*, 2018) have been reported to exhibit antilisterial activities. The antibacterial activities of essential oil (Ghaffar *et al.,* 2015) and flavonoid compounds (Takahashi *et al.,* 2004) from *Eucalyptus* leaf have been

previous reported. Ethanolic extracts of *E. camaldulensis* leaf exhibited antimicrobial activity against *S. aureus* (Nasr *et al.,* 2018).

Table 3. Antibacterial activity of *Eucalyptus camaldulensis* ethanolic leaf extract on *Listeria monocytogenes*

Source of *L. monocytogenes*	**Extract (µg/mL)**		**Sodium nitrite (mg/mL)**		**Sodium benzoate (mg/mL)**	
	MIC	**MBC**	**MIC**	**MBC**	**MIC**	**MBC**
Food processing environment (n=9)	64 - 128	256 - 512	16	>128	32 - 64	>128
Ready-to-eat food (n=10)	64 - 128	256 - 512	8 - 32	>128	32 - 64	>128
F2365 (reference strain)	128	256	16	>128	32	>128

2. Time-Kill Kinetic of *Eucalyptus camaldulensis* on *Listeria monocytogenes*

The time-dependent killing activity of the *E. camaldulensis* against representative isolates from the food-processing environment (PSU-KV-032), ready-to-eat food (PSU-KV-120), and strain F2365 were demonstrated (Figure 2). Time-kill assay revealed growth inhibitory effects after 4 h treatment of the bacteria with the extract. Approximately 2 to 3-log reduction in CFU/mL against all the tested food and environmental isolates was observed after challenging the pathogen with the extract at MIC for 6 and 8 h. The results suggested that the extract at MIC, 2MIC, and 4MIC were bactericidal to the test organisms, but at 1/2MIC, a bacteriostatic effect was observed. The effects of the extract on *L. monocytogenes* were both concentration and time dependent.

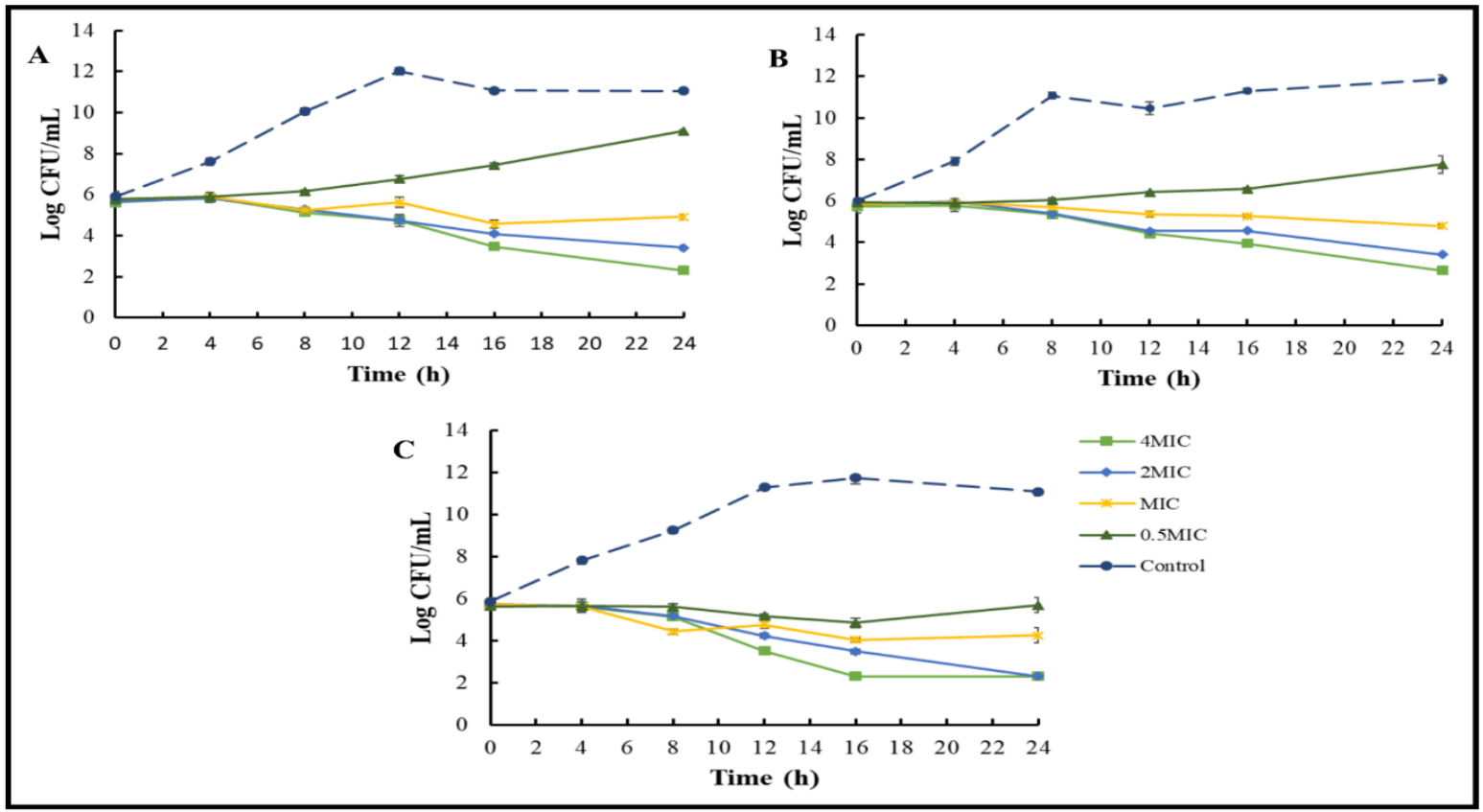

Figure 2. Time-kill curve of *Eucalyptus camaldulensis* extract *on Listeria monocytogenes* isolates (A) PSU-KV-032, (B) PSU-KV-120 and (C) strain F2365 at 37 °C. The experiments were performed in triplicate and recorded as Mean ± SD.

3. Effects of *Eucalyptus camaldulensis* Ethanolic Extract on Swarming Motility of *Listeria monocytogenes*

L. monocytogenes exhibits a thermo-sensitive swarming motility mediated by the production of five to six peritrichous flagella (O'Neil & Marquis, 2006). These flagella consist of thousands of flagellin monomers that are modified by β-O-linked glycosylation (Schirm *et al.,* 2004). Flagella formation and motility are thought to be responsible for *L. monocytogenes* biofilm formation and persistence within the food environment (Lemon, Higgins, & Kolter, 2007). However, in contrast, (Cabrita, Trigo, Ferreira, & Brito, 2015) noted that motility was not a critical feature for *L. monocytogenes* persistence in the food environment. The motility of *L. monocytogenes* isolates and the motility inhibitory effects of inhibitory and sub-inhibitory concentrations of the extract on significantly motile isolates at 30 ˚C, are presented (Figures 3 A and B). The results revealed a reduction in motility for most tested isolates. In addition, the tested concentrations significantly reduced the swarming motility of *L. monocytogenes* ($p<0.05$), except 1/4MIC and 1/8MIC that showed no significant difference on isolate PSU-KV-116 ($p<0.05$). The mechanism of *Listeria* motility inhibition by plant extracts and phenolic compounds is still unknown (Vazquez-Armenta *et al.,* 2018). However, scanning electron microscopy revealed a loss of *L. monocytogenes* flagella corresponding to loss of motility and membrane damage at sub-lethal doses of olive leaf extract (Yanhong Liu, McKeever, & Malik, 2017). A downregulation of flagellin encoding gene (fliC) accompanied by loss of motility was reported in *Escherichia coli* after treatment with cranberry extract (Hidalgo, Chan, & Tufenkji, 2011)

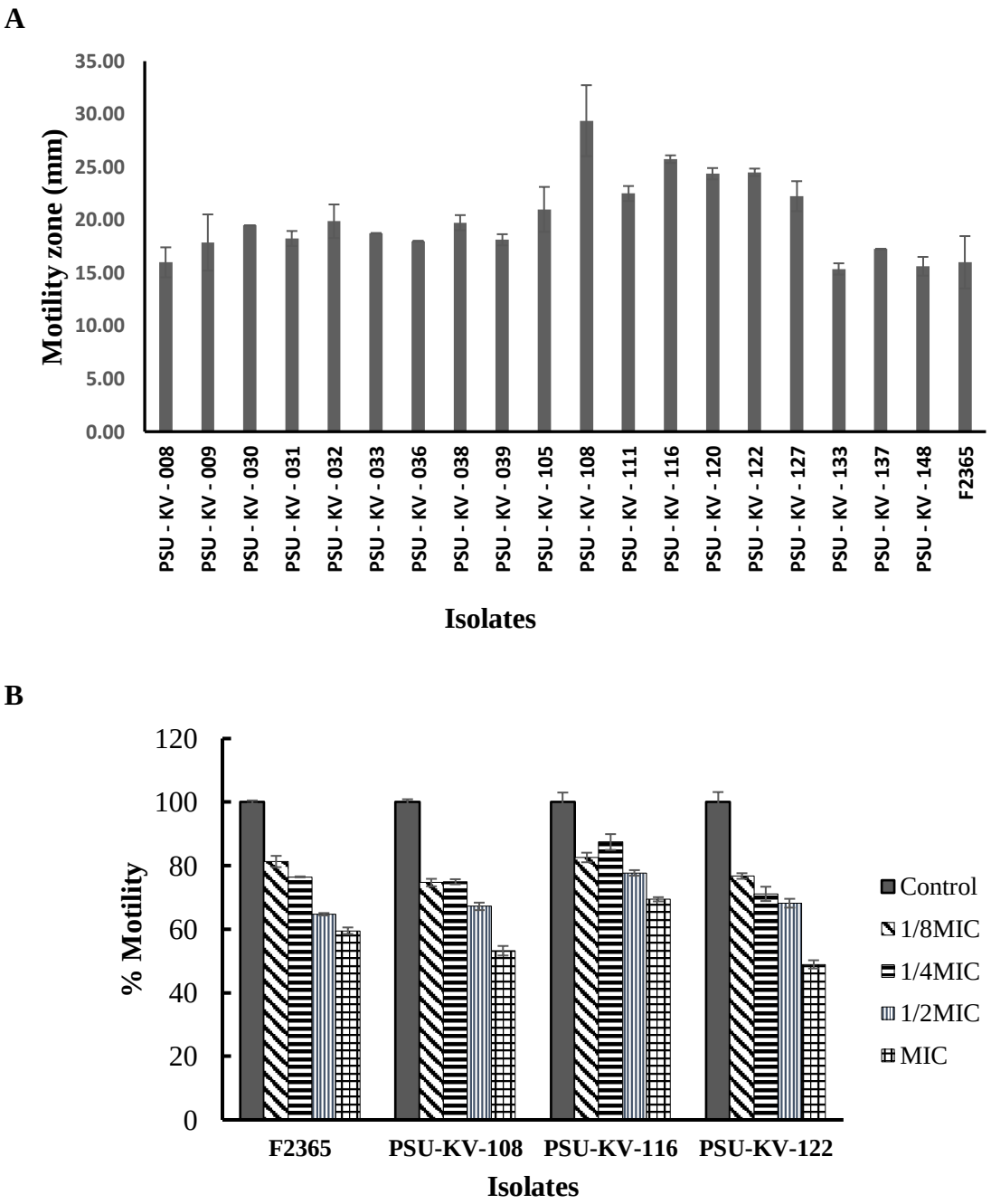

Figure 3. *L. monocytogenes* motility (A) and motility inhibitory effects of *E. camaldulensis* extracts at 30 °C (B). Result indicates values of the means % motility ± SD for two independent experiments performed in triplicate *Significant difference between treatment and control at ($p \leq 0.05$).

4. Inhibition of *L. monocytogenes* Attachment

Microbial attachment and adhesion to biotic and abiotic surfaces is a critical step mediated by cell-surface components or appendages generally known as adhesins. Attachment to surfaces represent the initial step in the process of biofilm formation, thus effective inhibition of bacterial attachment to contact surfaces in an important target in the control and eradication of biofilms. The effects of ethanolic leaf extract of *E. camaldulensis* towards the attachment of *L. monocytogenes* to model food contact material is presented in (Figure 4). The assay was conducted at the bacterial lag phase (2 and 4 h) and at the onset of exponential phase (6 h). The result showed a significant difference ($p < 0.05$) between treated and control at both lag phase and early exponential phase, suggesting that the observed difference was independent of growth inhibition. The anti-adhesion effects of natural products such as plant and microbial extracts have been previously reported (Klančnik et al., 2018; Mahyudin et al., 2018; Vazquez-Armenta et al., 2018). Natural products might inhibit adhesion of bacterial by interfering with cell surface properties and inactivation of adhesins.

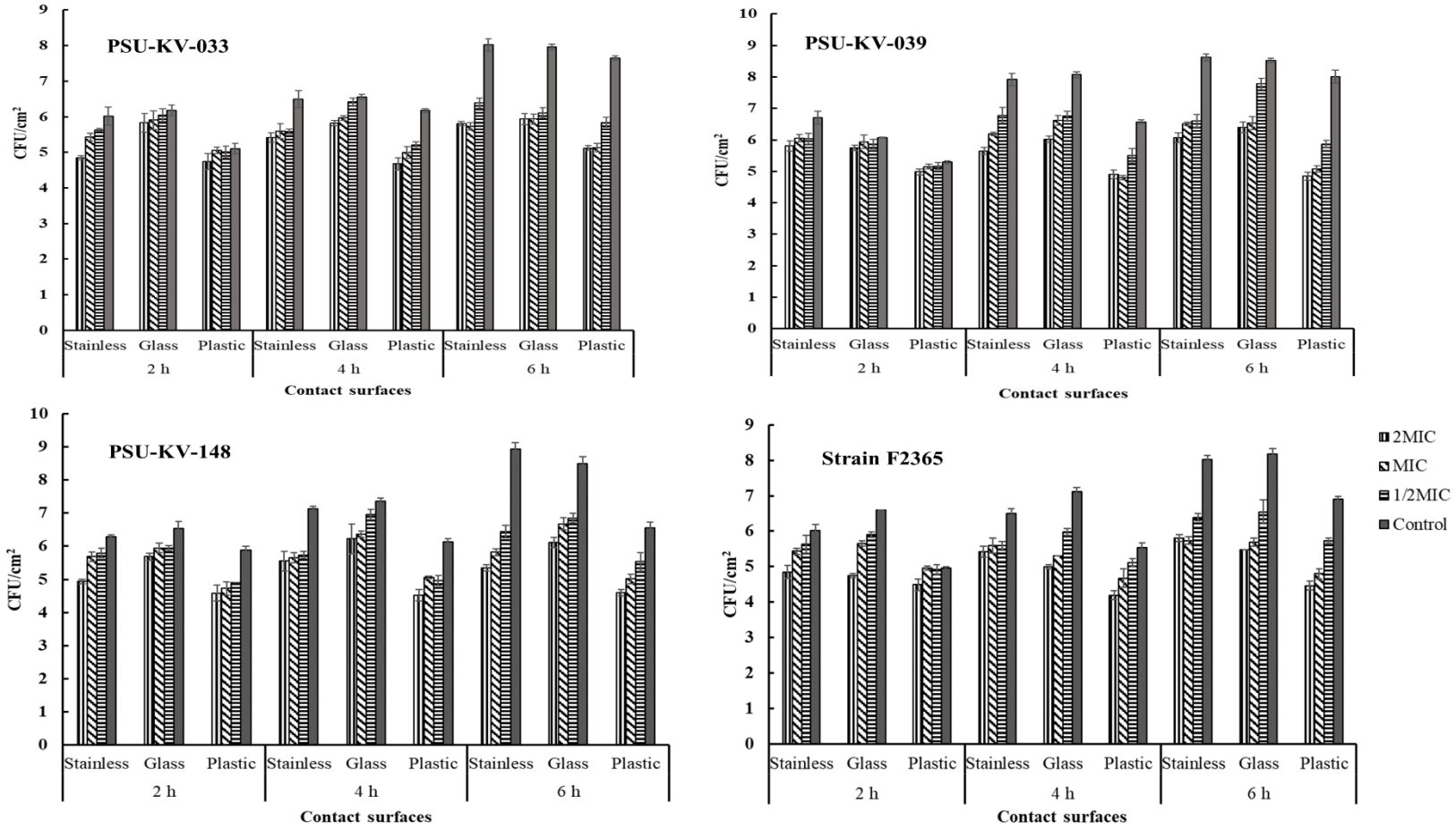

Figure 4. Effects of *Eucalyptus camaldulensis* extracts on *L. monocytogenes* attachment to food contact surfaces

5. Effects of *Eucalyptus camaldulensis* Ethanolic Extract on *Listeria monocytogenes* Biofilm Formation

Biofilm formation is an important microbial survival strategy. This sessile form of existence constitutes a food safety problem and serves as a source of recontamination of processed and finished products. Thus, biofilm inhibitory effect of sub-lethal concentrations of *E. camaldulensis* was further determined (Figure 5B). The results demonstrated that 1/2MIC and 1/4MIC inhibited biofilm formation, without growth inhibition. At 1/4MIC, biofilm formation for food isolate PSU-KV-148 and strain F2365 were significantly inhibited ($p<0.05$). In contrast, no significant effect on isolates PSU-KV-033 and PSU-KV-039 was observed ($p<0.05$). Previous researchers have suggested a correlation between flagella production, bacterial attachment, and biofilm formation (Gorski, Duhé, & Flaherty, 2009; Lemon et al., 2007). However, we observed that biofilm formation was higher at 37 ˚C than 30 ˚C, (motility temperature) (Figure 5A). In addition, highly motile isolates did not produce a corresponding higher amount of biofilm. The molecular mechanism governing biofilm production in *L. monocytogenes* remains uncertain (Schirm *et al*., 2004). However, population density dependent cell-cell communication (quorum sensing) is thought to regulate biofilm formation (Rutherford & Bassler, 2012). Plant phytochemical such as polyphenols and flavonoids inhibits biofilm by modulating bacterial cell-cell communication (Vikram, Jayaprakasha, Jesudhasan, Pillai, & Patil, 2010), interfering with surface charge, hydrophobicity and motility (Monte, Abreu, Borges, Simões, & Simões, 2014), and down regulation of genes required for biofilm formation (Kim et al., 2016)

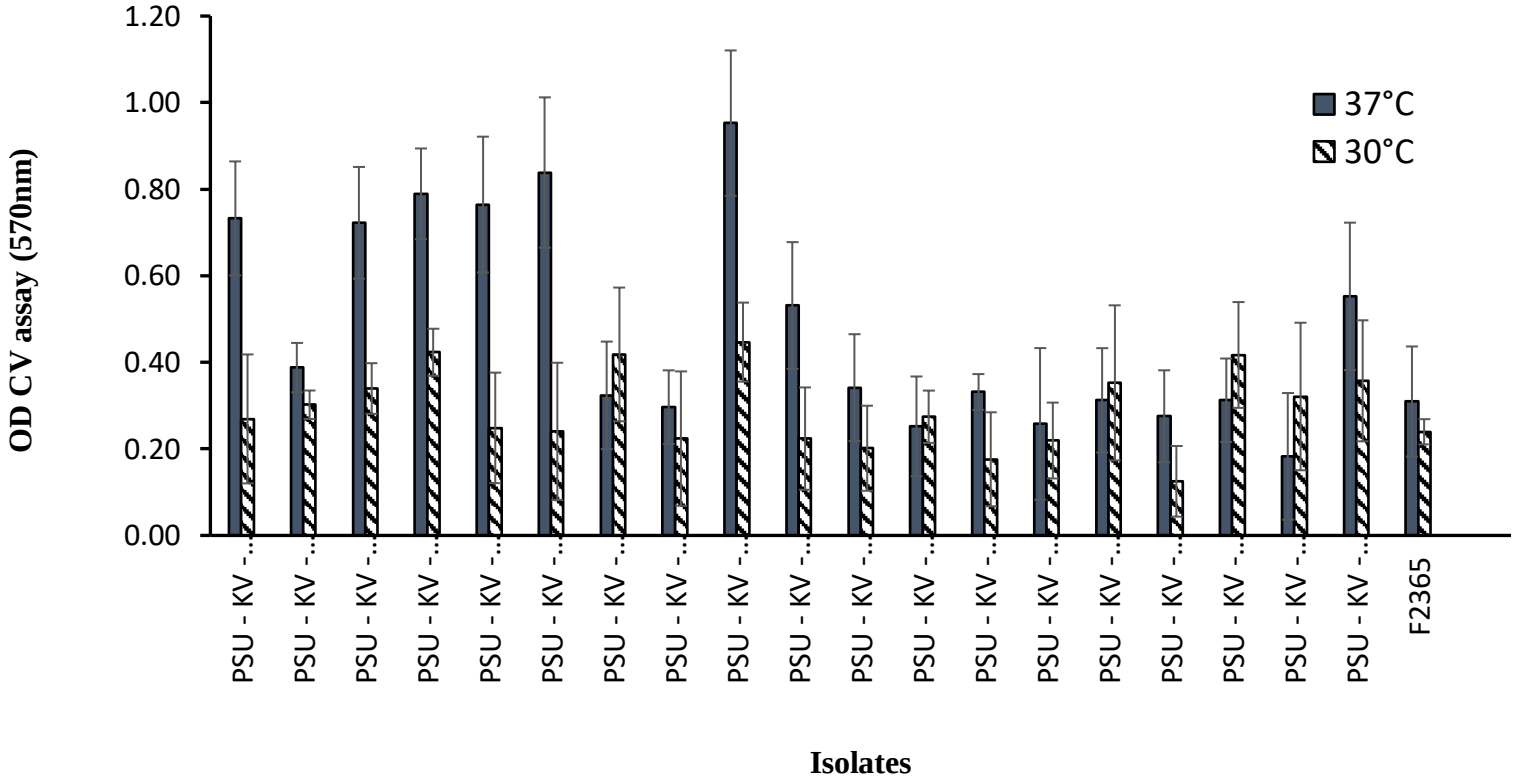

Figure 5A. Listerial biofilm formation at 30 °C and 37 °C on polyester 96-well microtiter plate

A

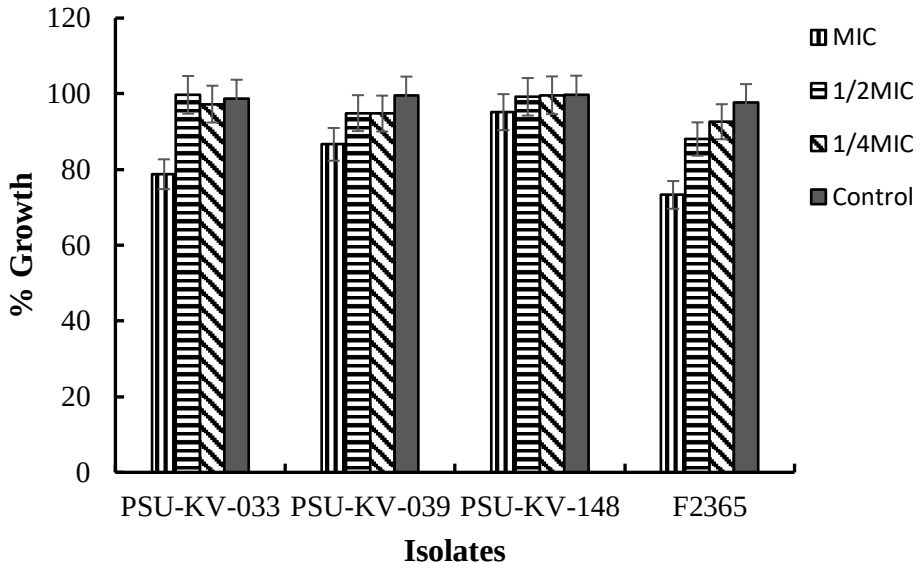

B

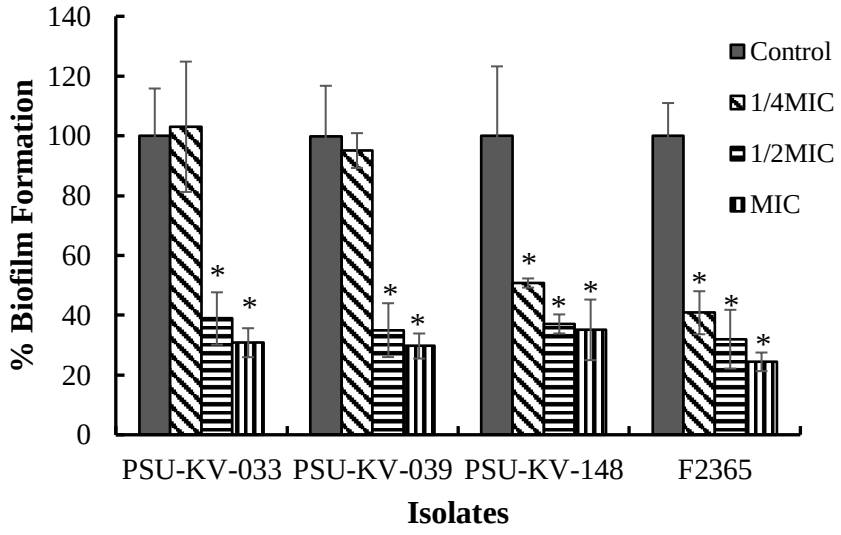

Figure 5B. Effect of *E. camaldulensis* extract on growth of listeria (A), and biofilm inhibitory effects of sub-inhibitory concentrations of *E. camaldulensis* determined by crystal violet assay (B). Untreated TSBYE cultures were maintained as negative control. Values indicates the means ± SD for three independent experiments performed in triplicate *Significant difference between treatment and control at ($p \leq 0.05$).

6. Effects of *E. camaldulensis* Ethanolic Leaf Extract on *L. monocytogenes* Biofilm Formation on Food Contact Surfaces

Biofilm formation on food contact surfaces presents a serious challenge to food industrialist as well as food safety. Formation of biofilm on food contact surface results to impaired heat transfer and contamination of finished products resulting in a compromise of food quality. In addition, microbial influenced corrosion resulting in pitting of stainless-steel amounts to huge economic lost to food processing scientist and technicians. Thus, inhibition of biofilm is an import aspect of food safety and quality control that can help prevent contamination of food and outbreaks of foodborne diseases. The twenty-four hours biofilm inhibitory effects of the extract were evaluated on food contact surfaces using crystal violet assay as well as by counting the number of viable biofilm cells in CFU/mL. The results revealed a concentration dependent biofilm inhibitory effects on all food contact surfaces. In addition, results of crystal violet assay suggested that biofilm formation was more on stainless steel and glass compared with plastic (Figure 6). This might be due to the surface characteristics such as hydrophobicity, roughness, as well as surface charges. Similarly, 24 h count of viable biofilm cells revealed a significant reduction ($p<0.05$) in the number of viable biofilm cells (Figure 7). The anti-biofilm inhibitory activity of various plant derived compounds have been reported. Extracts of *Salvia officinalis* was reported to mitigate microbial influenced corrosion of 304L stainless steel mediated by *Pseudomonas aeruginosa* (Lekbach et al., 2019).

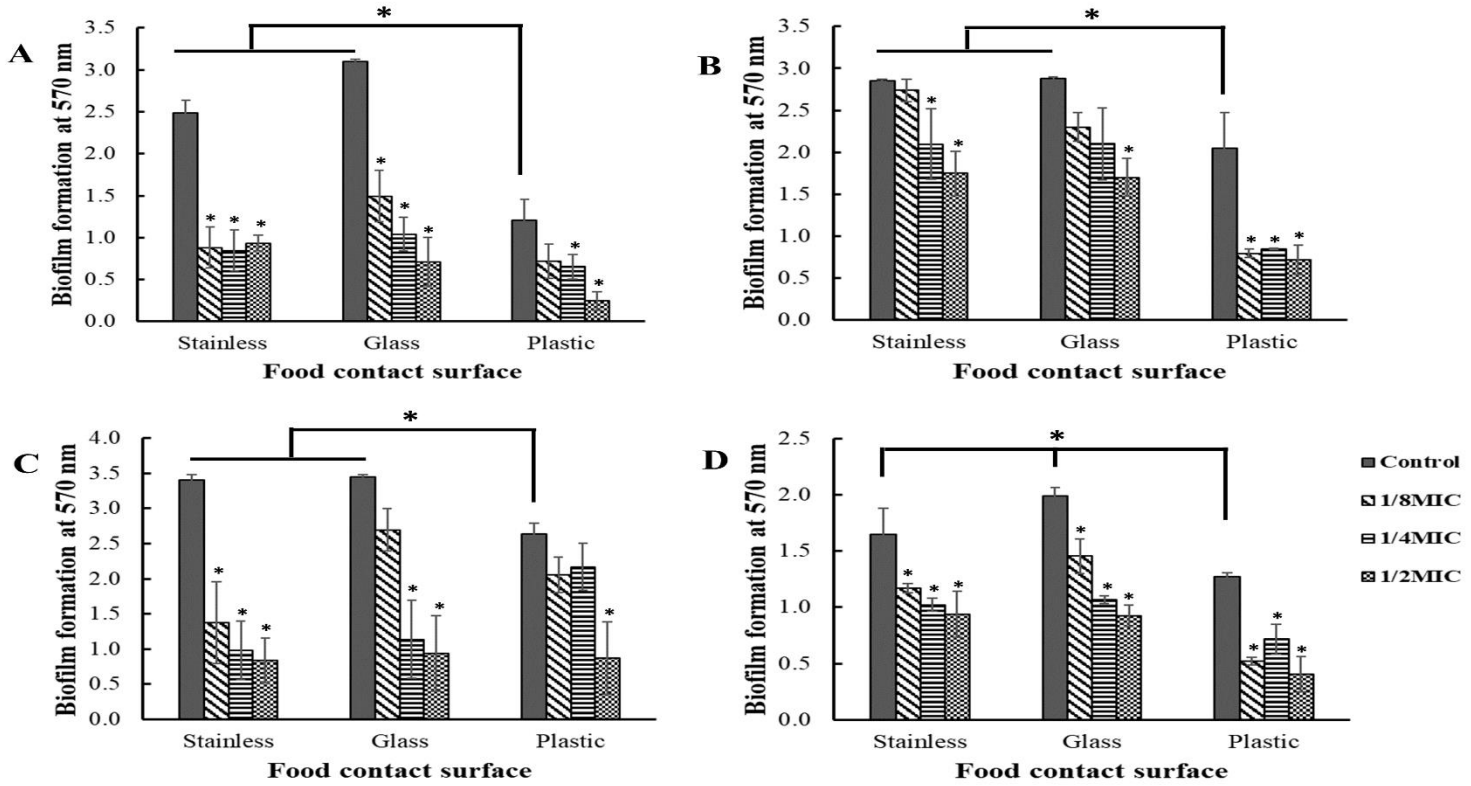

Figure 6. 24 h effects of sub-MIC *of E. camaldulensis* on *L. monocytogenes* biofilm formation on model food contact surface materials evaluated using CV assay. (A) PSU-KV-033, (B) PSU-KV-039, (C) PSU-KV-148, and (D) strain F2365. Values indicates the means ± SD for three independent experiments performed in triplicate *Significant difference between treatment and control at ($p \leq 0.05$).

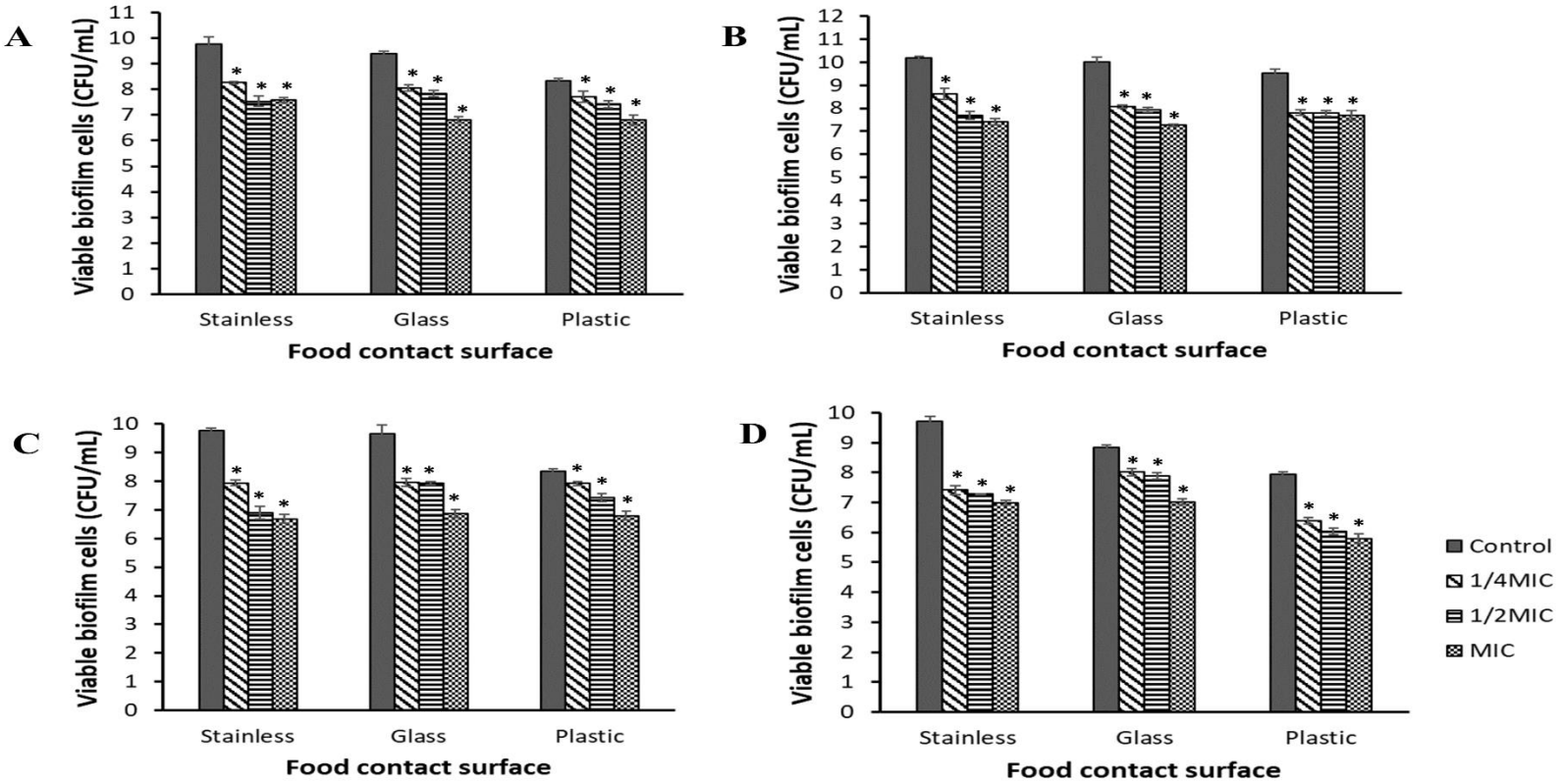

Figure 7. Effects of sub-inhibitory concentrations of *E. camaldulensis* extract on viable biofilm bacterial count on food contact surfaces after 24 h treatments. (A) PSU-KV-033, (B) PSU-KV-039, (C) PSU-KV-148, and (D) strain F2365.Values indicates the means ± SD for three independent experiments performed in triplicate *Significant difference between treatment and control at ($p \leq 0.05$).

7. Effects of The Extract on *L. monocytogenes* Established Biofilm on Food Contact Surfaces

Exo-polymer matrix associated with matured biofilm on food contact surfaces limits the diffusion and migration of antimicrobial sanitizers and cleaning agents. In addition, depositions of multi-layers biofilm structure results in formation of crevice resulting in the impairment of fluid flow and dynamics in food processing environments. Various studies reports the antimicrobial resistance of biofilm bacterial communities (Alvarez-Ordóñez, Coughlan, Briandet, & Cotter, 2019; Johani et al., 2018; Rodriguez-Lopez, Rodríguez-Herrera, Vazquez-Sanchez, & Lopez Cabo, 2018), which often is high cell density, EPS formation as well as social behaviors of biofilm communities (Mah & O'Toole, 2001; Rojo-Molinero, Macià, & Oliver, 2019). The results of this study indicated that treatment of *L. monocytogenes* established biofilm with bactericidal concentrations of 4MIC, 8MIC, and 16MIC the extract resulted in a reduction in the viable biofilm bacterial count (Figure 8). However, no significant difference ($p < 0.05$) was observed when analyzed using MTT and crystal violet assays (Data not shown). The reduction in viable bacterial count might have resulted from the disruptive effects of the extract or the killing activity at bactericidal concentrations.

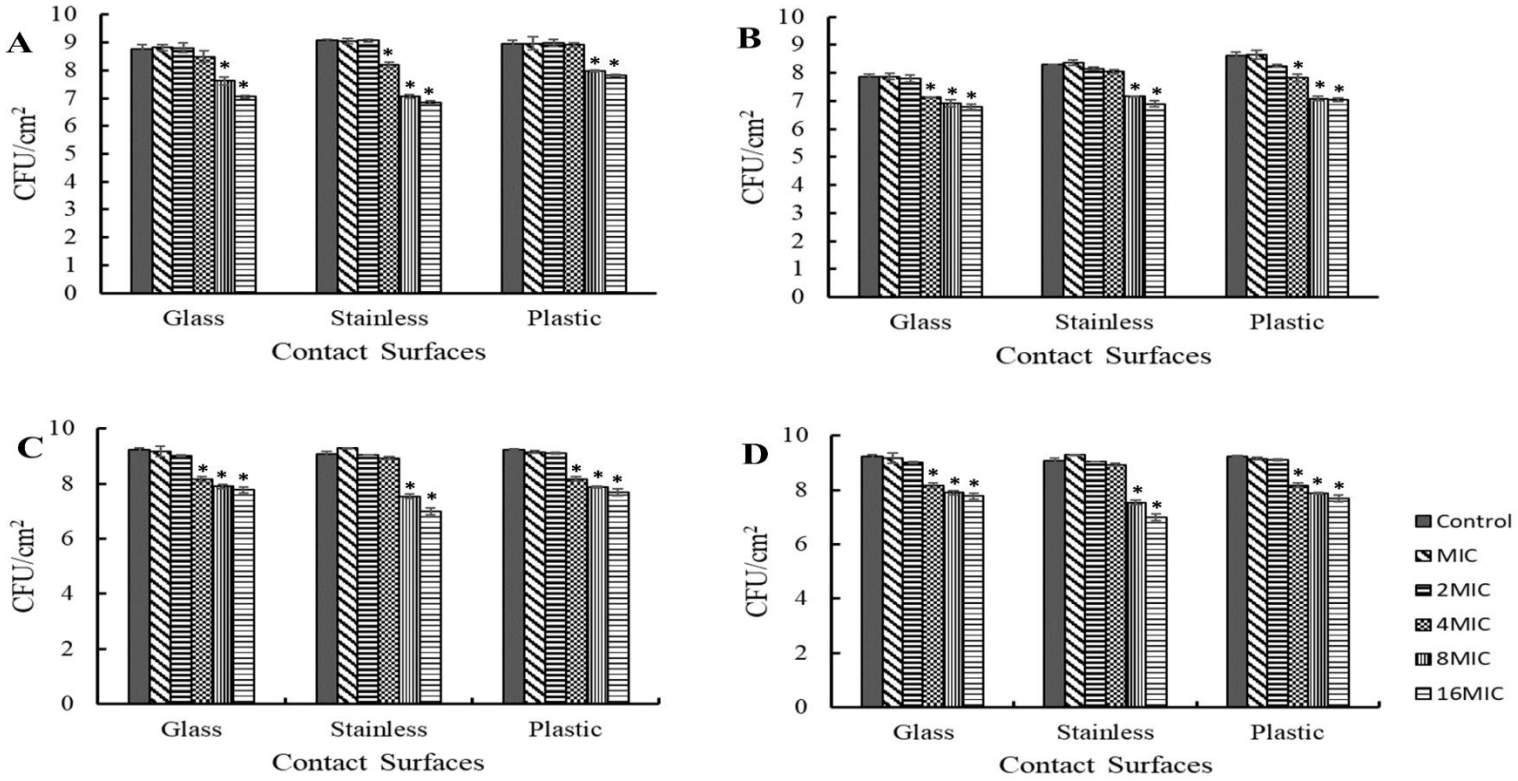

Figure 8. Effects of inhibitory and biocidal concentrations of *E. camaldulensis* extract on viable biofilm bacterial count of 96 h mature *L. monocytogenes* biofilm on food contact surfaces. (A) PSU-KV-033, (B) PSU-KV-039, (C) PSU-KV-148, and (D) strain F2365. Values indicates the means ± SD for three independent experiments performed in triplicate *Significant difference between treatment and control at ($p \leq 0.05$).

8. Time-Course *L. monocytogenes* Biofilm Development on Contact Surfaces

Surface properties such as topography, wettability and surface charge of a contact material are important parameter that might affect the dynamics of microbial attachment and biofilm formation. The time course development of biofilm on stainless steel, glass and plastic coupons was investigated over a 96 h period. The twenty-four hours micrograph revealed a dense cell biomass on the stainless steel and glass coupons, compared with the plastic coupon that showed a reduced biomass of cells. However, at maturation of biofilm (96 h), stainless steel and glass revealed a complex matrix with cells encased within, whereas plastic showed an increased cell biomass (Figure 9). The result indicated that stainless steel and glass displayed similar progression in biofilm development, which might be due to the similarities in wettability.

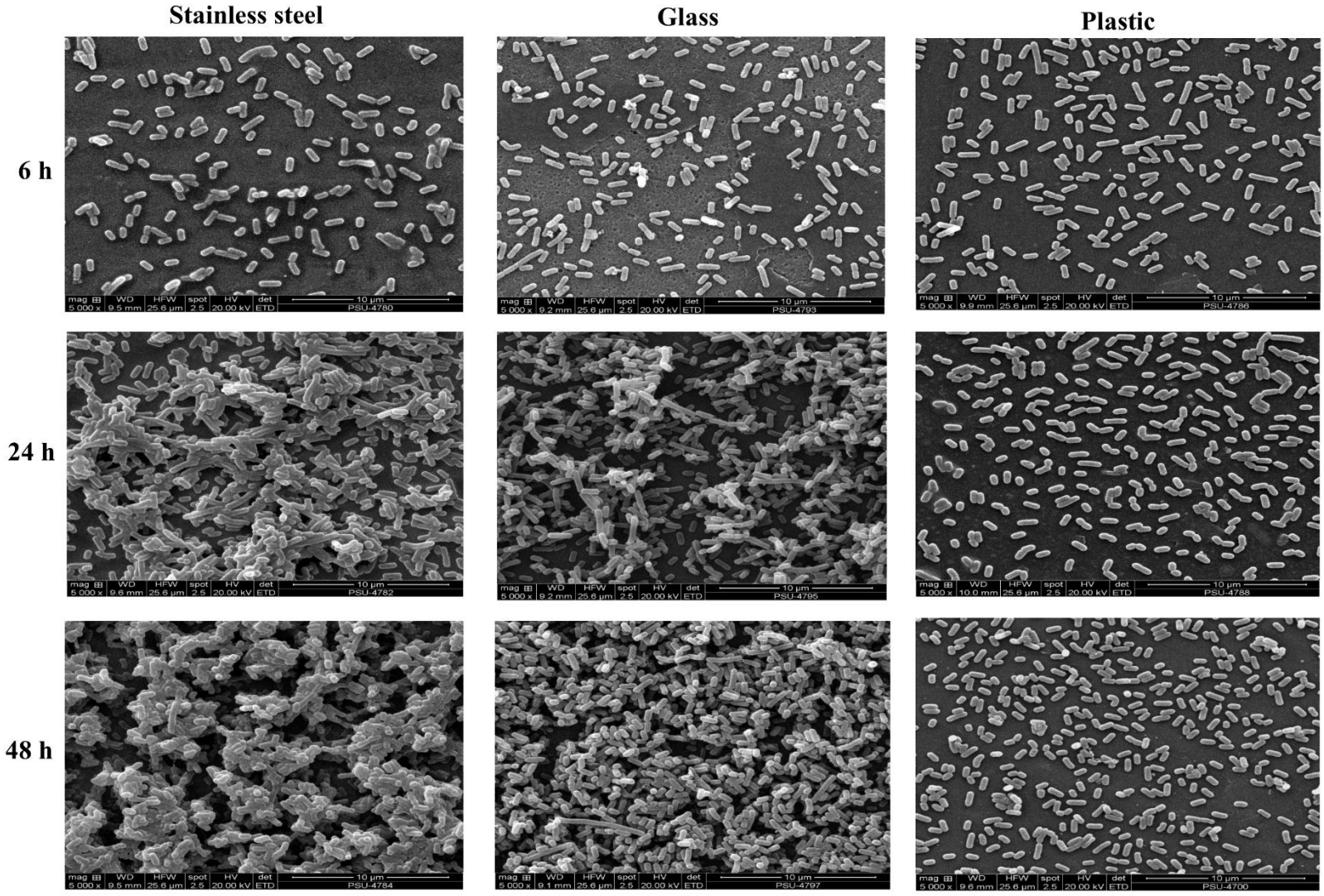
Stainless steel
Glass
Plastic
6 h
24 h
48 h

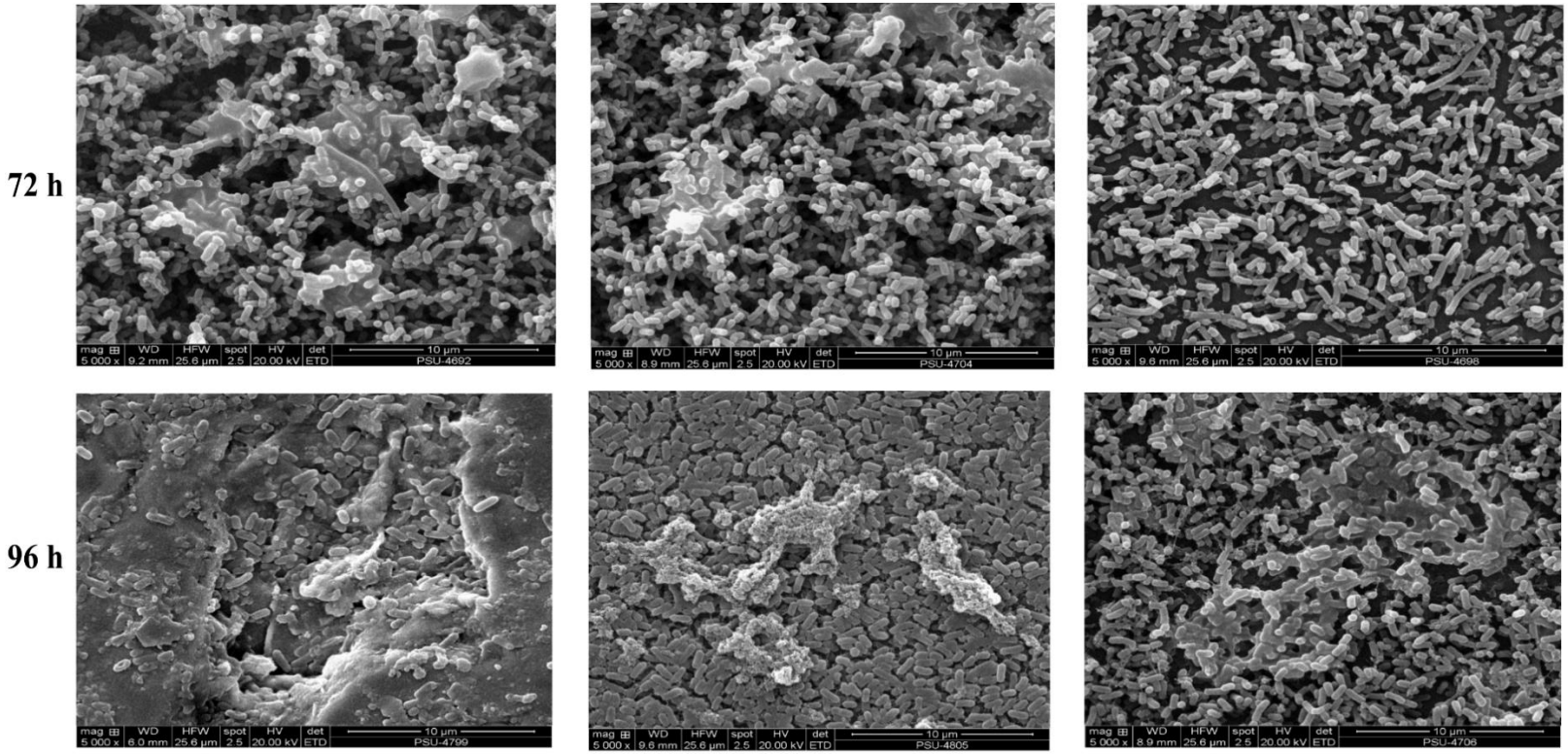

Figure 9. Time course *L. monocytogenes* biofilm development on food contact surface material visualized by scanning electron microscopy.

9. Attachment of *L. monocytogenes* to Solvents

Bacterial attachment to hydrocarbon assay (BATH) is a simple technique often employed to evaluate bacterial cell surface hydrophobicity. The hydrophobicity of 24 and 72 h culture of *L. monocytogenes* isolates obtained from ready to eat food (PSU-KV-033), food processing environment (PSU-KV-148) and strain F2365 was evaluated against a range of non-polar solvents. All the isolates showed higher affinity to chloroform, as compared to toluene, hexane, and petroleum ether (Figure 10A). Similar results were reported of *L. monocytogenes* exhibiting greater affinity to chloroform (an electron acceptor solvent) than to hexadecane (an apolar solvent) (Briandet, Leriche, Carpentier, & Bellon-Fontaine, 1999; Lee, Hébraud, & Bernardi, 2017). In addition, 72 h culture of isolate PSU-KV-033 and strain F2365 showed an increased affinity to hydrocarbon compared with the 24 h culture. This might be due to modifications in the cell surface chemistry resulting from aging of cultures. Various factors including temperature, culture condition and number of passages have been reported to influence cell surface hydrophobicity of a bacterial (Briandet et al., 1999; Lee et al., 2017). Cell surface hydrophobicity is an important criterion required for initial attachment to surface (Takahashi, Suda, Tanaka, & Kimura, 2010), however categorization of surfaces and bacterial cells based on hydrophobic– hydrophilic has been proved insufficient to make accurate predictions about bacterial attachment (Feng et al., 2015).

10. Effects of *E. camaldulensis* Extract on *L. monocytogenes* Cell Surface Hydrophobicity

Modification of *L. monocytogenes* cell surface properties such hydrophobicity has been reported to alter the attachment of bacteria to surfaces (Takahashi et al., 2010), thus alteration of bacterial cell surface chemistry might be possible target for disrupting the attachment of Listeria to food contact surfaces. The effects of the extract on listerial cell surface hydrophobicity was evaluated against isolate PSU-KV-148 and strain F2365 (Figure 10B). Treatment of the bacterial with sub-inhibitory concentrations of the extracts resulted in an increased hydrophobicity. An increase in hydrophobicity was reported after treatment of food-related bacteria isolates with antioxidant extracts of bearberry (Dykes, Amarowicz, & Pegg, 2003). The results suggested that extracts of *E. camaldulensis* could be used to alter listeria cell surface hydrophobicity.

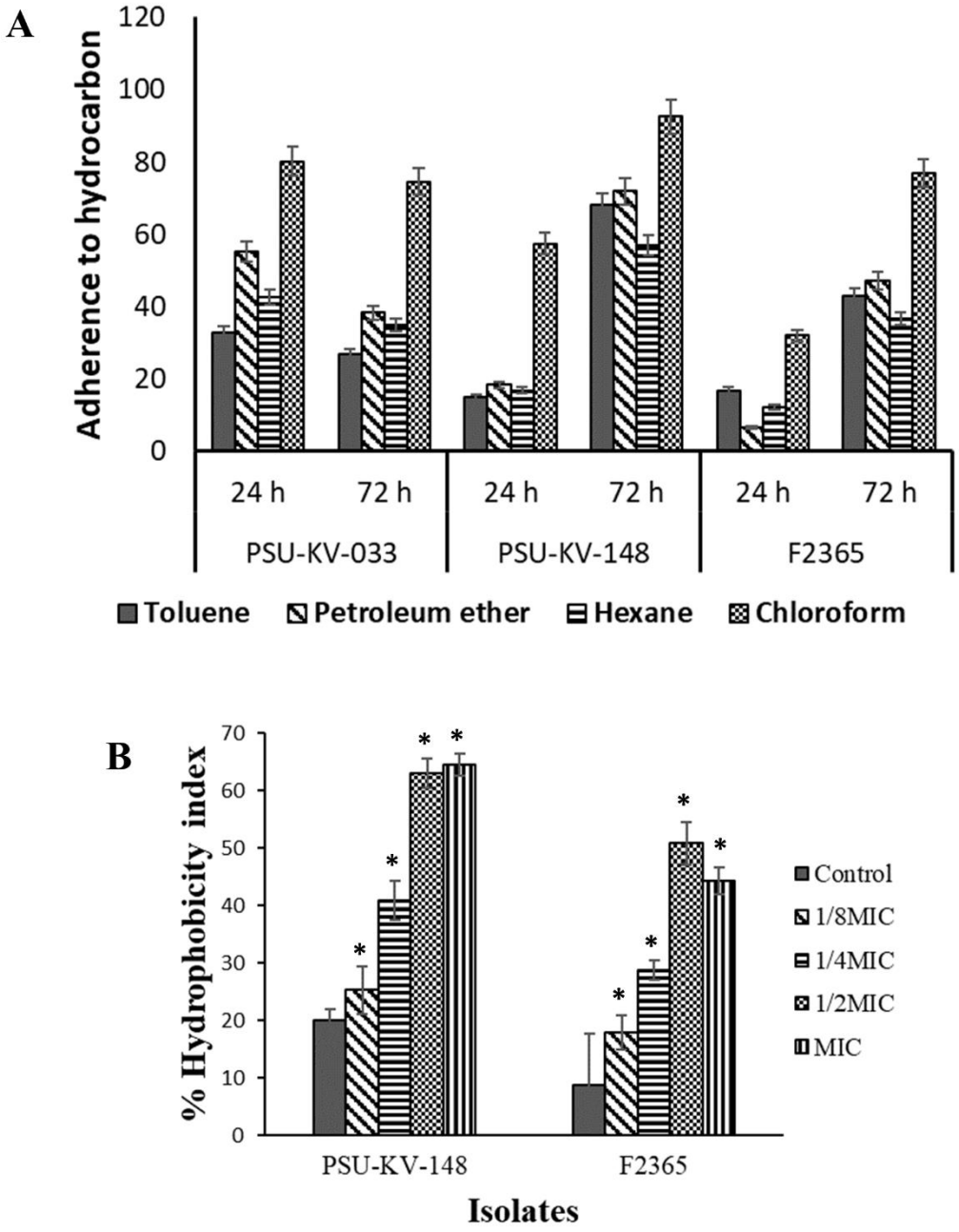

Figure 10. Affinity of *L. monocytogenes* 24 and 72 h cultures to hydrocarbon (A), and effects of *E. camaldulensis* extract on the hydrophobicity of *L. monocytogenes* (B). Values indicates the means ± SD for three independent experiments performed in triplicate *Significant difference between treatment and control at ($p \leq 0.05$).

11. Effects of *Eucalyptus camaldulensis* Ethanolic Extract on Listeriolysin O Production

Listeriolysin O is a cholesterol-dependent cytolysin, a family of pore-forming toxins commonly present in Gram-positive bacteria. Listeriolysin O is a primary virulence factor of *L. monocytogenes*, necessary for intracellular survival and escapes from host acidic phagolysosomal compartments. In this study, listeriolysin O production ability of all the test isolates was evaluated. Eighty-five percent (17 isolates) showed 27 to 97% haemolysis on red blood cells after exposure for 30 min (Figure 11A). The effect of sub-inhibitory concentrations of the extract on listeriolysin O production was further determined (Figure 11B). The results showed that sub-inhibitory concentrations of *E. camaldulensis* effectively inhibited listeriolysin O production after treatment for 18 h. Minimum inhibitory concentrations of the extract, completely inhibited listeriolysin O production, probably due to growth inhibition at this concentration. Treatments indicated a consistent concentration-dependent effect that was significantly different from the control ($p<0.05$). However, concentration of 1/16MIC showed no significant difference from the control against strain F2365. Previous researchers have reported listeriolysin O inhibitory activities of plant extracts and plant derived compounds (Du et al., 2018; Sansano et al., 2017). However, a detailed understanding of the inactivation and inhibitory mechanism of listeriolysin O is still lacking. Repression of the *L. monocytogenes* listeriolysin O gene (*hly*) was observed after treatment with sub-inhibitory concentrations of tea tree oil (Liu et al., 2016). Fisetin, a natural flavonoid was observed to inhibit haemolytic activity of listeriolysin O by competitively engaging

loop 2 and loop 3 of LLO, thus preventing the binding of cholesterol and reduction of oligomerization (Wang et al., 2014).

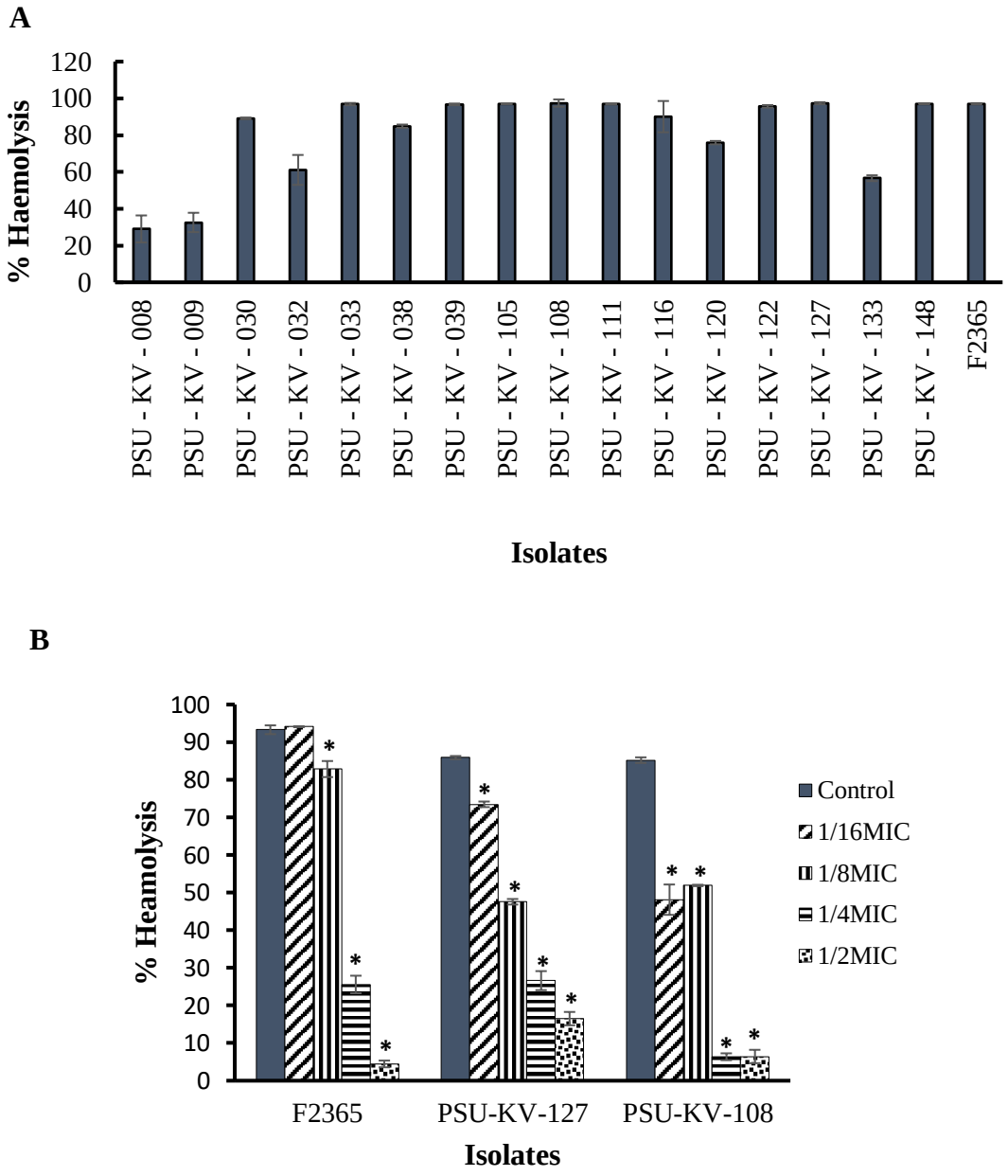

Figure 11. Haemolytic effects of *L. monocytogenes* culture supernatants (A) and effects of *E. camaldulensis* extracts on haemolysis of *L. monocytogenes* (B). Values were recorded as mean ± SD of triplicate values.

12. Effects of *Eucalyptus camaldulensis* Ethanolic Extract on *Listeria monocytogenes* Cell Membrane Permeability

Bacterial membrane serves as a permeable barrier that protects cytoplasmic contents from the damage that might arise from the influx of extracellular molecules. Alteration in membrane integrity might disrupt its permeability machinery, and thus lead to cell leakage. In this study, crystal violet uptake assay was used to evaluate the effect of the extract on the membrane integrity of *L. monocytogenes* after 30 min treatment. The results suggest that *E. camaldulensis* extract compromised the cell membrane integrity of *L. monocytogenes* at all the concentrations (Figure 12). Crystal violet uptake for all tested isolates increased significantly in a concentration dependent manner. The increased uptake of crystal violet reflects an increase in cell membrane permeability that could have resulted from the disruptive effects of the extract.

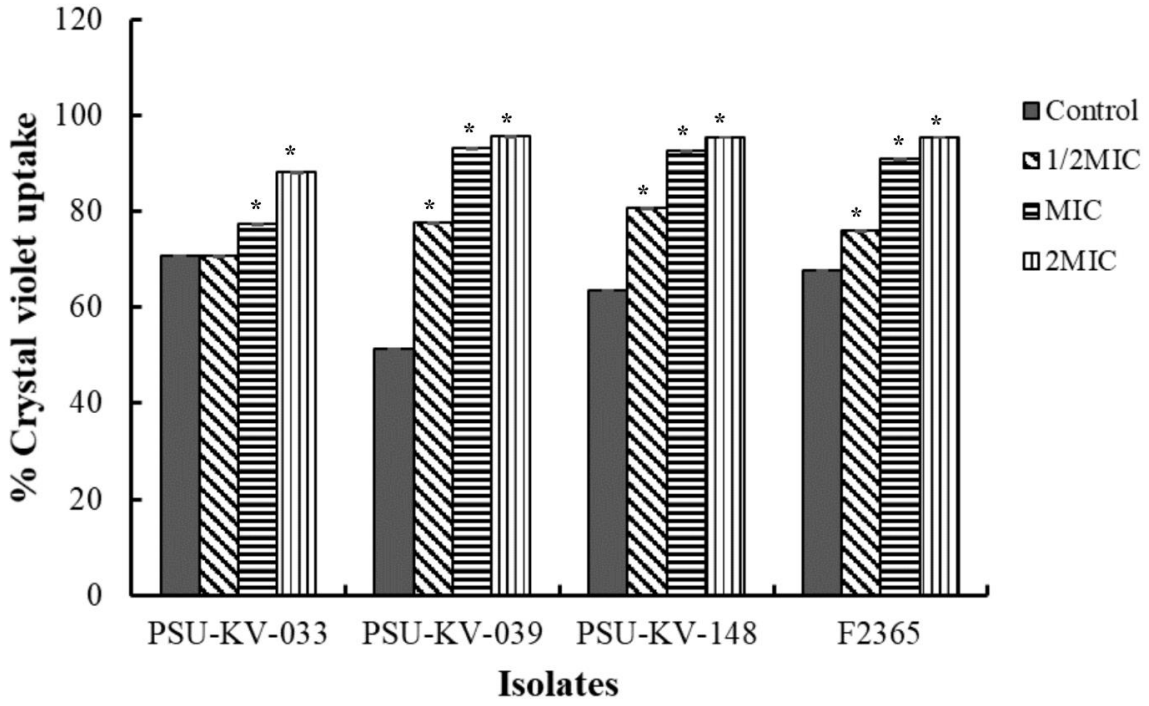

Figure 12. Effects of *Eucalyptus camaldulensis* extract on membrane permeability of *Listeria monocytogenes* evaluated using CV uptake assay. The value indicates the means ± SD for three independent experiments performed in triplicate *Significant difference between treatment and control at ($p \leq 0.05$).

13. Free Radical Scavenging Activity of *E. camaldulensis* Ethanol Leaf Extract

Free radical scavenging or quenching extends the shelf life of food products. In this study, the free radical scavenging activities of *E. camaldulensis* was evaluated using the DPPH and ABTS assays (Table 4). The result showed an IC_{50} of 57.07 and 29.01 µg/mL for DPPH and ABTS, respectively. The IC_{50} of the *E. camaldulensis* methanolic leaf extract on DPPH was previously reported as 89.11 µg/mL and 601.8 µg/mL, and 1279.58 µg/mL for the ethanolic extracts (Ashraf et al., 2015; Upreti et al., 2018). ABTS assay demonstrated better activity with IC_{50} lower than ascorbic acid (40.52 µg/mL) and trolox (50.90 µg/mL), respectively. The low IC_{50} shown by ABTS might indicate the presence of lipophilic constituents not detected by the hydrophilic based DPPH (Floegel, Kim, Chung, Koo, & Chun, 2011; Kedare & Singh, 2011). Enzymatic oxidation resulting from the generation of free radical species is a major cause of food spoilage during storage (Petruzzi *et al.*, 2017). Thus, the antioxidant results suggest that oxidative degradations such as lipid oxidation of food can be reduced by the applications of bioactive extracts of *E. camaldulensis*, leading to a delay of spoilage, extension of shelf-life, and maintenance of food quality and safety.

14. Total Phenolic, Total Flavonoid Contents and Ferric Reducing Antioxidant Power

Eucalyptus spp. are rich sources of phenolic and flavonoid compounds with excellent antioxidant activities. Total phenolic and flavonoid contents of the extract measured using the Folin-Ciocalteu and $AlCl_3$ calorimetric assays yielded values equivalent to 11.10 mg GAE/mg extract and 15.05 mg QE/mg extract, respectively. The total antioxidant contents of *E. camaldulensis* leaf extract estimated by FRAP test demonstrated high ferric reducing antioxidant power of 92.93 µM AAE/mg extract. The antioxidant power of the extract might be due to the phenolic and flavonoid contents of the extract. Ferric reducing antioxidant power of *E. camaldulensis* leaf was previously reported as 34.81 ± 0.67 mg GAE/g of plant extract for hexane extract, 15.02 ± 0.35 mg GAE/g of plant extract for methanol extract and 9.54 ± 0.04 mg GAE/g of plant extract for chloroform extract (Ashraf *et al*., 2015)

Table 4. Total phenolic, total flavonoid contents and antioxidant activities of *E. camaldulensis* extract

Test/Samples	Extract	Ascorbic acid	Trolox
2,2-diphenyl-1- picrylhydrazyl (DPPH) IC_{50} µg/mL	57.07	23.01	34.66
2,2′-azino-bis-ethylbenzthiazoline-6-sulphonic acid (ABTS) IC_{50} µg/mL	29.01	40.52	50.90
Ferric reducing antioxidant power (FRAP) (µg AAE/mg extract)	92.93	NA	NA
Total phenolic content (mg GAE/mg extract)	11.10	NA	NA
Total flavonoid content (mg QE/mg extract)	15.05	NA	NA

NA-Not applicable

Part II. Microencapsulation of *Eucalyptus camaldulensis* Crude Ethanolic Extract by Freeze Drying Technique, Using Sodium Alginate and Sodium Carboxymethyl Cellulose as Wall Materials

1. Particle Size

The particle size of alginate–CMC encapsulated extract is shown in (Table 5). In this study, the particle size of microcapsules was reported based on the equivalent sphere concept (D_{10}: 10th percentile of cumulated volume distribution, D_{50}: median particle diameter (50th percentile) of cumulated volume distribution and D_{90}: 90th percentile of cumulated volume distribution) and span. The D_{50} values of the microcapsules ranged from 6.7–26.6 µm, with the blank microcapsules presenting the lowest particle size of 6.7 µm. Addition of extract resulted in a significant ($p<0.05$) increase in the diameter of the microcapsules, however particle size diameter was not extract concentration dependent. Various factors including needle diameter, distance between needle and collecting solution (Pasukamonset, Kwon, & Adisakwattana, 2016) as well as concentration of crosslinking agent, homogenization speed and time might affect the size of the microcapsules. Polyphenols in the extract can establish firm hydrogen bonding, mediated by hydrophilic phenolic hydroxyl groups with the polymers resulting in increase in interfacial tension between aqueous and organic phase (Pasukamonset et al., 2016), which might affect the size of the microcapsules. Low span values were observed for the microcapsules, indicating a narrow particle size distribution.

2. Percentage Yield and Encapsulation Efficiency

Percentage yield and encapsulation efficiency are important factors for a microencapsulation process. Percentage yield is the ratio of the actual yield of microcapsule to the theoretical yield, which reflects the amount of recovered inputted material. In this study a high percentage yield (70.4–81.5%) was observed, demonstrating a minimal loss of material (Table 6). Various factors including concentration of polymers, solubility, concentration of the crosslinking agent and viscosity of the mixture might affect the yield. Similarly, encapsulation efficiency is a measure of the percentage of the core material loaded in the microcapsules (Choi & Chang, 2018). In addition, it reflects the degree of protection provided by the encapsulant (Binsi et al., 2017). Encapsulation of the extract using alginate–CMC demonstrated %EE of 74.2±0.011–82.43±0.772%. The high encapsulation efficiency shows the compatibility of alginate with CMC and further suggest the formation of stable interactions between reactive sites of the polymers and the extract.

3. Physicochemical Properties of Microcapsules

Physicochemical parameters of the microcapsules including zeta potentials, polydispersity index, swelling index and solubility are presented in (Table 6). Zeta potential is an important parameters that indicates charge and stability of the colloidal systems against coalescence and aggregation (Sezgin-Bayindir, Antep, & Yuksel, 2015). The alginate–CMC encapsulated extract showed a zeta potential of -11.01, -17.01, 2.23 and -2.45 for F0, F1, F2 and F5, respectively. As zeta potential decreases, the particles attract one another forming aggregates. Zeta potentials $\geq \pm 30$ mV are

generally regarded as stable (Wang et al., 2016), hence the formulations showed low electrostatic stabilization with net charges closer to zero. It has been reported previously that the ratio of polymers is an important surface charge modulating factors (Caetano, Almeida, & Gonçalves, 2016).

Polydispersity index (PDI) of a polymer colloidal system indicates the uniformity of the colloidal particles in the solution (distribution of size populations within a sample). The PDI scale ranges from 0.0 for uniform particle sized samples to 1.0 for highly polydisperse samples. For polymer-based particles, PDI values ≤ 0.2 are considered acceptable (Danaei et al., 2018). In this study, PDI values of the microcapsules ranged from 0.344–0.489, indicating a high size dispersion. The result confirms the high range between the D_{10} and D_{90} values of the microcapsules.

The microcapsules exhibited high swelling index that reduced with increased extract concentration. The high swelling index of the alginate–CMC co-polymer microcapsules reflects the hydrophilic nature of alginate and hydrocolloidal properties of CMC. Alginate has been reported to exhibit high swelling properties at neutral and alkaline pH (Akalin & Pulat, 2018), whereas Na-CMC demonstrates a pH independent swelling property (El-Hag Ali, Abd El-Rehim, Kamal, & Hegazy, 2008). Swelling properties of polymer-based formulations can be affected by several factors, including properties of the polymer, ionization degree, pH, concentration of the crosslinker and hydrophobicity or hydrophilicity. Results revealed that addition of the extract significantly ($p<0.05$) reduced the swelling index. Increase in extract concentration further lowered the swelling index of the microcapsules. This might be as a result of pH

alterations and the formation of intra-molecular hydrogen bonds. For effective release of core material, the microcapsules must absorb solvent and swell significantly (Patel et al., 2016), thus the results suggests that alginate–CMC co-polymer blend might be an effective release wall material for the encapsulation of bioactive compound.

The microcapsules demonstrated approximately 19–22% solubility. Addition of the extract revealed slight concentration dependent reduction in solubility. Reduction in solubility might be due to alterations in pH resulting in the insolubility of alginate and sodium CMC or the formation of complex electrostatic bonding between the polymers and the extract.

4. Loss on Drying and Swelling Index

The moisture loss of the microcapsules shown in Table 7 indicates a less than 20 % moisture content. Formulation F1 displayed the least moisture content while F5 showed the highest percentage of moisture loss. The presence of simulative water content might be due to improper drying of microcapsules and hygroscopic nature of the polymers used. The swelling index of the microcapsules varied inversely with the concentration of the loaded extract. Blank microcapsules showed the highest swelling index, while the formulation F5 showed the least (Table 6). The reduction in swelling index observed in the extract loaded microcapsules is attributed to the decrease in water holding capacity resulting from the increase in concentration of extract.

5. Micromeritic Properties of Microcapsules

The bulk density of particles is the density when packed or stacked in bulk, while the tapped density represents its random dense packing. Bulk density and the angles of

repose are important parameters used to describe the fluidity of the particles. The micromeritics properties, including bulk density, tapped density, angle of repose, carr's index and hausner's ratio of the microcapsules were evaluated (Table 7). The results indicated that the tapped density ranged between 0.33 ± 0.03 to 0.44± 0.01 g/cm^3 and the bulk density ranged between 0.22 ± 0.02 to 0.27 ± 0.01 g/cm^3, respectively. The prepared microcapsules showed poor flow property as shown be Carr's index between 27 to 40, angle of repose between 27.9° to 30.9°, and hausner's ratio greater than 1.5, indicating a passable flow behaviour of the microcapsules. The results further revealed that the F1 formulation had the highest tapped density, which might be due to the relatively larger particle size as revealed by the D_{50} suggesting a reduction in the cohesive force between particles. In addition, moisture content of the microcapsules might also affect its flowability due to liquid bridge forces because of the presence of thin film liquids on the surface of the microparticles.

Table 5. Particle size of microcapsules measured using particle analyzer and expressed in terms of equivalent sphere concept

Formulations	Extract content (mg)	Particle Size (µm)			
		D_{10}	D_{50}	D_{90}	Span
F0	0	3.07	6.70	14.63	1.73
F1	1.25	11.85	26.59	59.70	1.79
F2	2.50	4.99	10.03	20.15	1.51
F5	5.00	4.41	9.06	18.61	1.56

D_{10}: 10th percentile of cumulated volume distribution
D_{50}: median particle diameter (50th percentile) of cumulated volume Distribution
D_{90}: 90th percentile of cumulated volume distribution

Table 6. Physicochemical properties of microencapsulated ethanolic leaf extracts of *E. camaldulensis* and blank sodium alginate and sodium carboxymethyl cellulose capsules

Formulations	**% Yield**	**Encapsulation efficiency (%)**	**Swelling index (%)**	**Polydispersity index**	**Zeta potential (mV)**	**Solubility (%)**
F0	80.7	NA	84.0	0.450	-11.01	22.2±1.1
F1	76.5	74.2 ± 0.011	81.4	0.489	-17.01	22.1±1.6
F2	81.5	80.11 ± 0.008	71.8	0.344	2.23	19.9±0.1
F5	70.4	82.43 ± 0.772	54.4	0.370	-2.45	18.8±0.2

NA-not applicable

Table 7. Micromeritics properties of microencapsulated extract and blank sodium alginate and sodium carboxymethyl cellulose

Samples	Bulk Density (gm/cc)	Tapped Density (gm/cc)	Moisture Loss (%)	Angle of Repose (°)	Carr's Index	Hausner's Ratio
F0	0.22 ± 0.02	0.38 ± 0.04	14.7 ± 0.02	30.9 ± 1.41	40	1.66
F1	0.24 ± 0.03	0.44 ± 0.01	9.0 ± 0.03	29.24 ± 1.15	44	1.8
F2	0.27 ± 0.01	0.41 ± 0.06	14.0 ± 0.01	29.68 ± 0.83	34	1.5
F5	0.24 ± 0.07	0.33 ± 0.03	15.0 ± 0.04	27.9 ± 3.22	27	1.38

6. FTIR

The FTIR spectra of the polymers, extract and microcapsules is shown in Figure 13**.** The spectra shows molecular interactions between functional groups resulting in the formation of new groups and /or alteration of already existing groups. Similar bands were observed for all the spectra with broad bands at 3400–3600 cm^{-1} attributed to the O-H vibrations, while the peaks at 2900–2950 cm^{-1} relates to the C-H bands. Peaks between 1600–1650 cm^{-1} and 1420–1450 cm^{-1} represented the assymetric and symmetric strechings of the –COO– (Capanema et al., 2018). Further, peaks around 1300–1370 cm^{-1} belonged to the streching vibration peak of C–N (Wang et al., 2018), and bending vibration of O–H (Dai, Ou, Huang, Liu, & Huang, 2018). The extract spectra showed a peak at 1726 cm^{-1} which was ascribed to C=O group. The spectra around 2360 cm^{-1} represents CO_2 streching that might have resulted from measurement condition. Addition of the extract resulted in minor shifts in bands as shown by the difference between spectra of blank microcapsule an microcapsule with extract. The prominent C-H peak located at 2928 cm^{-1} and 2950 cm^{-1} in the extract and blank capsules combined, resulting in a minor shift to 2926 cm^{-1}. In addition, the extract lost its carbonyl peak at 1732 cm^{-1} as a result of fussion with the -COO- group resulting in band shift from 1618 to 1622 cm^{-1}. Furthermore the streching of the primary alkane at 1051 cm^{-1} in the extract also fussed with the peak at 1032 cm^{-1} resulting in a shift to 1026 cm^{-1}.

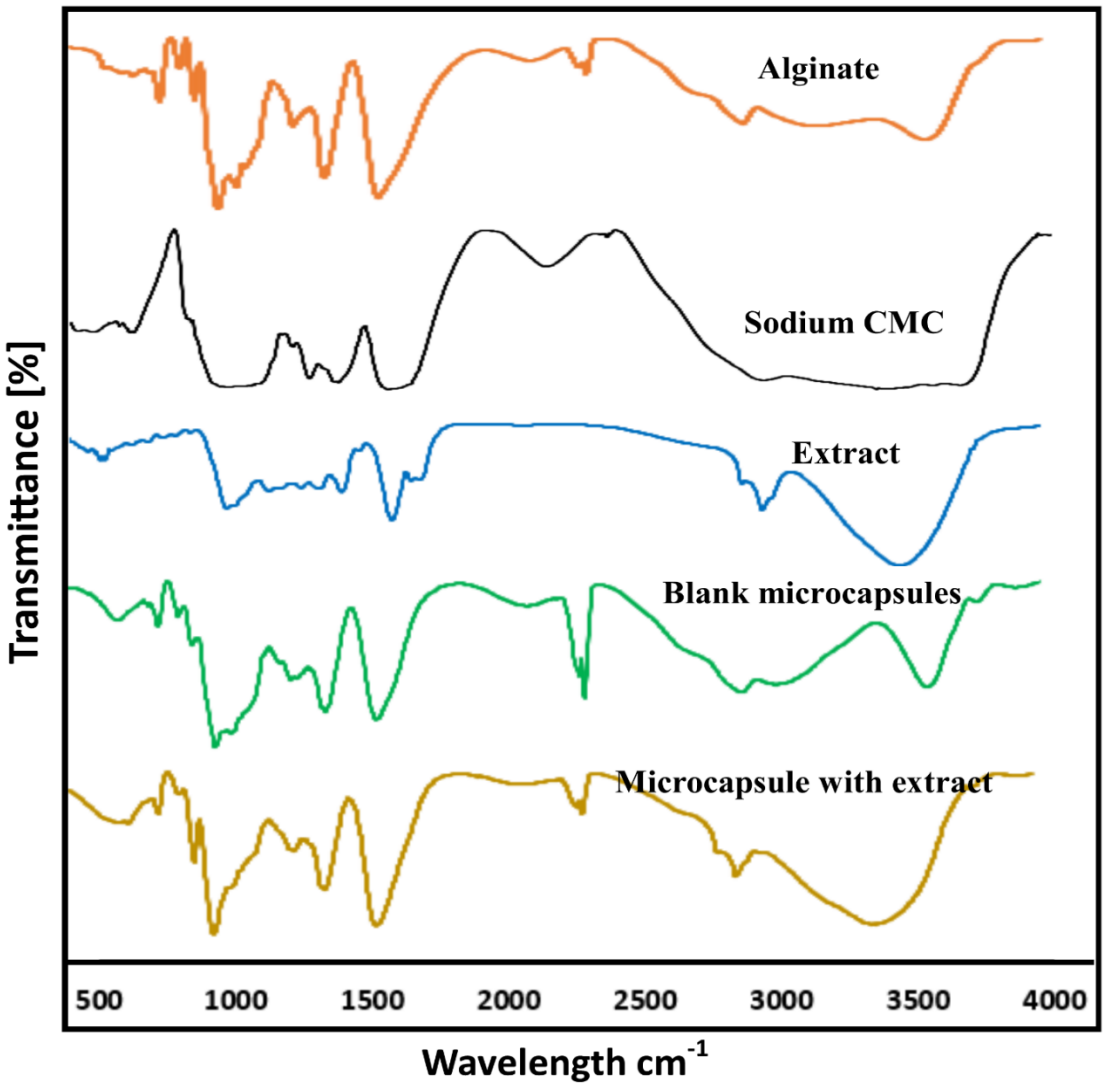

Figure 13. FTIR spectra of polymers, extract, blank microcapsules, and microencapsulated extract recorded between 500–3900 nm, showing molecular interaction of components following the encapsulation process.

7. Release of Polyphenols

Release of bioactive core material from polymer matrix is an important property of microcapsules and determines the bioavailability and activity of the core as preservatives. The release of polyphenols from the alginate–CMC matrix, evaluated at 37 °C and 4 °C (Figure 14)**.** The results indicated a significant difference in the release profile at the tested temperatures ($p<0.05$). The microcapsules at both temperatures showed rapid release of polyphenols within 1 h. Encapsulation of *Stevia rebaudiana* leaf extract and *Clitoria ternatea* petal flower extract with alginate showed similar results (Arriola et al., 2016; Pasukamonset et al., 2016). However, our study indicated a slow and regulated release of polyphenol over a wide time range. In addition, the microcapsules showed enhanced polyphenol release at 37 °C than at the storage temperature of 4 °C. This might be ascribed to increased collision due to increase in Brownian movement of particles.

Release of polyphenols at 37 °C, followed the first-order kinetics with dependence on concentration and a zero-order kinetics independent of concentration at 4 °C. The Higuchi kinetic model showed a time dependent controlled release at 37 °C, and a time independent controlled release at 4 °C.

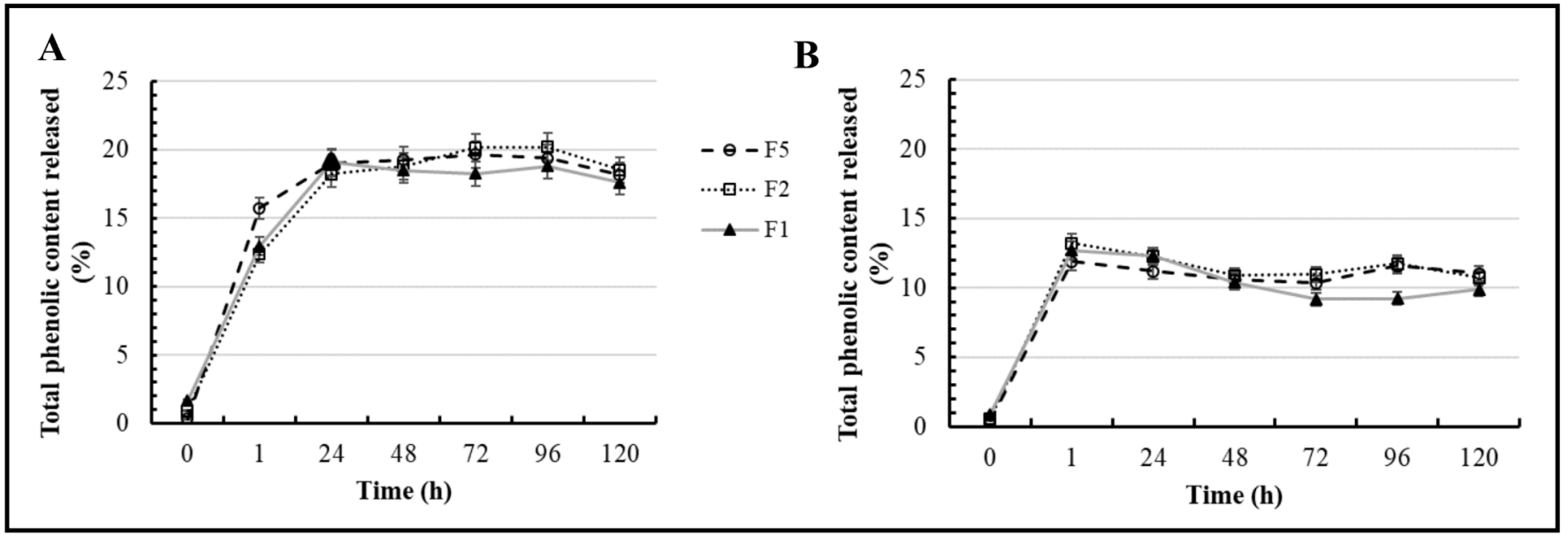

Figure 14. Release of polyphenol from microcapsules at 37 ℃ (A), and 4 ℃ (B)

8. Total Phenolic and Flavonoid

The total phenolic and flavonoid contents of the microcapsules are presented in Figure 15**.** The results indicate a TPC content of 0.26, 0.15, and 0.09 mg garlic acid equivalent/mg sample for formulation F5, F2 and F1 and a TFC of 0.21, 0.09 and 0.06 mg catechin equivalent/mg sample for F5, F2 and F1, respectively. *E. camaldulensis* extract contains numerous phenolic and flavonoid compounds with a TPC of approximately 148, 76 and 39 µg GAE/mg extract and TFC of approximately 20, 11 and 6 µg QE/mg extract for methanol, chloroform and hexane extracts (Ashraf et al., 2015). TPC of ethanolic leave extracts of *E. camaldulensis* was recorded as 11.10 mg GAE/mg extract, while TFC was 15.05 mg QE/mg extract (Nwabor et al., 2019). The phenolic and flavonoid contents of the microcapsules indicate a release of surface entrapped bioactive compounds. Formulation F0 showed no phenolic and flavonoid content (data not shown) confirming that the polymers contained no phenolic or flavonoid.

9. Antioxidant Efficacy of Microcapsules

The antioxidant activities of the microcapsules, demonstrated by DPPH and ABTS assay is shown in Figure 16**.** The capsules showed a concentration dependent inhibition for both DPPH and ABTS. The concentration of the extract in the microcapsules reflects the antioxidant properties, hence F5 showed the highest antioxidant properties whereas F1 showed least antioxidant activity. The blank (F0) capsules did not show any antioxidant activity at all the concentrations tested (data not shown). This is due to the absence of the bioactive extract and the lack of antioxidant

properties for both sodium alginate and sodium CMC. The antioxidant also demonstrates the release of the bioactive core from across the wall material or the interaction of surface bioactive components with the stable radical compounds.

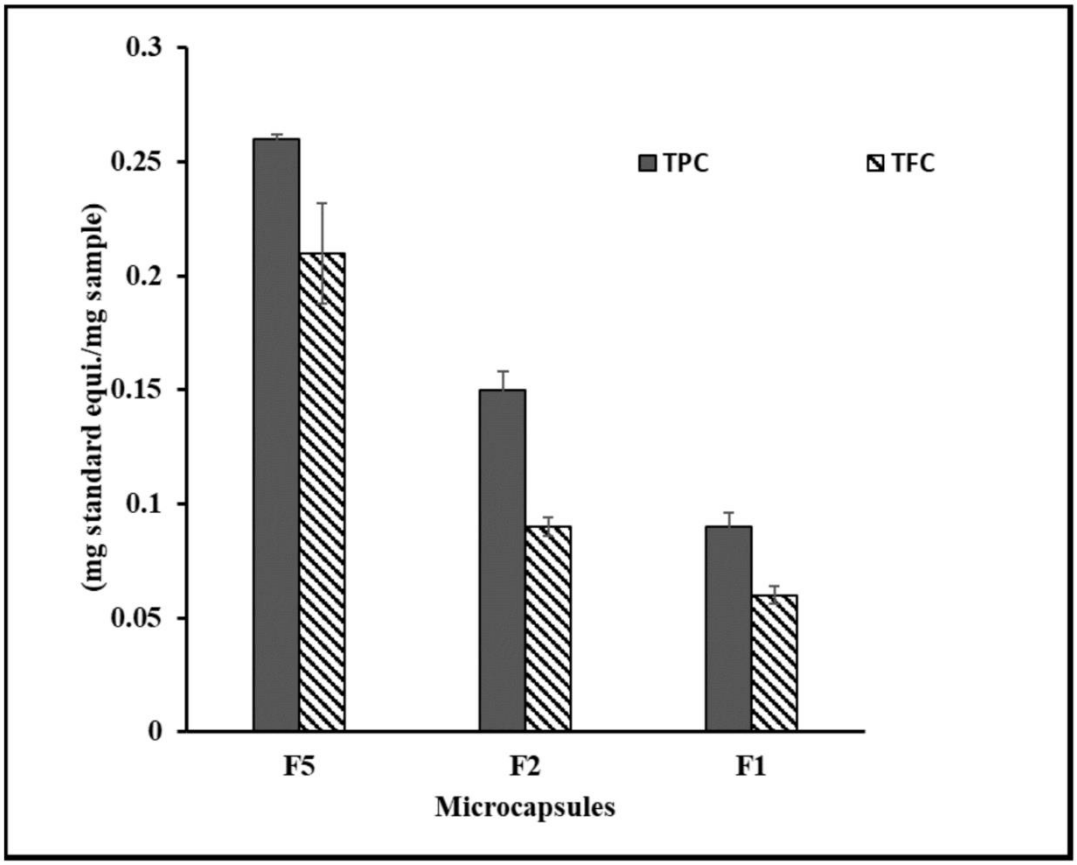

Figure 15. Total phenolic and total flavonoid contents of the microcapsules tested using Folin-Ciocalteu and $AlCl_3$ assay. Values represents mean of triplicate measurements.

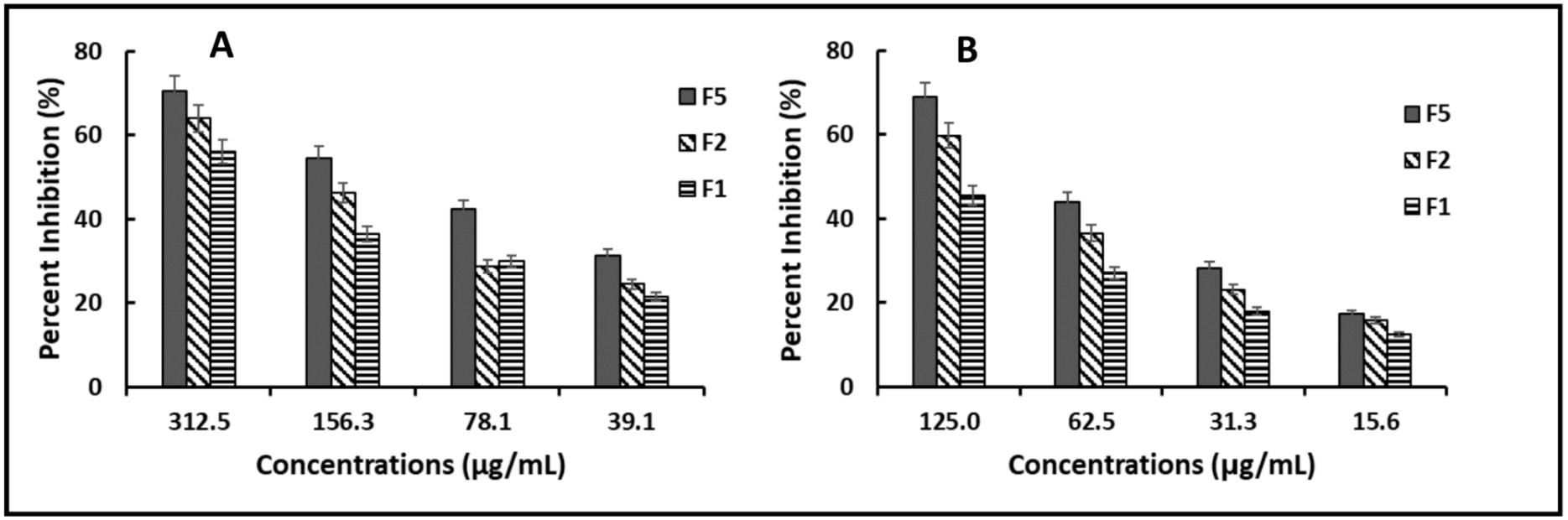

Figure 16. Antioxidant properties of microencapsulated extract evaluated using DPPH (A) and ABTS (B). Measured as percentage inhibition. Values represents mean of triplicate measurements.

10. Antimicrobial Activity of Microcapsules

Microencapsulation is a suitable method for the incorporation of bioactive compounds into products such as food, pharmaceuticals, and cosmetics. Encapsulated bioactive compounds are incorporated into food as additives, enhancers, binders, antioxidants, as well as antimicrobial preservatives. Release of encapsulated core material helps maintain the food qualities by inhibiting oxidation and microbial mediated spolage. Antimicrobial activities of the encapsulated extracts of *E. camaldulensis* against foodborne pathogenic bacteria is shown in (Table 8). The microencapsulated extracts demonstrated antimicrobial effects with minimum inhibitory concentrations and minimum bactericidal concentrations ranging from 0.19–3.12 and 0.19–12.25 mg/mL, respectively. Both the extract and the microcapsules did not show any activity against Gram–negative *E. coli* (data not shown). In addition no antimicrobial activity was observed for the blank microcapsules. The results suggests an antimicrobial activity dependant on the concentration of the extract. In addition, the antimicrobial activity observed suggests release of core material across the walls of the particles into media.

Table 8. Antimicrobial activities of microcapsules and extract on foodborne bacterial isolates

Isolates	**MIC/MBC (mg/mL)**				
	F0	**F1**	**F2**	**F5**	**Extract**
Bacillus cereus	>24	0.39/1.56	0.19/0.39	0.19/0.19	0.064/0.128
Listeria monocytogenes F2365	>24	1.56/6.25	0.39/6.25	0.19/0.78	0.128/0.512
Staphylococcus aureus ATCC 25923	>24	3.12/12.25	1.56/6.25	0.39/1.56	0.128/0.256

11. Scanning Electron Microscopy

The morphology of the microcapsules, observed using scanning electron microscopy is presented in (Figure 17)**.** The micrograph showed irregular shape and compact structure similar to previously observed micrograph for freeze dried microcapsules (Hussain et al., 2018; Kuck & Noreña, 2016; Yang et al., 2019). The high speed homogenization and breakage of microbeads formed after cross-linking into irregular shapes, and the crushing procedure employed for size reduction after lyophilization might be responsible for the irregular shaped observed. In addition, no difference in structure was observed from the scanning electron micrograph of the different formulations. However, the micrograph showed a larger particle size for F0 and F1.

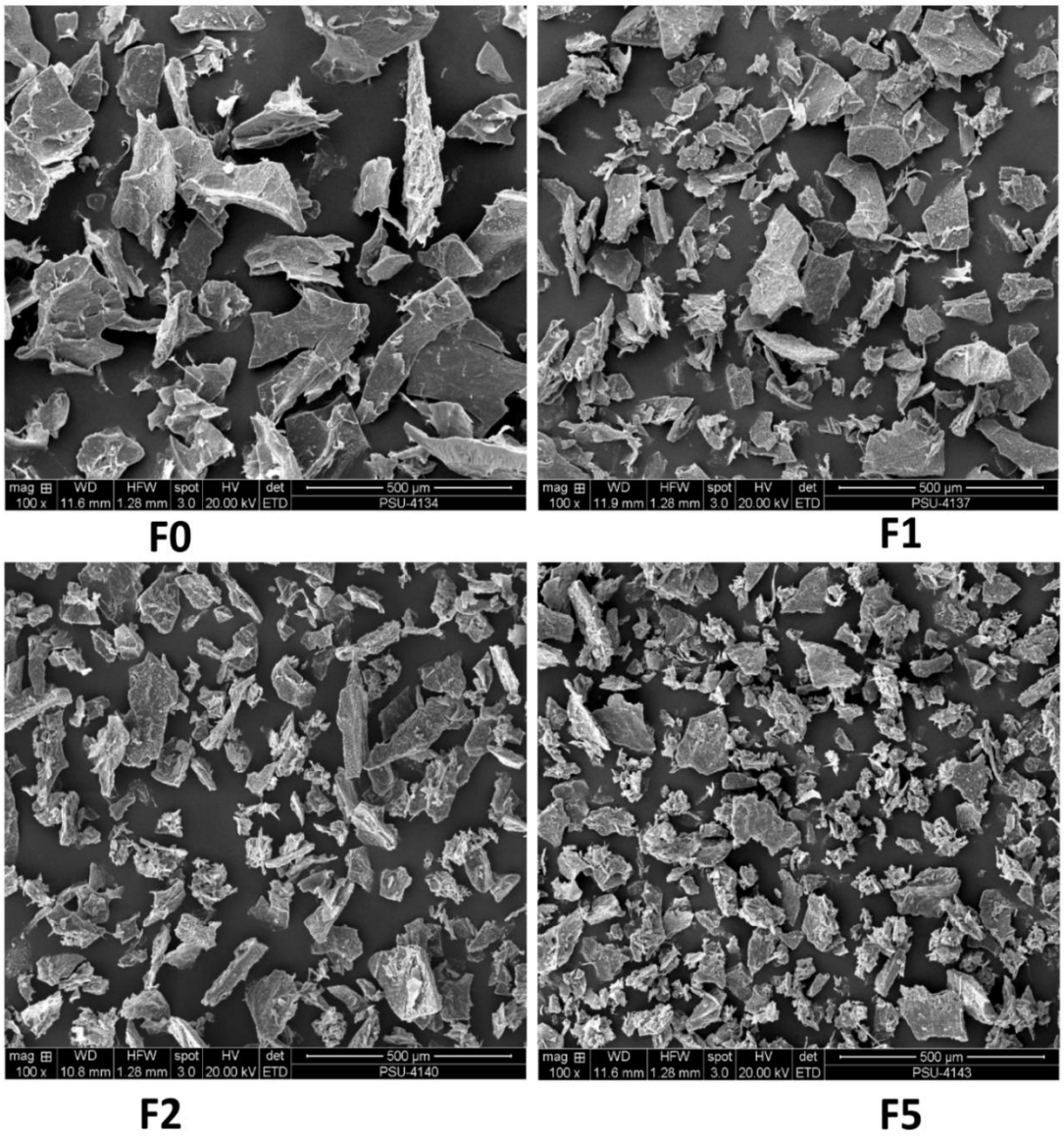

Figure 17. Scanning electron micrograph of *E. camaldulensis* extract encapsulated in sodium alginate and sodium carboxymethyl cellulose matrix, showing the shape and surface morphology of the microcapsules.

12. Cytocompatibility Testing of Microcapsules

The cytotoxicity evaluation of eluates obtained from microcapsules at various time intervals against human embroyonic colon cell Caco-2 is shown in (Figure 18)**.** At the tested time intervals, eluates from the formulations showed >80% cell viability when compared with the control (100%), indicating a general low toxicity to the test cell line. The cytocompatibility of microencapsulated plant extracts and phytochemicals have been reported for various mammalian cell lines (Condurache et al., 2019; Mohammed et al., 2019; Ruiz-Montañez et al., 2019). Encapsulation of active compounds can reduce the adverse effects through regulated slow release with prolonged activity.

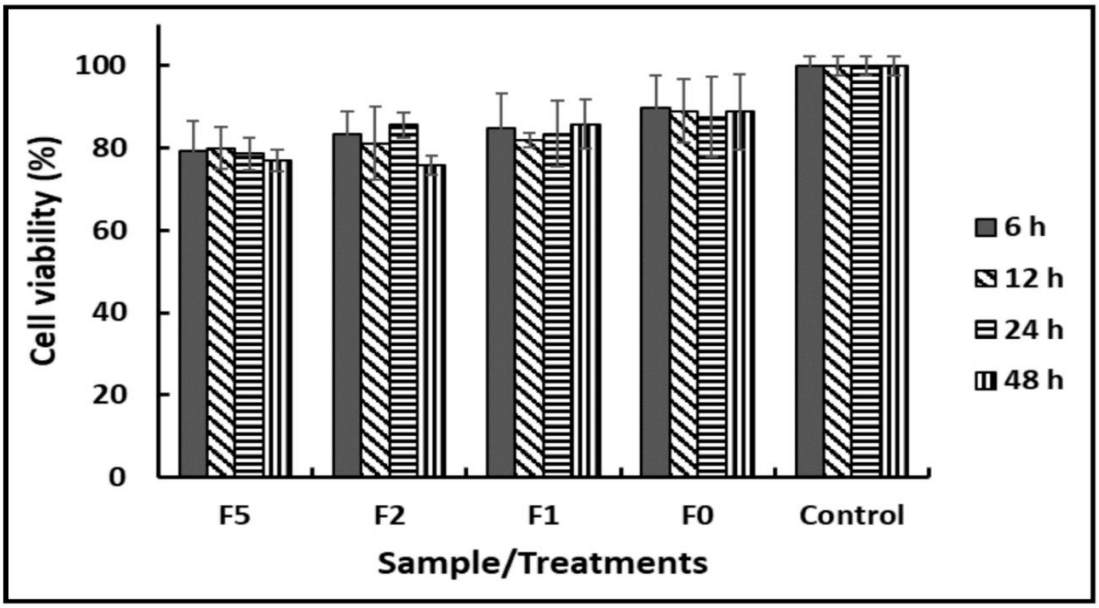

Figure 18. Cytocompatibility of microcapsules on human embryonic colon cell Caco-2, evaluated by indirect method using eluates released from microcapsules at different time intervals. Values represents means of triplicate values, and experiments were performed for two independent times

13. Colour Analysis

Encapsulation of natural bioactive products is extensively employed for masking of unfavourable qualities such as colour, smell and taste. These qualities often impairs the oganoleptic, sensory and aestetic qualities of products. In this study, the Lightness (L*), Chroma and Hue angle of the microcapsules ranged from 9.17±0.13–29.43±0.12, 1.72±0.06–19.20±0.46.9, and -1.41±0.01–1.15±0.20°, respectively (Table 9). The redness and yellowness values a* and b* of the blank microcapsules were -0.69±0.13 and -1.54±0.15. The redness/blueness values increased in formulation F1 but reduced with addition of more extract in F2 and F5. Yellowness/greenness values displayed a significant ($p < 0.05$) extract concentration dependent increase. A negative correlation was observed between redness a*, greenness b* values and the lightness values L*. Chroma was positively correlated with L* whereas Hue displayed a negative correlation (Table 10). The brownness index BI of the microcapsules increased with increase in the extract concentration added. The results revealed that encapsulation of the extract using alginate–CMC did not effectively mask the colour of the extract.

Table 9. Colour parameters of microencapsulated extract and blank microcapsules obtained by freeze drying

Samples	***L****	***a****	***b****	ΔE	**Chroma**	**Hue**	**BI**
F0	9.17±0.13^{a}	-0.69±0.13^{a}	-1.54±0.15^{a}	9.33±0.13^{a}	1.72±0.06^{a}	1.15±0.20^{a}	-20.26±0.98^{a}
F1	29.43±0.12^{a}	-5.13±0.09^{ab}	8.78±0.22^{a}	31.14±0.18^{ab}	10.17±0.23^{a}	-1.04±0.01^{ab}	20.38±0.77^{a}
F2	28.05±0.10^{ab}	-4.83±0.05^{ac}	13.26±0.44^{a}	31.40±0.18^{ac}	14.11±0.41^{a}	-1.22±0.01^{acd}	46.91±2.79^{a}
F5	27.97±0.04^{ac}	-3.15±0.08^{a}	18.94±0.47^{a}	33.93±0.24^{a}	19.20±0.46^{a}	-1.41±0.01^{abe}	93.45±4.14^{a}

Values represent mean values ± standard deviation. Same superscript within the same column indicates significant difference while different superscript indicates no significant difference at ($P < 0.05$)

Table 10. Pearson correlation coefficients (r) between colour parameters (L*, a*, b*, ΔE, Chroma, Hue, and BI)

	L*	***a****	***b****	**Δ*E***	**Chroma**	**Hue**	**BI**
L*	**1**						
a*	-.918**	1					
b*	.846**	-.596**	1				
Δ*E*	.987**	-.849**	.921**	1			
Chroma	.833**	-.575**	1.000**	.911**	1		
Hue	-.979**	.848**	-.927**	-.995**	-.917**	1	
BI	.735**	-.432	.981**	.835**	.986**	-.841**	1

**. Correlation is significant at the 0.01 level (2-tailed).

Part III. Synthesis, Characterization, and Antibacterial Activities of Biogenic Silver Nanoparticles Using Ethanolic Extract of *Eucalyptus Camaldulensis* as Reducing and Capping Agent

1. Synthesis and Characterization of Biogenic Silver Nanoparticles

Reduction of metal salts with plant extracts and phenolic compounds has been described as an eco-friendly alternative method for the synthesis of NPs with excellent bioactive properties. Ethanolic extracts of *E. camaldulensis* was successfully used as a reducing and capping agent for $AgNO_3$. The formation of silver nanoparticles was signaled by colour change and confirmed using UV-visible spectroscopy (Figure 19A). The peak at 437 nm represented the surface plasmon resonance of silver nanoparticles. DLS analysis showed that the silver nanoparticles had an effective diameter of 138.6 nm with a polydispersity of 0.244 (Figure 19B, C). Elemental analysis of the silver nanoparticles by EDS indicated Ag concentration of 23.7 %Wt (Figure 19D). Furthermore, visualization of the NPs by TEM (Figure 19E) showed spherical shaped nano-sized particles with mean diameter of 13.11 nm. In addition, the silver nanoparticles revealed a zeta potential of –35.85 mV. The high negative zeta potentials indicate high stability of the silver nanoparticles due to electrostatic repulsive force (Paosen, Saising, Septama, & Voravuthikunchai, 2017). Previous researchers have reported the synthesis of silver nanoparticles with extracts of plants belonging to the genus Eucalyptus (Mohammed, 2015; Wintachai, Paosen, Yupanqui, & Voravuthikunchai, 2019). The FTIR spectra of the extract and silver nanoparticles were also obtained (Figure 20), using a Vertex 70 FTIR (Bruker, Ettlingen, Baden-Württemberg, Germany).

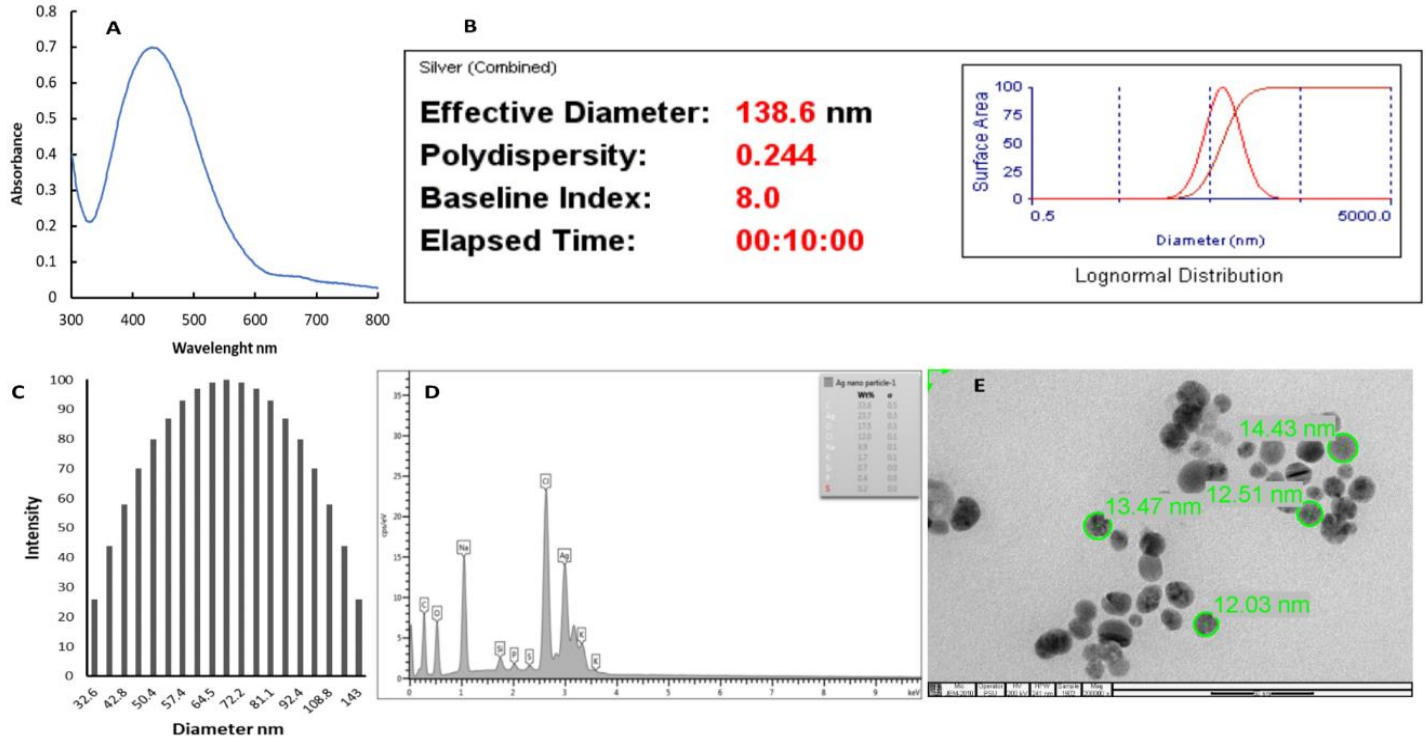

Figure 19. Characterization of synthesized silver nanoparticles using UV-visible spectroscopy (A) showing the Ag plasmon resonance peak at 437 nm, Dynamic light scattering (B and C) showing the effective diameter of the silver nanoparticles, polydispersity index and the size distribution of the particles, Energy dispersive X-ray spectroscopy (D) showing the elemental components of the silver nanoparticles with a silver concentration of 23.7%Wt, Transmission electron microscopy (E) showing the shape and average size of the particles.

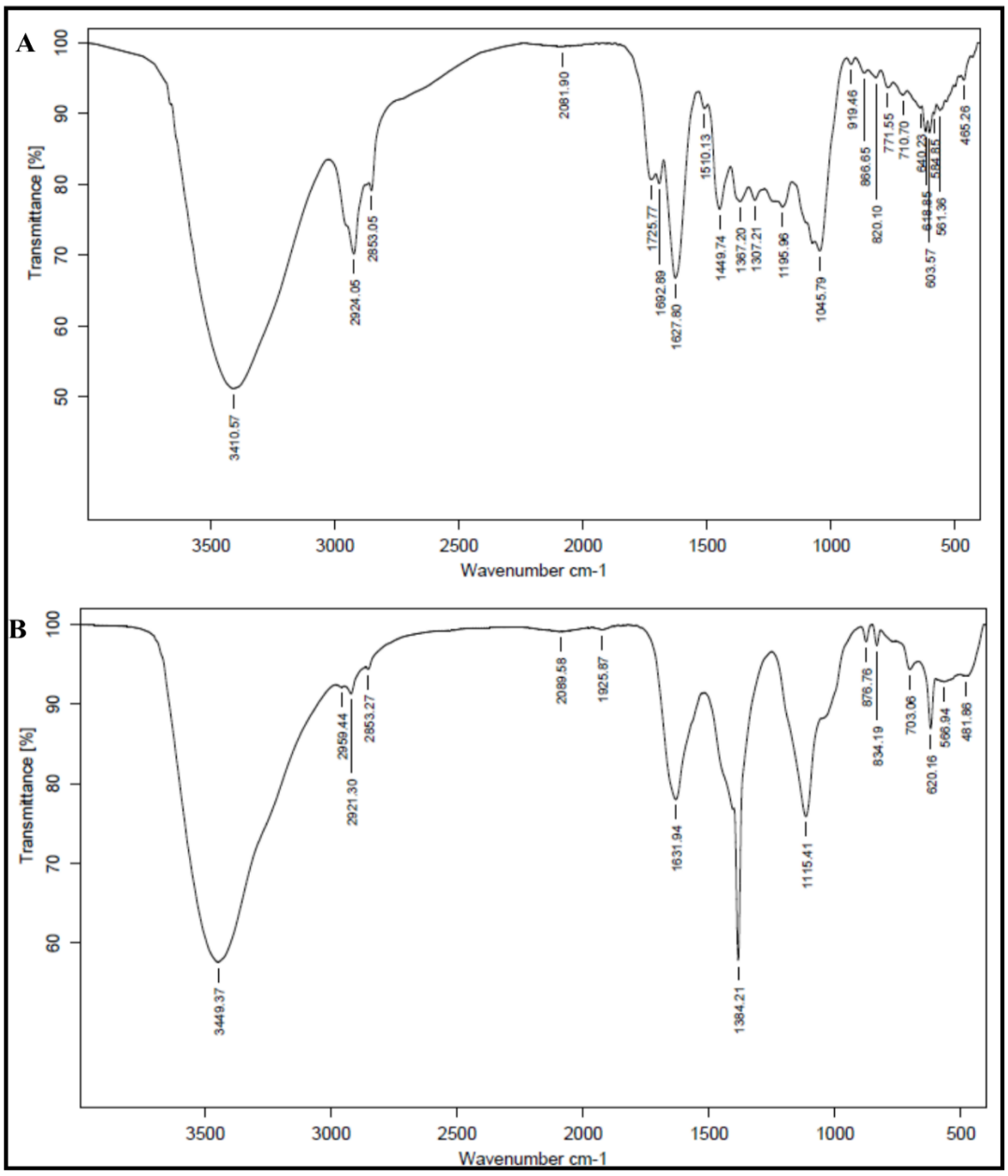

Figure 20. Fourier transformed infrared spectra of (A) Ethanolic extract of *E. camaldulensis*, and (B) Silver nanoparticles synthesized using the extract as reducing and capping agent.

2. Antimicrobial Activities of Biogenic Silver Nanoparticles on Foodborne Pathogens

Plant synthesized silver nanoparticles have demonstrated a broad-spectrum antimicrobial activity against various foodborne pathogenic and spoilage microorganisms. In this study, the synthesized silver nanoparticles exhibited good bactericidal activities against foodborne pathogenic bacteria, including *B. cereus, E. coli*, *L. monocytogenes* and *S. aureus* (Table 11). The minimum inhibitory concentrations and the minimum bactericidal concentrations ranged from 0.99–1.99 and 3.98–15.91 µg/mL, respectively. Similar findings have earlier been reported (Loo et al., 2018). Although the antimicrobial properties of silver nanoparticles have been extensively explored, the exact mechanism of action is still not fully elaborated. However, the extent of antimicrobial effects of silver nanoparticles is dependent on factors including the size, morphology, physicochemical properties of the silver nanoparticles as well as the culture medium, microbial environment, and method of synthesis (Qasim, Udomluck, Chang, Park, & Kim, 2018).

Table 11. Minimum inhibitory and minimum bactericidal concentrations of silver nanoparticles against pathogenic foodborne bacteria

Bacterial isolates	**MIC (µg/mL)**	**MBC (µg/mL)**
Bacillus cereus	0.99	3.98
Escherichia coli O157:H7	1.99	3.98
Listeria monocytogenes (F2365)	1.99	7.96
Staphylococcus aureus (ATCC 25923)	1.99	15.91

3. Silver Nanoparticles Induced Potassium Ion Leakage

Bacterial plasma membrane constitutes a permeable barrier that regulates the movements of molecules in and out of the cell cytoplasm. Thus, alterations and poration of the plasma membrane by antimicrobial agents results in the loss of functionality leading to increased efflux of important cellular electrolytes that are required for proper cell functions. The membrane disruption activities of biogenic silver nanoparticles evaluated by potassium leakage is presented in Figure 21. The results indicated silver nanoparticles concentration dependent K^+ release. Increase in the K^+ leakage after treatment with silver nanoparticles suggest an increase in the efflux of important ions from the cell and might be due to structural and functional alterations of the membrane by the silver nanoparticles or formation of pores on the plasma membrane. The results further suggested low K^+ release from *S. aureus*, this might be to the difference in MBC value observed.

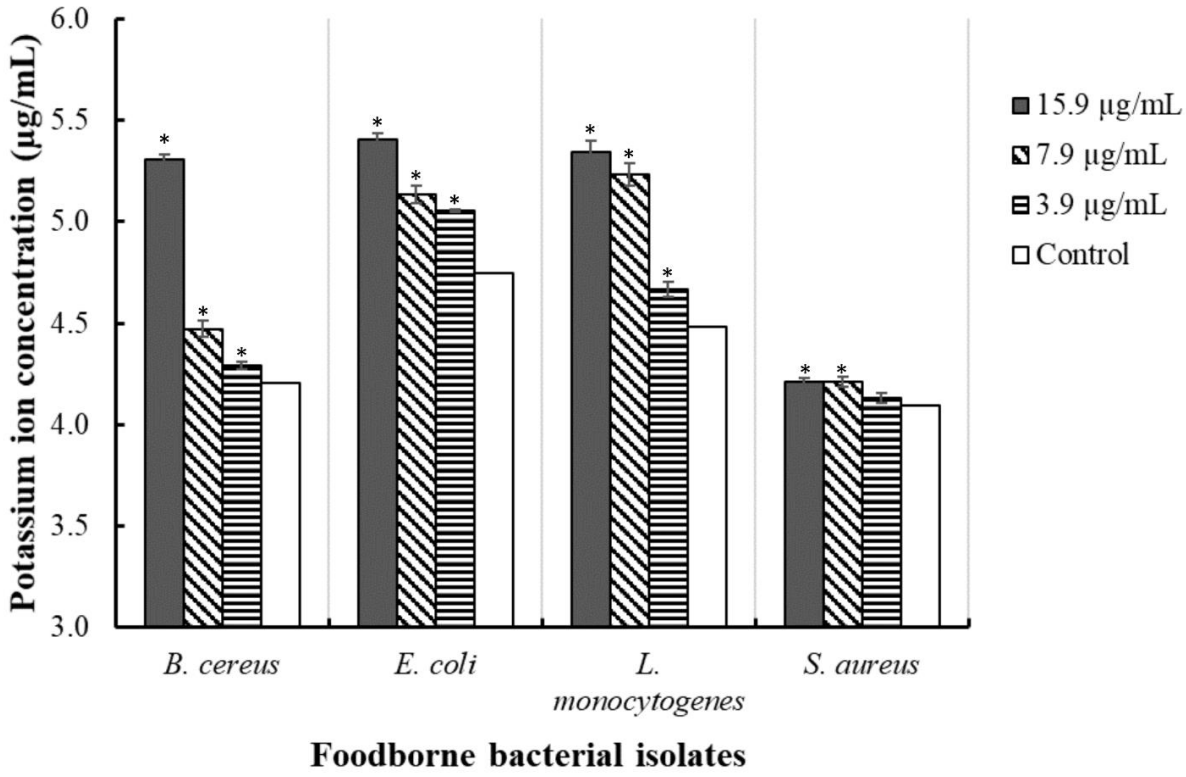

Figure 21. Silver nanoparticles induced potassium ion leakage, evaluated by measuring the concentration of potassium ion in cell free supernatants of bacterial isolates after 4 h of treatment with inhibitory and biocidal concentrations of silver nanoparticles. Values represents mean of triplicate measurements and *represents significant difference between treatment and control at ($P<0.05$).

4. Effect of Silver Nanoparticles on Bacterial Cell Membrane

The effects of the silver nanoparticles on the cell membrane of pathogenic bacterial isolates and strains was confirmed by scanning electron microscopy (Figure 22). The micrograph presented intact and healthy cell membrane for untreated control cells, whereas silver nanoparticles treated cells were observed to exhibit extensive membrane damage with structural deformation, poration and shrinkage. Bacterial cell membrane plays an important role as selective permeable barrier. Disruption of the cell membrane due to treatment with silver nanoparticles alters the membrane functionality, resulting in the influx of extracellular molecules into the cell, leading to lysis of the cell. The micrograph confirms that silver nanoparticles exerts its antibacterial effects by disrupting the cell membrane of the cell and thus enhancing the influx and efflux of extracellular materials and intracellular components, respectively.

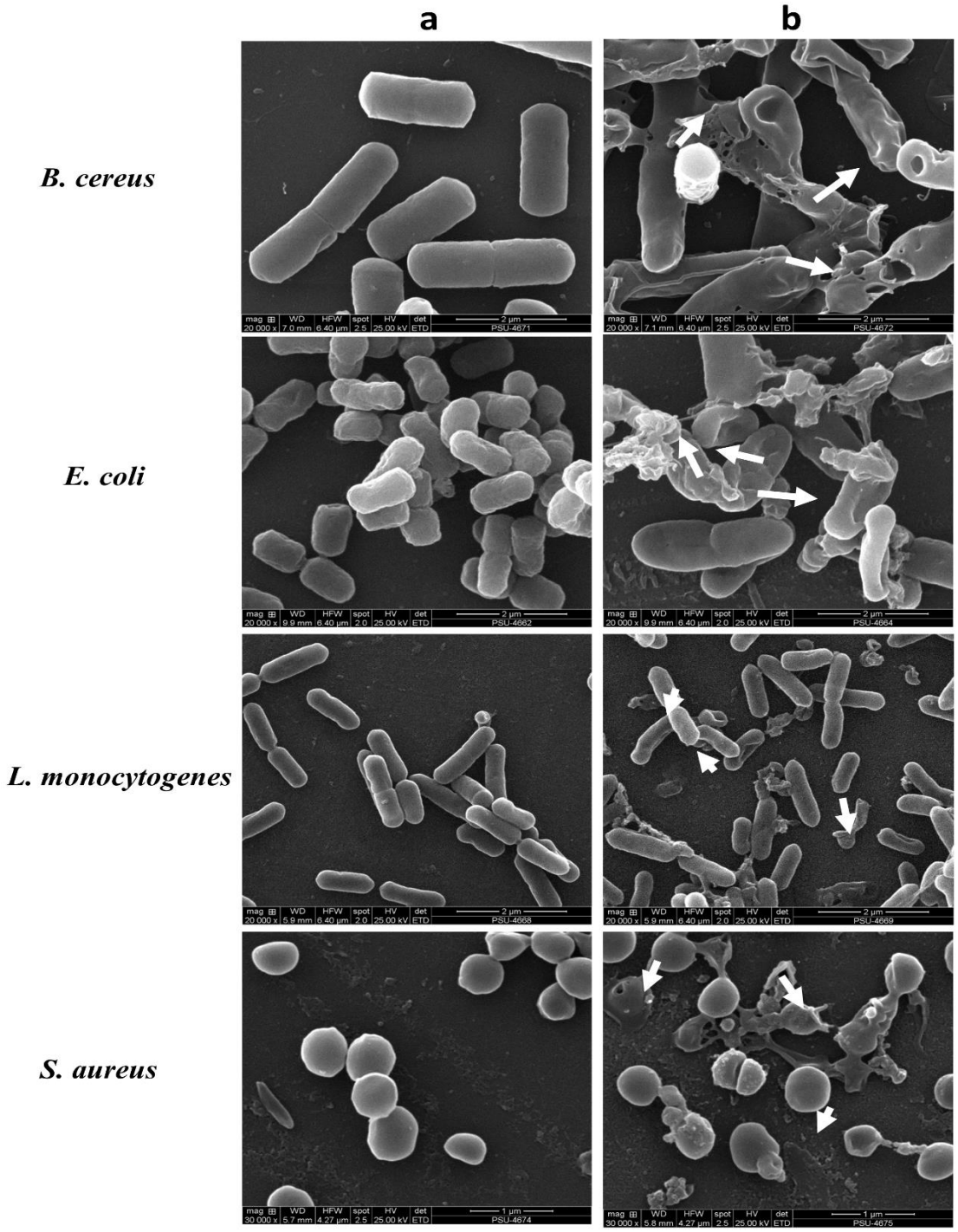

Figure 22. Effects of silver nanoparticles on bacterial cell membrane, observed using scanning electron microscopy, showing (a) healthy control cells, (b) treated cells with membrane disruption, poration and lysis (arrow in whites).

Part IV. Fabrication of Antibacterial Chitosan-PVA Based Nanocomposite Food Packaging Functionalized with Biogenic Silver Nanoparticles

1. Fabrication of Nanocomposite Films

UV–visible spectroscopy of the film forming solutions showed the characteristic peak at 437 nm corresponded to the surface plasmon resonance signature of Ag nanoparticles (Figure 23), suggesting the formation of Ag nanoparticles by the reduction of $AgNO_3$ with the ethanolic extracts of *E. camaldulensis.* The ICP–OES results for film forming solution showed Ag concentration of 2.83 ± 0.03, 0.89 ± 0.06 and 0.15 ± 0.05 µg/mL for 1:1, 1.5:0.5, and 1.75:0.25 (Table 12). The pure PVA–CH film solution did not show this peak, thus confirming that the peaks resulted from the addition of the Ag nanoparticles. In addition, the intensity of the peak varied with the concentration of the Ag nanoparticles incorporated. The result showed that Ag nanoparticles were stable and detectable in the film forming solution.

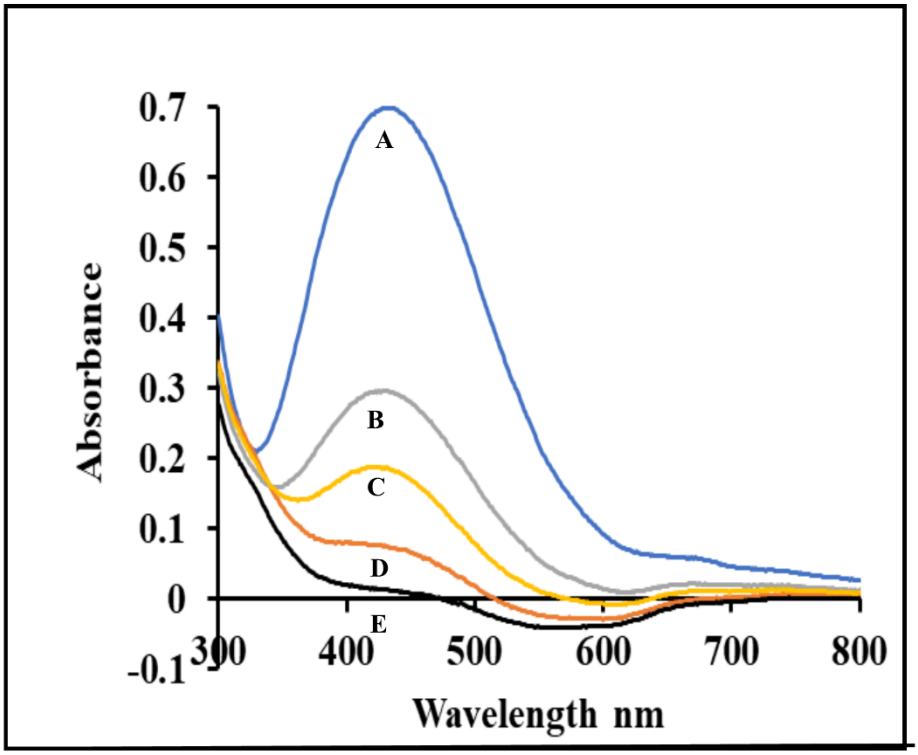

Figure 23. UV-vis spectra of silver NPs, polyvinyl alcohol–chitosan, and polyvinyl alcohol–chitosan/silver nanoparticles film forming solutions. Colloidal Silver nanoparticles (A), PVA-CH/Silver nanoparticles 1:1 (B), PVA-CH/Silver nanoparticles 1.5:0.5 (C), PVA-CH/Silver nanoparticles 1.75:0.25 (D), and PVA-CH (E)

Table 12. Silver nanoparticles content in filmogenic solution expressed in (mg/L) as revealed by ICP-OES (n=3).

Samples	**Ag^+ Concentration (mg/L)**			**Mean**	**SD**
1:1	2.84	2.86	2.79	2.83	0.03
1.5:0.5	0.83	0.88	0.95	0.89	0.06
1.75:0.25	0.18	0.10	0.18	0.15	0.05

2. FTIR Spectra

The FTIR spectra of the films, Ag nanoparticles, chitosan and polyvinyl alcohol are shown (Figure 24). The PVA and chitosan spectra were similar to those previously reported (Kumar, Krishnakumar, Sobral, & Koh, 2019; Mauricio-Sánchez, Salazar, Luna-Bárcenas, & Mendoza-Galván, 2018). Both PVA and chitosan showed an absorption broad band between 3300–3500 cm^{-1} and 2900–2940 cm^{-1} which were ascribed to the O–H and N–H stretching vibrations and the asymmetric stretching of the $–CH_2$. The chitosan peak at 1650 cm^{-1} was ascribed to amide group, while the PVA peak around 1720 cm^{-1} indicates the stretching vibration of C=O (Siripatrawan & Vitchayakitti, 2016). Absorption bands between 1380–1373 cm^{-1} indicated the CH_2 and C–H vibrations, respectively (Mohanapriya et al., 2017). Band at 1115 cm^{-1} in the PVA spectrum was assigned to the CH (Abdelrazek, Elashmawi, & Labeeb, 2010). The spectrum for the green synthesized silver Nanoparticles showed similar bands at 3449, 2921, 1631, and 1384 cm^{-1} corresponding to the O–H, $–CH_2$, C=O and C–H vibrations. The PVA–CH/Ag nanoparticles film showed the same pattern of bands as the PVA–CH (control) film, with a prominent band at 1030 cm^{-1} corresponding to C–O stretching from alcohols, ethers, esters, carboxylic acid, and C–N stretching vibrations of the amine (Paosen et al., 2017).

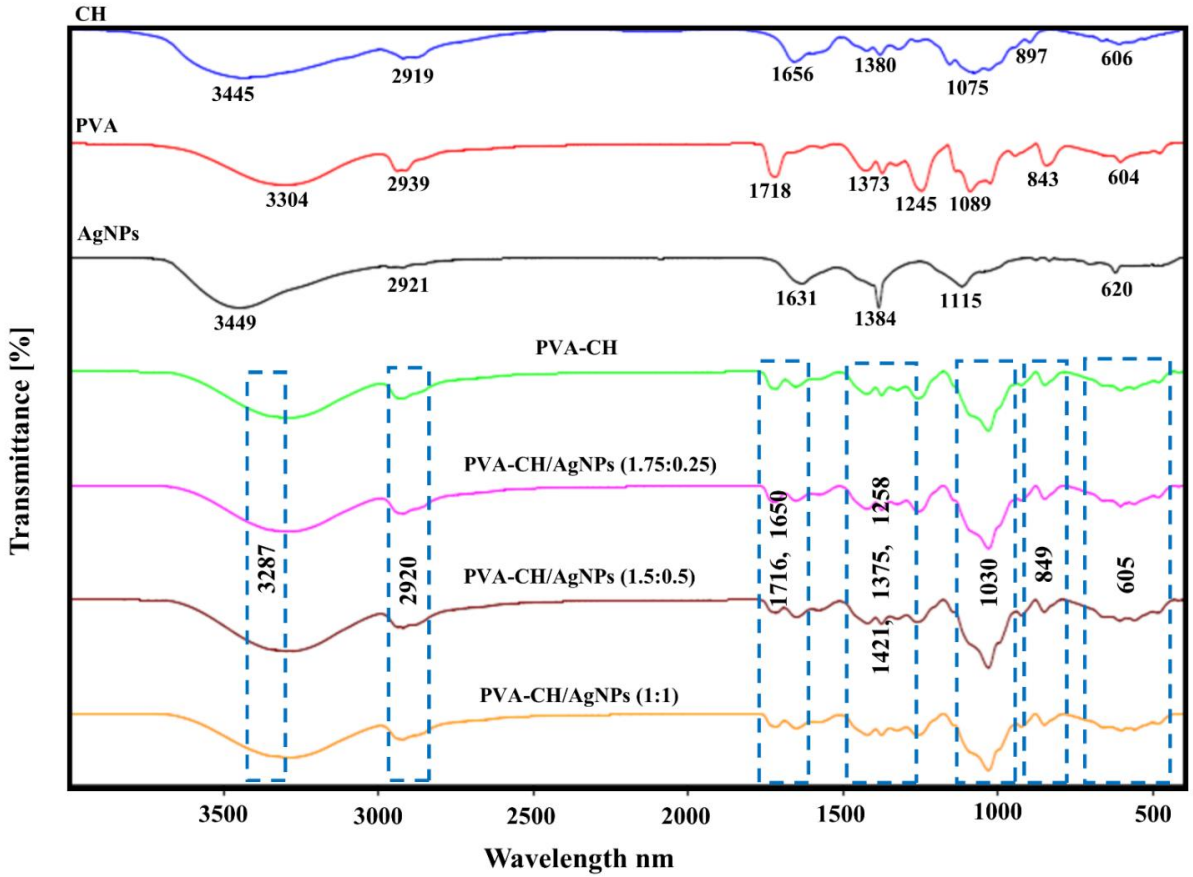

Figure 24. FTIR spectra of chitosan, polyvinyl alcohol, polyvinyl alcohol-chitosan films, and polyvinyl alcohol-chitosan films incorporating silver nanoparticles.

3. X–ray Diffraction

The X–ray diffractograms of the films are shown (Figure 25A). The PVA–CH film exhibited three characteristic peaks representing the crystalline phase at 2θ = 9.5º, the amorphous phase with a broad peaks at 19.5º and a low intensity band at 28.6º similar to previous reports (Azizi, Ahmad, Ibrahim, Hussein, & Namvar, 2014; Choo, Ching, Chuah, Julai, & Liou, 2016). The diffractogram of the PVA–CH/Ag nanoparticles films showed peaks similar to that of the pure PVA–CH film. However, the intensity of the peaks at 2θ = 9.5º and 2θ = 28.6º increased in the PVA–CH/Ag nanoparticles 1:1 and 1.5:0.5 films. The diffractogram revealed that the films showed amorphous to crystalline form. It further reveals that the addition of the green synthesized silver nanoparticles did not affect the structural uniformity of the co–polymer blended film. Previous works have demostrated the presence of silver peaks in the diffractogram of silver nanoparticles loaded chitosan films with peaks at 2θ range of 30–50º, corresponding to the (111) and (200) planes of the silver nanoparticles (Djerahov, Vasileva, Karadjova, Kurakalva, & Aradhi, 2016; Vimala et al., 2010). Silver peaks were detected at 2θ = 38.0º, in the presence of 1.5% silver (López-Carballo, Higueras, Gavara, & Hernández-Muñoz, 2012). However, peaks corresponding to the reflection plane of silver were not observed in this study. This might be as a result of the low concentrations of silver used in this study.

4. Water Permeability of Films

The water vapor permeability is an important parameter in the design of food packaging material. High WVP exposes products to contact with water, resulting in speedy deterioration and decay of packaged foods (Wu, Huang, Li, Xiao, & Wang, 2018). The result suggested that an increase in water vapor permeability for sample 1.75:0.25 (Figure 25B). However, a decrease in the WVP was observed for samples (1:1 and 1.5:0.5). Previous studies had reported a decrease in the WVP of polymer films after the incorporation of Ag nanoparticles (Ortega, Giannuzzi, Arce, & García, 2017; Shankar, Rhim, & Won, 2018). The decrease in WVP might be due to the decreased mobility of the polymer chains attributable to the existence of Ag nanoparticles as a discontinuous phase in the film matrix, thus creating a tortuous path for the diffusion of water vapor (Shankar et al., 2018). Factors including the nature of polymer matrix, type of nanofiller, and the concentration of nanofiller might also influence the WVP of polymer films (Roy et al., 2019).

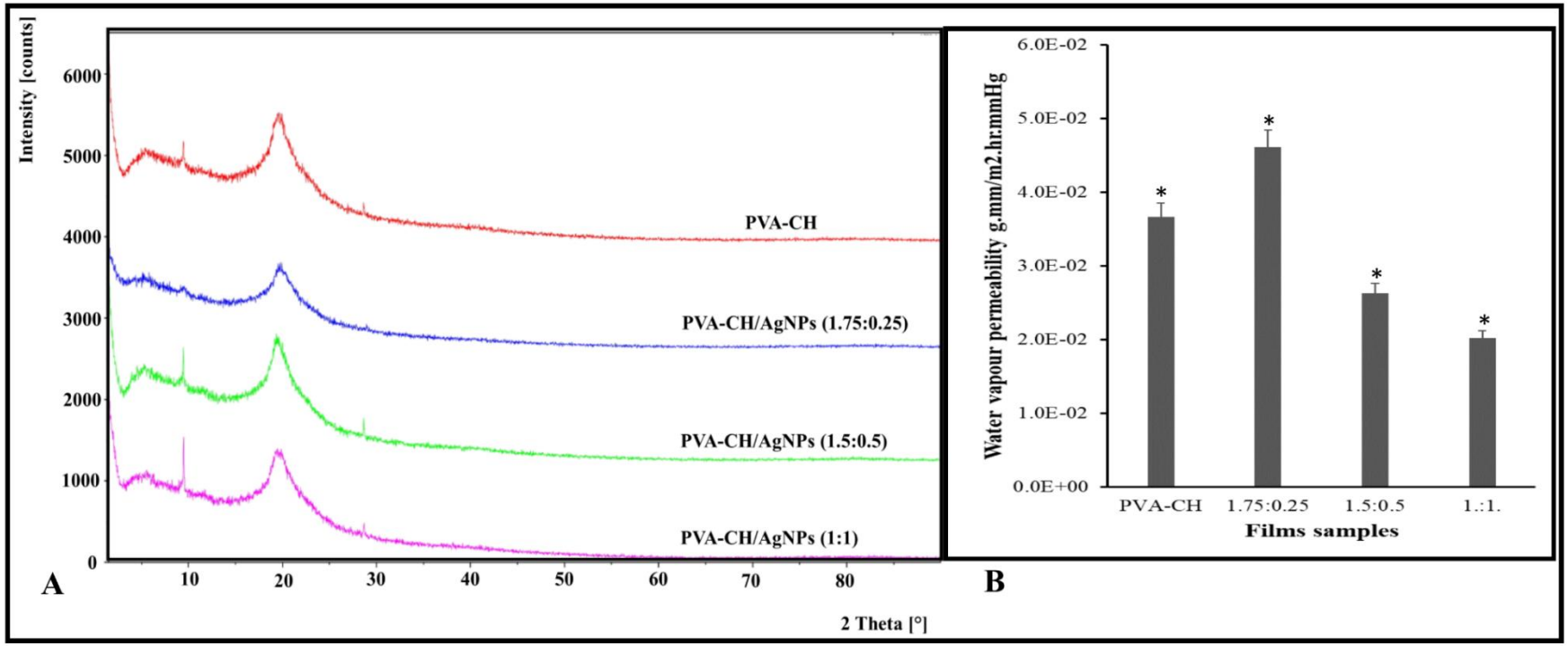

Figure 25. XRD diffractograms (A) and water vapour permeability of polyvinyl alcohol-chitosan films (A) and polyvinyl alcohol-chitosan films incorporating silver nanoparticles (B). * represent significant difference ($p < 0.05$).

5. Thermal Analysis of Films

The DSC thermogram of the control film had two endothermic peaks at temperatures of 52.2 ºC and enthalpy of 114 J/g (Figure 26A), corresponding to the water vapourization temperature and 195 ºC and enthalpy of 58 J/g, representing the melting temperature of PVA (Pervez & Stylios, 2018; Vega-Cázarez et al., 2018). The thermogram of the Ag nanoparticles incorporated films (1.75:0.25, 1.5:0.5, and 1:1) showed single peaks at temperatures 52, 58, and 55 ºC with enthalpies of 187, 255, and 256 J/g, respectively. The results suggested a slight increase in the energy needed to vapourize the moisture contained within the film. In addition, the decomposition peak of PVA was not detected in the Ag nanoparticles films.

Thermogravimetric analysis was used to evaluate the stability and thermal decomposition of the polymer blend films (Figure 26C). Initial weight loss of 4–15% at the temperature range of 31–175 $^{\circ}$C due to the evaporation of trapped water (moisture content) in the polymer films. The second and third stages of weight loss observed at temperature range 140–270 $^{\circ}$C and 270–310 $^{\circ}$C were attributed to the degradation of the PVA and chitosan polymer (Abu-Saied et al., 2017; Merlusca et al., 2018). The fourth and fifth degradation phase occurred at temperature range of 300–420 ºC and 400–550 ºC, respectively. The TGA thermogram of the films showed similar pattern, with no visible changes in the thermal degradation patterns of the films. Thus, confirming the compatibility between the polymers and the Ag nanoparticles.

DTA results of the films showed two broad endothermic peaks between 29–127 ºC and 178–284 ºC with T_{max} at 78–93 ºC and 222–244 ºC, corresponding to a cumulative weight loss of 25–46% as shown in the TGA. The initial weight loss is

probably due to loss of structured water in parallel with a transformation to semi amorphous state. The second phase of weight loss suggested thermal decomposition of film samples (Figure 26B). The results suggest good thermal stability of films to temperature above 200 ºC.

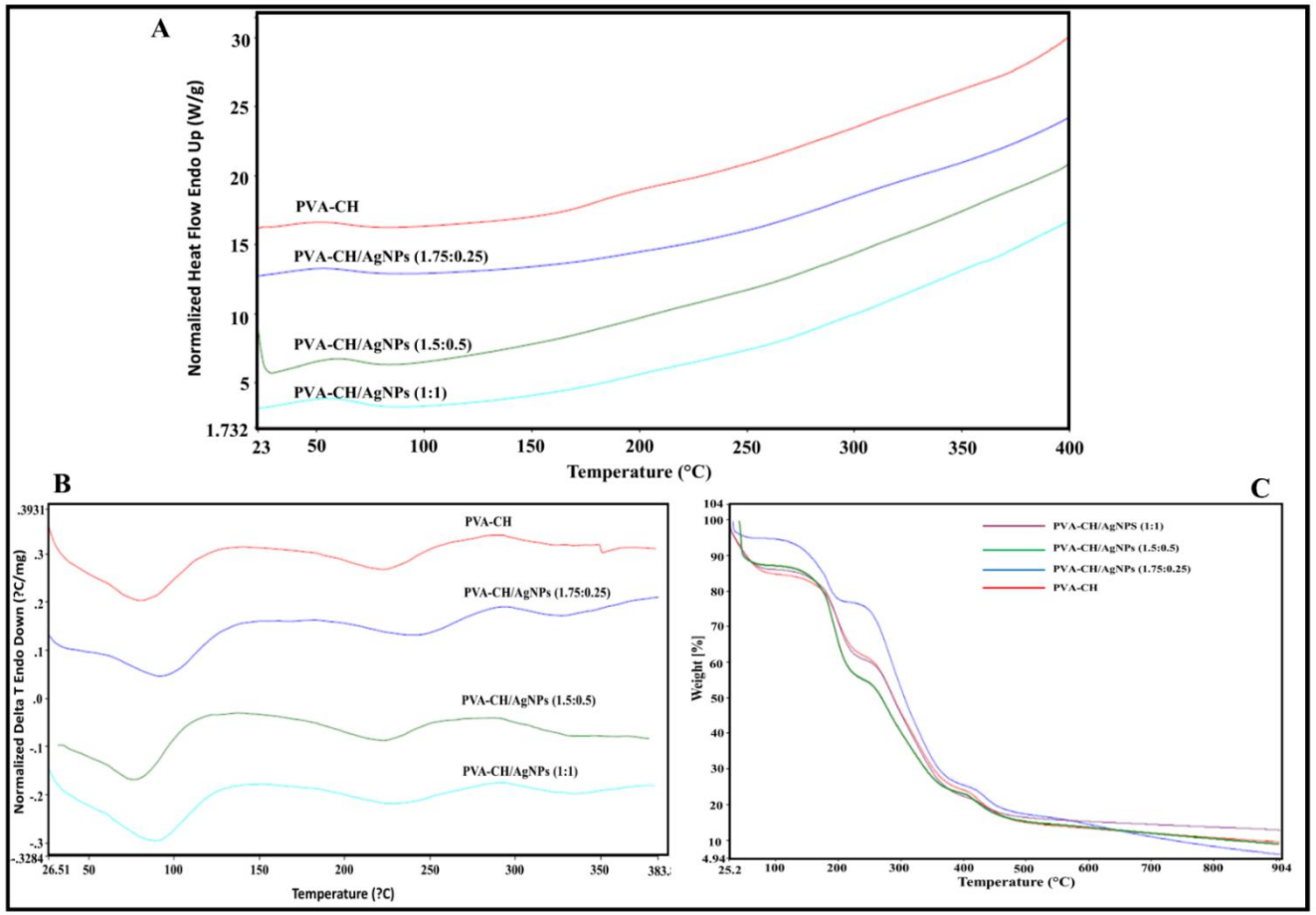

Figure 26. Thermal properties of PVA-CH (control) film and PVA-CH/silver NPs film. Differential scanning calorimeter (A), Differential thermal analysis (B) and the thermogravimetric profile (C).

6. Mechanical Properties of Film

The mechanical properties of packaging materials are important factors that determines the applicability of the material. In this study, the thickness, tensile strenght, young's modulus, elongation at break, water content, and swollen ratio of the samples were measured (Table 13). An insignificant reduction in the thickness of the films was observed, resulting from the addition of the Ag nanoparticles ($p < 0.05$). The reduction in thickness observed after the addition of the green synthesized silver nanoparticles resulted from the variations in water content and decrease in polymer content Ag nanoparticles incorporated films. The tensile strength of the films increased with increase in the Ag nanoparticles ratio. However, the effects of the Ag nanoparticles on tensile strength were not significant ($p<0.05$). Previous studies have reported similar tensile strength for PVA/CH films (Cheng, Hong, Lee, Lai, & Tsai, 2018; Merlusca et al., 2018). Variations in the tensile strength and elongation at break of the PVA–CH film is dependent on the PVA and chitosan contents, concentration of the plasticizer (Kasai et al., 2018; Wu, Ying, Liu, Zhang, & Huang, 2018). In addition, the PVA–CH (control) film showed the highest water content compared to the Ag nanoparticles incorporated films. This might be due to the variation in thickness and higher surface area for entrapment of water molecules. The results suggested that the incorporation of the synthesized Ag nanoparticles had no negative effects on the mechanical properties of the film.

7. Physical and Optical Properties

The PVA–CH (control) films showed limited protection against UV–light with a transmittance of at 600 nm. Incorporation of the green synthesized Ag nanoparticles into the film significantly ($p<0.05$) decreased the transmittance values (Table 14). The transmittance value of the PVA–CH/Ag nanoparticles films ranged from 60–80%. Transmittance reduced with the increase in the ratio of Ag nanoparticles. This indicates that incorporation of Ag nanoparticles in the PVA–CH film had good barrier property against light transmission to the food product. However, the transparency of the PVA–CH/Ag nanoparticles films showed no significant differnce when compared with the control film ($p<0.05$). Thus, the difference in transmission resulting from the variations in the colour and thickness of the films had no effects on the transparency of the film. Reduction in transmittance with the addition of Ag nanoparticles has previously been reported (Dairi et al., 2019; Roy et al., 2019). The true density values of the Ag nanoparticles incorporated films were also similar to that of the control film, with no significant differnce at ($p<0.05$). Furthermore, viscosity evaluation of film forming solutions showed that the control solution were more viscous, as a result of higher polymer contents and reduced water content. Viscosity reduced with the increase in the ratio of incorporated Ag nanoparticles.

Table 13. Mechanical properties of the polyvinyl alcohol-chitosan films and polyvinyl alcohol-chitosan films incorporating silver nanoparticles; (Mean ± SD), n = 4.

Samples	Tensile Strength (MPa)	EAB (%)	Thickness (mm)	Young's modulus (MPa)
Control	12.9 ± 0.44^{b}	53.6 ± 0.28^{b}	0.044 ± 0.002^{a}	0.046 ± 0.002^{a}
1.75:0.25	13.4 ± 0.48^{b}	59.4 ± 0.84^{b}	0.041 ± 0.002^{a}	0.043 ± 0.004^{a}
1.5:0.5	18.1 ± 0.85^{b}	62.0 ± 0.71^{b}	0.033 ± 0.001^{a}	0.037 ± 0.004^{a}
1:1	19.8 ± 0.55^{b}	52.3 ± 0.83^{b}	0.030 ± 0.002^{a}	0.039 ± 0.006^{a}

Values represents mean ± standard deviation, ^{a} = significantly difference, ^{b} = not significantly difference, ($p < 0.05$).

Table 14. Physicochemical properties of the polyvinyl alcohol-chitosan films and polyvinyl alcohol-chitosan films incorporating silver nanoparticles; (Mean ± SD), n = 4.

Samples	Transmission (%)	Transparency (A_{600}/mm)	True density (g/cm^3)	Viscosity (cP)	MC (%)	Swollen ratio (%)
Control	86.6 ± 0.005^a	3.29 ± 0.00^b	1.19 ± 0.002^b	46.6 ± 0.40^a	31.4 ± 0.02^b	4.78 ± 0.11^a
1.75:0.25	79.8 ± 0.002^a	3.29 ± 0.00^b	1.20 ± 0.002^b	32.0 ± 0.22^a	29.2 ± 0.93^b	6.78 ± 0.66^b
1.5:0.5	75.3 ± 0.003^a	3.36 ± 0.00^b	1.16 ± 0.003^b	23.6 ± 0.10^a	24.6 ± 0.16^a	6.98 ± 0.35^b
1:1	60.0 ± 0.005^a	3.30 ± 0.00^b	1.16 ± 0.004^b	12.2 ± 0.05^a	24.6 ± 1.65^a	8.32 ± 0.21^a

Values represents mean ± standard deviation, ^{a} = significantly difference, ^{b} = not significantly difference, ($p < 0.05$).

8. Water Contact Angle and Surface Energy of Films

The contact angle and surface energy are important surface parameters for the evaluation of wettibility and hydrophillicity. The results suggested that all the samples were hydrophilic with contact angle < 90º (Figure 27). The results are similar to previous works that reported that PVA, chitosan and PVA/CH blended films were hydrophilic (Cheng et al., 2018; Parsa, Paydayesh, & Davachi, 2019; Shankar & Rhim, 2018). A significant increase was observed ($p<0.05$) in the films containing Ag nanoparticles when compared to the control, indicating an increase in the hydrophobicity of the PVA–CH/Ag nanoparticles films. Increase in contact angles of polymer nanocomposite films, resulting from the addition of ZnS and Ag^{+} nanoparticles has been previously reported (Yun, Kim, Shim, & Yoon, 2018) and (Shankar & Rhim, 2017). The observed low contact angle of the films is a reflection of the hydrophilicity of the polymers (Merlusca et al., 2018; Parsa et al., 2019). In addition, a decrease in the free energy of the film was observed for films (1.5:0.5 and 1:1), indicating a disruption of intermolecular bonds of adhesion.

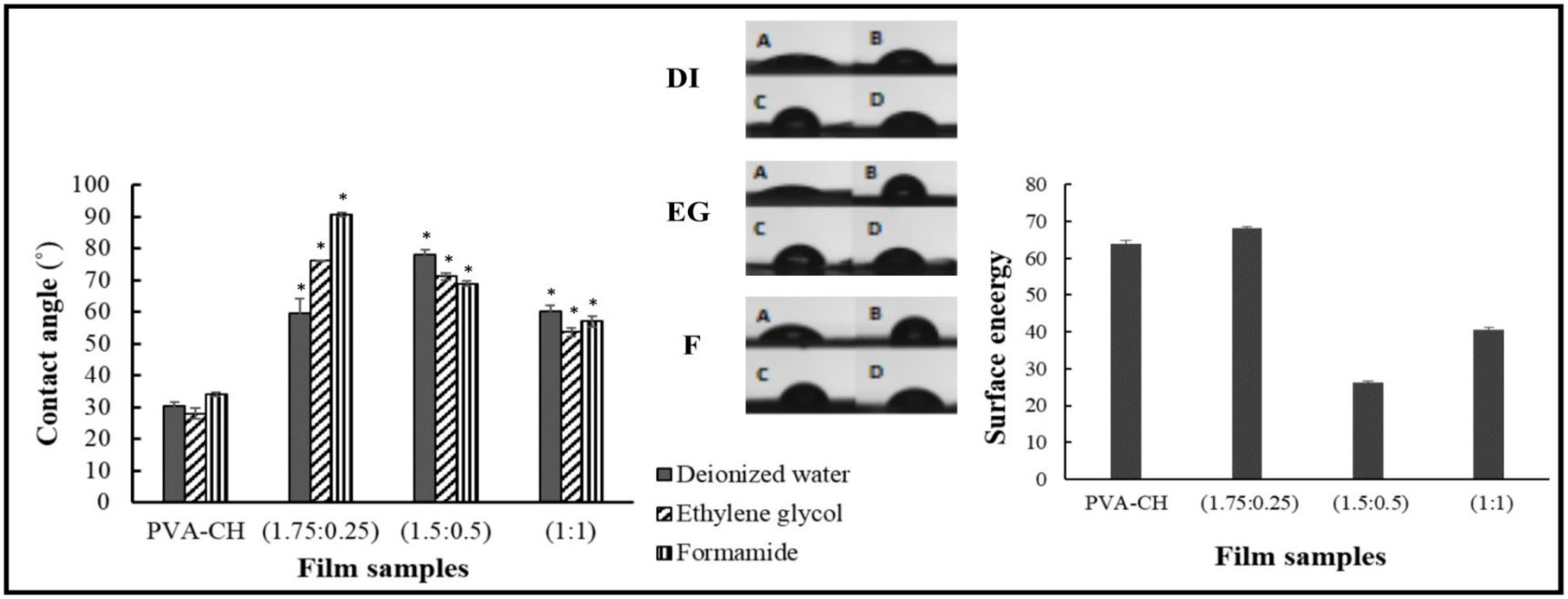

Figure 27. Contact angle and free energy of the polyvinyl alcohol-chitosan films and polyvinyl alcohol-chitosan films incorporating silver nanoparticles analyzed using sessile drop method with deionized water, ethylene glycol and formamide as the probe solvents.

9. Atomic Force Microscopy

The 2D and 3D surface topographic images of the samples are shown in (Figure 28). The results showed that the addition of the Ag nanoparticles resulted in a significant ($p \leq 0.05$) reduction in the average roughness (Ra) and the root mean square roughness (Rq) for film (1.5:0.5 and 1:1) with less cavities when compared to the control film. The addition of nanoparticles was previously reported to result in an increase in surface roughness (Wu et al., 2019). The difference in the observed result might be due to the difference in the polymer used or difference in the methods employed for the fabrication of the films. Moreover, the formation of cavities in polymer films has been related to the slow evaporation (mass transfer) of the solvent from the film forming solution, and consequently, a slower drying speed (Espitia et al., 2013). Thus, the high polymer content of the PVA–CH (control) film might have impaired water evapouration resulting in the formation of cavities and increased roughness.

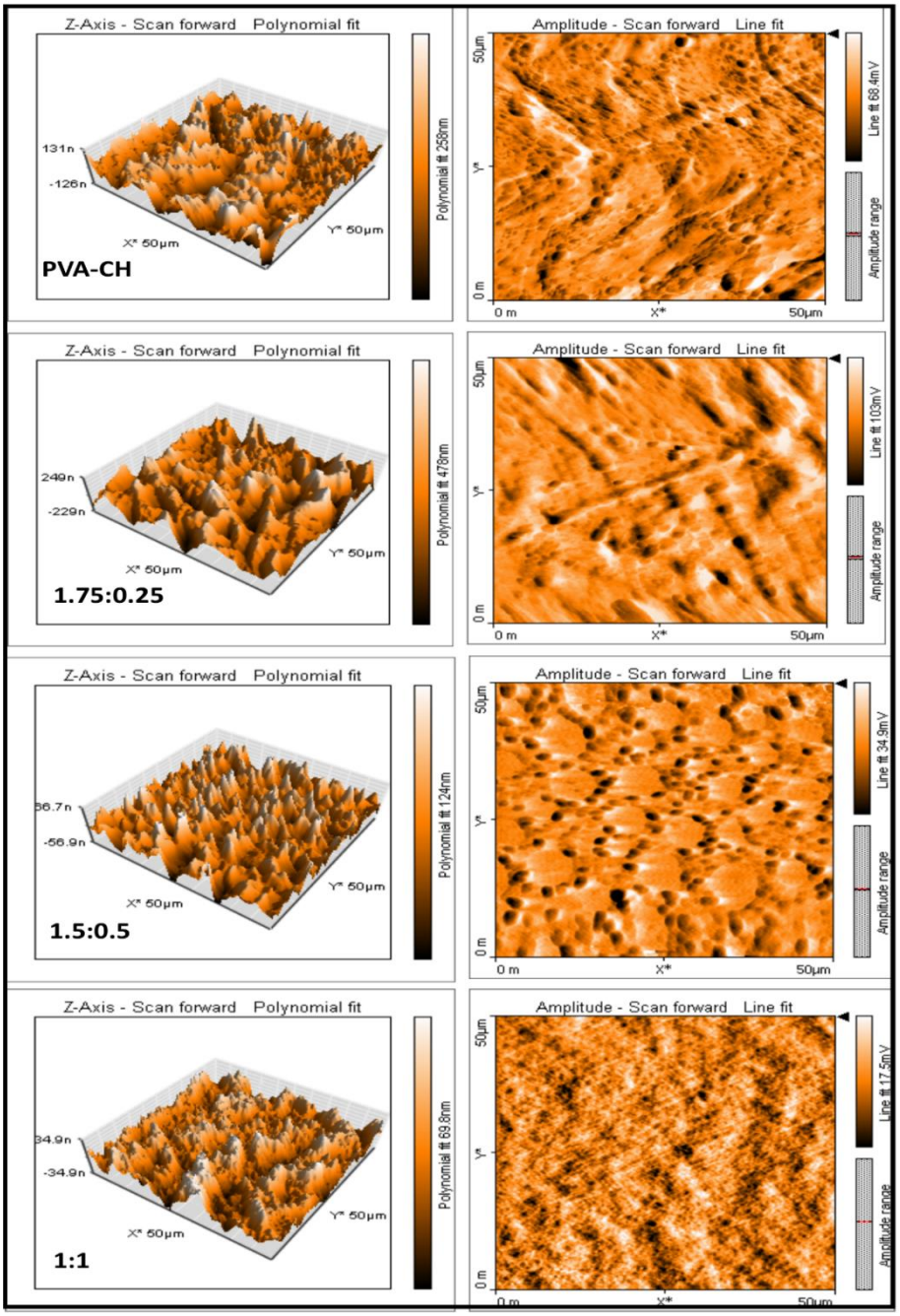

Figure 28. Atomic force micrographs (2D and 3D) of polyvinyl alcohol-chitosan films and polyvinyl alcohol-chitosan films incorporating silver nanoparticles.

10. Antimicrobial Activity of The Film

The efficacy of PVA/CH and the Ag nanoparticles incorporated films is shown (Figure 29). The Ag nanoparticles incorporated films showed good antimicrobial activities that varied directly with the concentration of the Ag nanoparticles. Film (1:1) showed bactericidal activity against all the tested organisms with a 99.9% reduction in CFU/mL. At 12 h, ≥ 3log reduction in CFU/mL was observed against *L. monocytogenes* F2365 and *S. aureus* ATCC 25923 when compared with the control. A more pronounced antimicrobial activity was observed against *E. coli* O157:H7 and *B. cereus* with ≥ 4 log and ≥ 6 log reduction in CFU/mL after 6 h treatment, respectively. Film (1.5:0.5), showed an inhibitory effect on the pathogens within 6–12 h of treatment. However, after the initial 12 h of treatment, a rapid increase was observed. Previous studies reported similar results showing antimicrobial activities of polymer films that were dependent on the concentration Ag nanoparticles against *E. coli* and *S. aureus* (López-Carballo et al., 2012) and *E. coli, Salmonella typhimurium*, *Salmonella enterica, Pseudomonas aeruginosa, Klebsiella pneumonia*, *B. cereus, S. aureus* and *Micrococcus luteus* (Hajji et al., 2017). In addition, the antimicrobial activities of chitosan have been demonstrated in various studies. However, the PVA–CH control films did not exhibit antimicrobial effects against the tested bacteria. The results revealed that the antimicrobial activities of the PVA–CH/Ag nanoparticles films resulted from the incorporation of Ag nanoparticles. Ag nanoparticles exhibits excellent antimicrobial activities with broad applications in various fields. The antimicrobial properties of Ag nanoparticles have been ascribed to properties such as, the surface charge and nano-size of the particles. The mechanism mainly involves cell membrane damage, disruption of energy

metabolism, generation of oxidative stress due to ROS formation, and inhibition of transcription (Singh, Garg, Pandit, Mokkapati, & Mijakovic, 2018).

11. Antioxidant Activity of Films

The results of the DPPH and ABTS assays suggested that all the films showed antioxidant activity (Figure 30). However, an increased antioxidant activity correlating with the concentrations of Ag nanoparticles was observed in the PVA–CH/Ag nanoparticles films. Antioxidant activity against DPPH, has previously been related to the chitosan and silver amount in the nanocomposite films (Hajji et al., 2017). The (1:1) film showed the highest antioxidant activity with a percentage inhibition equavalent to 19.4 and 16.7 µg/mL of ascorbic acid for DPPH and ABTS assays, respectively. Films (1.5:0.5 and 1.75:0.25) also had antioxidant activities that were higher than the PVA–CH (control) film, with percentage inhibition values of 12.3, 1.9 and 10.1, 8.8 µg/mL of ascorbic acid equivalents for DPPH and ABTS assays, respectively. The antioxidant properties of the PVA–CH control films reflects the radical scavenging ability of chitosan (Yen, Yang, & Mau, 2008). Free radical oxidative chain reaction is a basic mechanism of lipid and protein peroxidation, and thus are significant triggers of food spoilage process. Addition of antioxidants and free radical scavenging agents inhibits the generation of free radical molecules, thus inhibiting peroxidation of food products (López de Dicastillo et al., 2011).

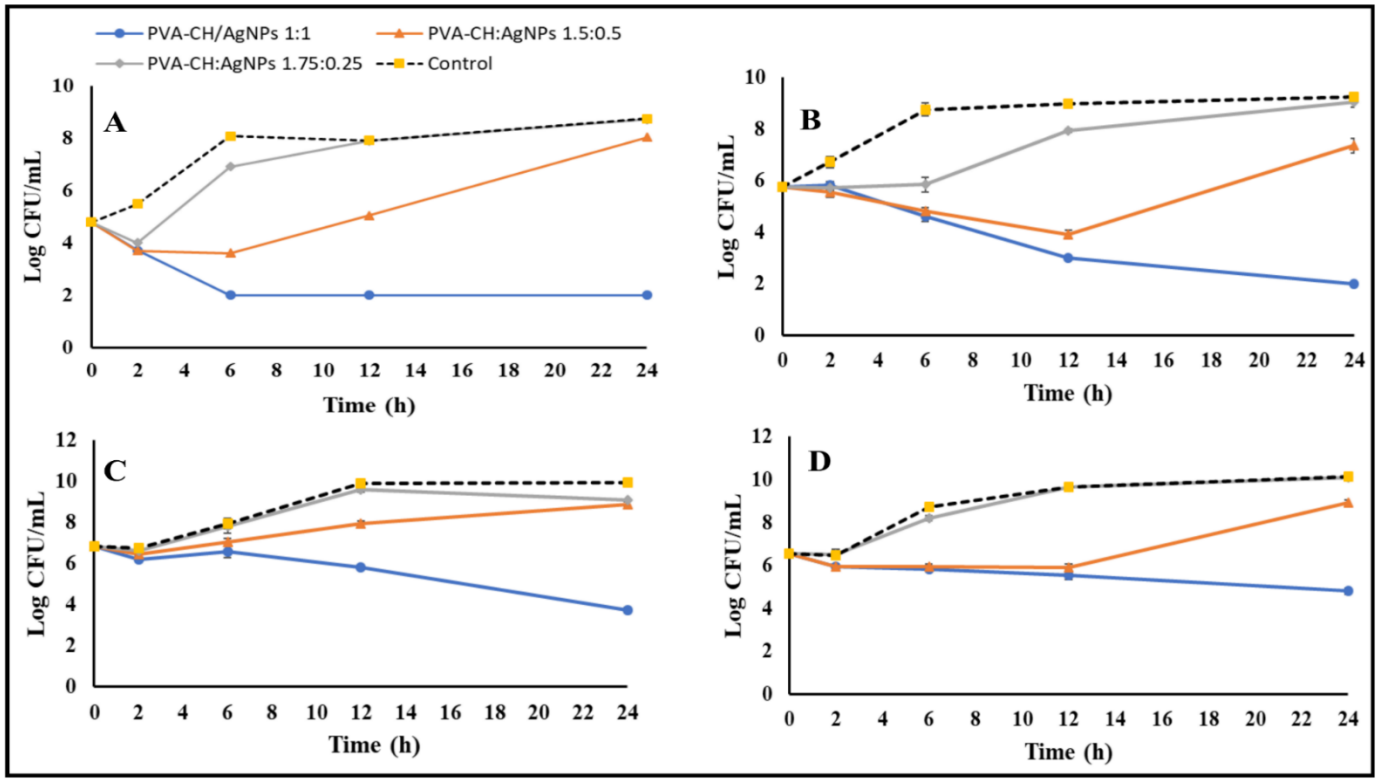

Figure 29. Antimicrobial activity polyvinyl alcohol-chitosan films and polyvinyl alcohol-chitosan films incorporating silver nanoparticles against foodborne pathogenic bacteria *Bacillus cereus* (A), *Escherichia coli* O157:H7 (B), *Listeria monocytogenes* F2365 (C) and *Staphylococcus aureus* ATCC 25923.

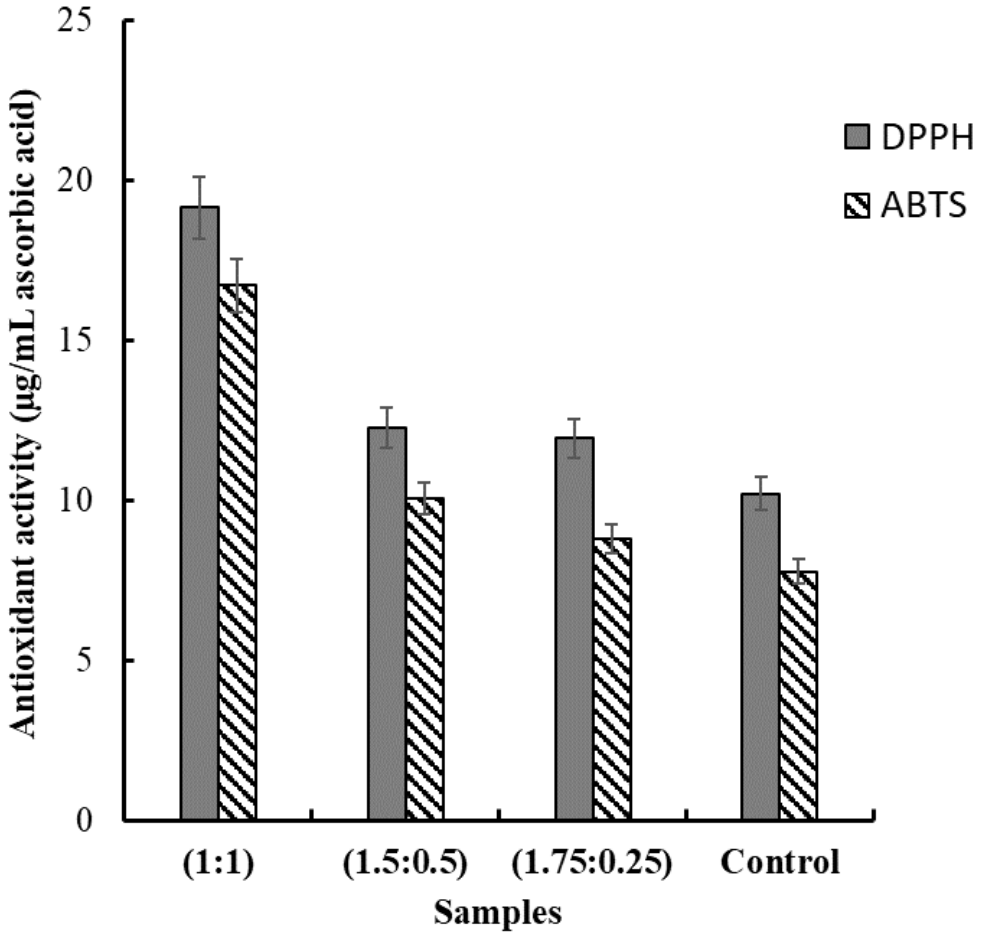

Figure 30. Antioxidant activity of polyvinyl alcohol-chitosan films and polyvinyl alcohol-chitosan films incorporating silver nanoparticles, measured using DPPH and ABTS free radical scavenging assays.

12. Effects of Film Wrap on The Shelf Life of Chicken Sausage

The spoilage retarding effects of the films monitored on sausage slices are presented (Figure 31). The films (1:1 and 1.5:0.5) showed good shelf life extension effects over the storage period. Compared with the control, the (1.5:0.5) film showed signs of deterioration after 15 days storage, whereas the 1:1 film remained visually intact without any sign of spoilage. However, early spoilage signs were visible for PVA–CH film without Ag nanoparticles and the unwrapped control on day 7 and 15 but were more pronounced in the unwrapped sample. This variation might be due to the already documented antifungal properties of chitosan present in the film (Avelelas et al., 2019). The results further revealed that the Ag nanoparticles incorporated films could serve as an active packaging material for the extension food products shelf life.

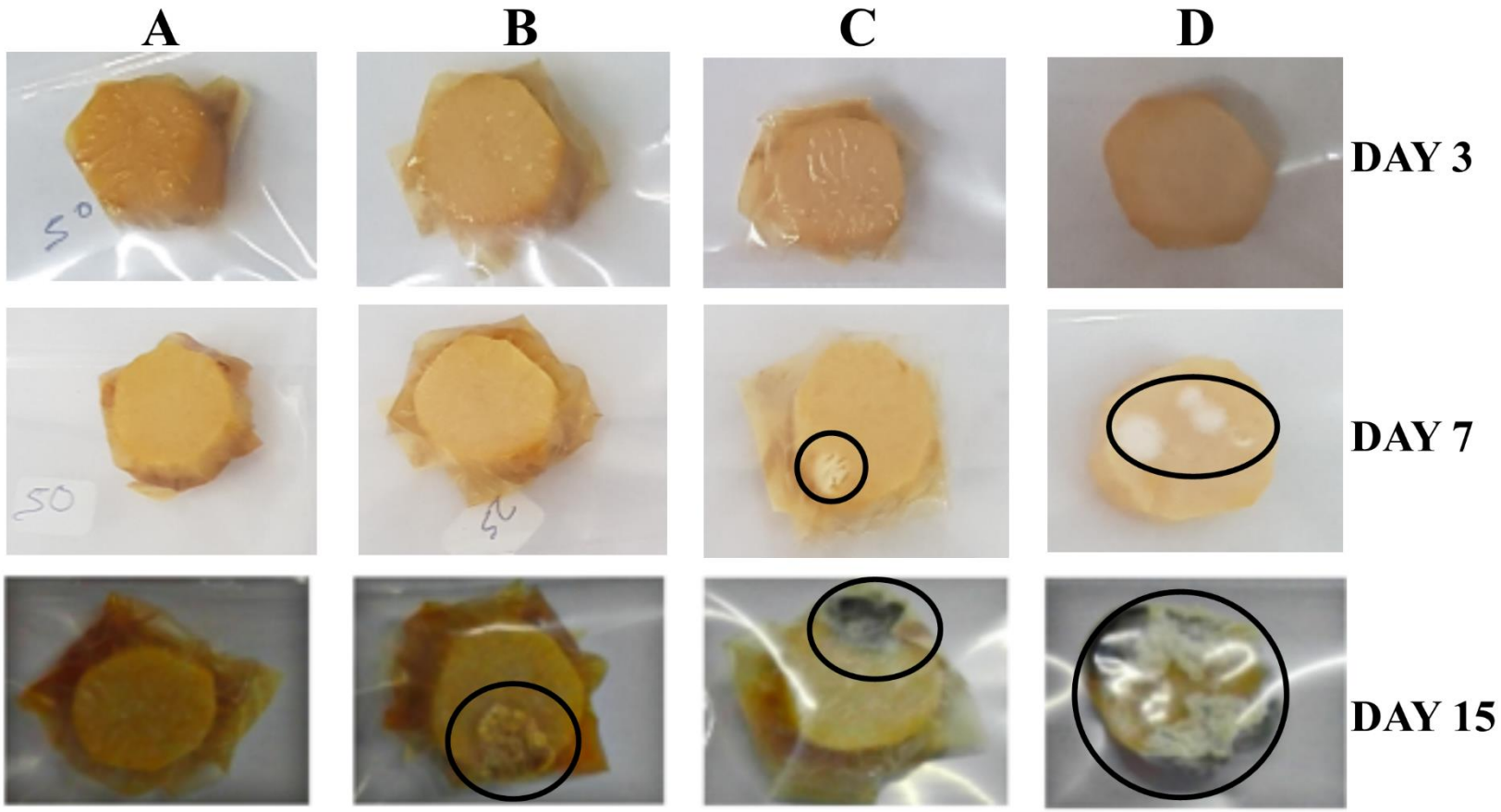

Figure 31. Shelf-life extension effects of polyvinyl alcohol-chitosan films incorporating silver nanoparticles on chicken frank sausage stored at 20 °C. Films: 1:1 (A), 1.5:0.5 (B), PVA-CH control (C) and unwrapped sausage (D).

13. *In vitro* Ag^+ Release

The *in vitro* release profile of Ag nanoparticles from the PVA–CH/Ag nanoparticles films is shown in (Figure 32). The total Ag content obtained from digesting 100 mg of films were 1.42 ± 0.05 µg/mL for film 1:1, 0.51 ± 0.03, and 0.27 ± 0.05 µg/mL for 1.5:0.5, and 1.75:0.25. As shown in the results, a burst release of Ag nanoparticles was observed at the first 6 h, amounting to a percentage cumulative release of 7.38, 8.26, and 7.46% for 1:1, 1.5:0.5, and 1.75:0.25. At 12–96 h a reduction in Ag nanoparticles release was witnessed with percentage cumulative release of 15.2, 18.3, and 17.9% for the respective films at 96 h. The overall results showed a rapid and continuous release of Ag nanoparticles from the composite film. In addition, no significant difference ($p<0.05$) was observed between the percentage cumulative Ag nanoparticles release of the three samples indicating the release was independent of the Ag nanoparticles concentrations in the films. The results showed that the fabricated PVA–CH/Ag nanoparticles films were stable, with a slow and controlled Ag nanoparticles release.

The release kinetics of Ag from PVA–CH/Ag nanoparticles films showed "r" value range of 0.77–0.83 for first order kinetics indicating a concentration dependent *in vitro* release. The interpretation of release exponent values (n) was studied to understand release mechanism of Ag nanoparticles from PVA–CH/Ag nanoparticles films. The Higuchi and Korsmeyer-Peppa's model showed a linearity of (0.91–0.94) for Ag nanoparticles, whereas Peppa's model suggests classic Fickian diffusion with n values of (0.07–0.08) (Table 15).

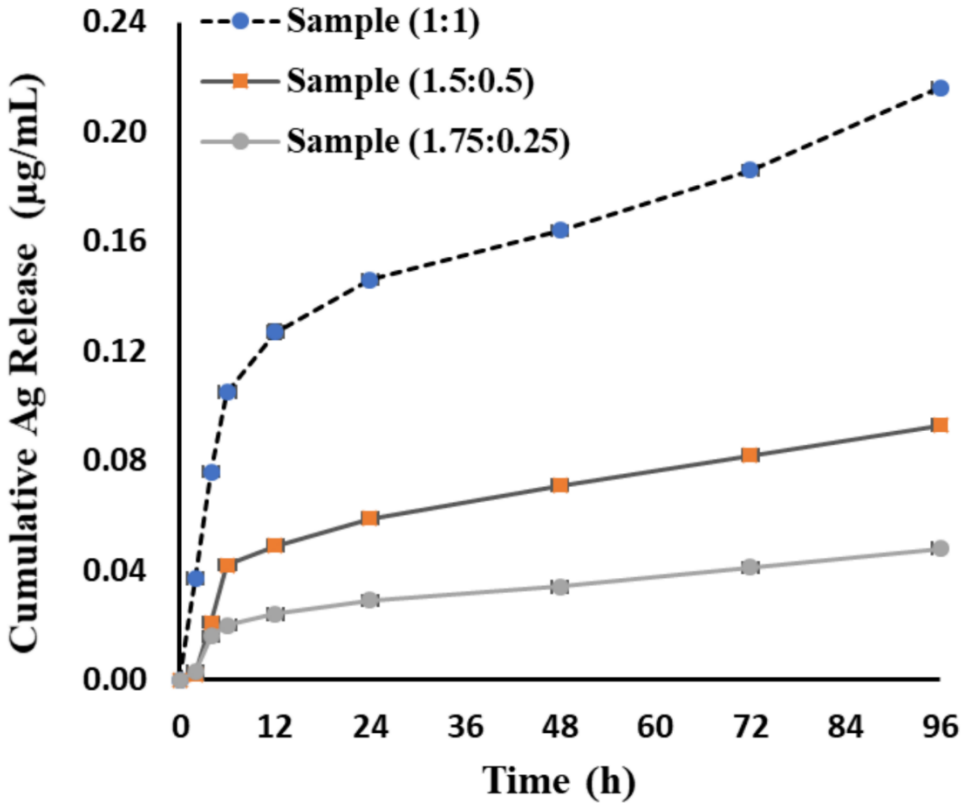

Figure 32. Cumulative release of silver nanoparticles in µg/mL from samples at various time intervals, measured using ICP-OES. Values represents mean of triplicate measurements.

Table 15. *In vitro* release kinetics models of PVA-CH/silver nanoparticles films

Samples	Zero Order	First Order	Higuchi	Peppas (n)
Film 1:1	0.75	0.77	0.91	0.07
Film 1.5:0.5	0.79	0.81	0.92	0.09
Film 1.75:0.25	0.81	0.83	0.94	0.08

14. Cytotoxicity of PVA–CH/Ag Nanoparticles

Toxicity of PVA-CH/Ag nanoparticles and PVA-CH control films measured using MTT assay showed that Ag nanoparticles composite film exhibited significant cell viability ($p<0.05$) when cells were treated with eluent from 1 mg/mL of film samples. However, at a concentration of 5 mg/mL a mild toxicity was observed (Figure 33). Cytotoxicity of Ag nanoparticles composite films depends on the release of Ag nanoparticles (Wu et al., 2018). It has been shown that controlled release of Ag nanoparticles can minimize the toxicity of the composite film (Wu et al., 2018). Moreover, in practical applications as food wrap, lower concentrations of Ag nanoparticles will be released since migration of nano material is dependent on the nature and moisture content of the food matrix. Ag nanoparticles shows higher migration in liquid based food models and soft food products such as fruit juice and cheese (Metak & Ajaal, 2013).

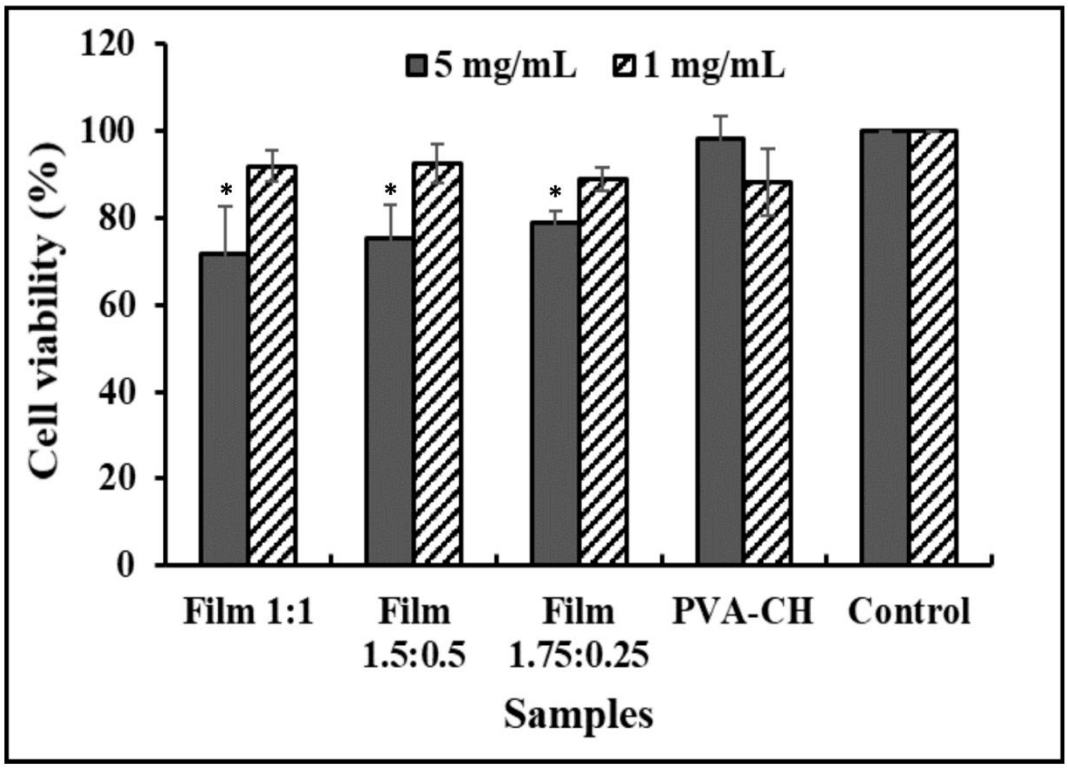

Figure 33. Cytotoxicity of PVA-CH/silver nanoparticles and PVA-CH control films on human colon cells Caco-2 evaluated using MTT assay. Values represents means of triplicate measurements, * represents significant difference at $p<0.05$.

Part V. Fabrication of Nanocomposite Food Packaging from Recycled Wastepaper and Functionalization with Biogenic Silver Nanoparticles.

1. FTIR Analysis

The FTIR spectra of the biogenic silver nanoparticles, extract, blank paper, and synthesized silver nanoparticles paper is presented in (Figure 34). Synthesized silver nanoparticles and ethanolic extract of *E. camaldulensis* spectra showed a broad band between 3400–3450 cm^{-1} representing the O–H stretching vibration of the phenolic and flavonoid compounds. Peak at 2920–2925 cm^{-1} is ascribed to the $–CH_2$ and C–H stretching of alkanes. The prominent peaks at 1620–1640 cm^{-1} reflects the N–H presence of amine group. The extract and silver nanoparticles spectra displayed visible interaction between functional groups. The absence of the aliphatic saturated aldehydes carbonyl group C=O (1690–1750 cm^{-1}) observed in the extract, merging of the multiple weak bands of polyols C–O, alkanes C–H and C-H deformation vibrations (1190–1450 cm^{-1}) present in the extract into a single sharp and prominent peak at 1384 cm^{-1} and shift of –C–O– stretching of alcohols, carboxylic acids, esters and ethers from 1045–1115 cm^{-1} indicates the reduction of Ag ions by plant phytochemicals or adsorption of phytochemical compounds from the extracts onto the nanoparticle surface (Alghoraibia et al., 2019). The FTIR spectra of the recycled blank paper and silver nanoparticles paper displayed similar peaks, with minor peak shifts at 3331 to 3329, 2898 to 2900, 1726 to 1722, 1639 to 1637, 1426 to 1413, 1023 to 1021. The absence of major changes in the functional groups is attributed to the usage of an already reduced Ag^{+}. Previous researchers have demonstrated slight alterations in the functional groups of cellulose paper following the reduction of $AgNO_3$ (Thiagamani et al., 2019; Yu et al., 2019).

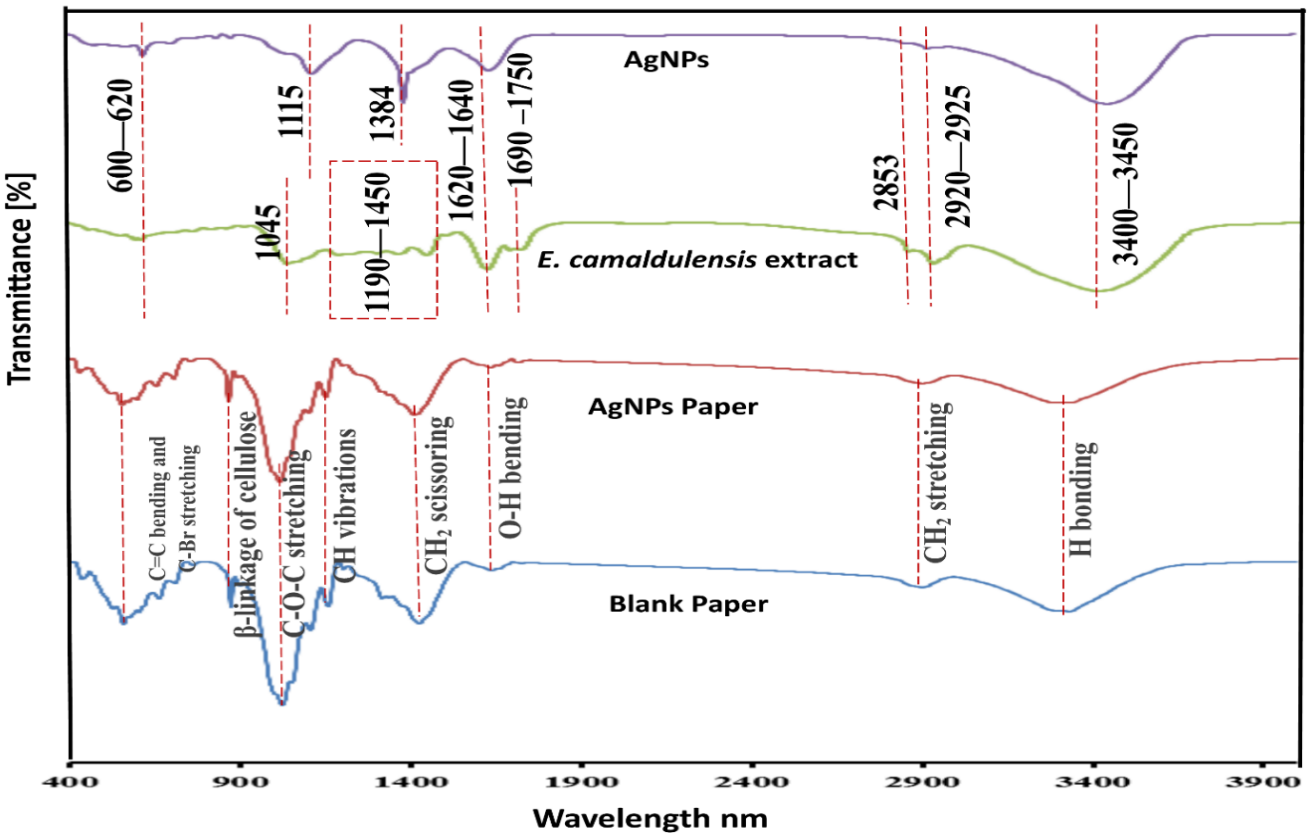

Figure 34. FTIR spectra of synthesized silver nanoparticles, *E. camaldulensis* extracts, silver nanoparticles paper and blank control paper showing the functional groups present in the samples and the chemical interactions between functional groups.

2. XRD Analysis

The XRD spectra presented in Figure 35, showed that both blank control and Silver nanoparticles paper presented similar amorphous to crystalline peaks. The XRD peaks at 2θ = 16.5°, 22.6°, and 22.9° were ascribed to (1–10), (110), and (200) planes of cellulose II crystalline structure (Kishanji, Mamatha, Obi Reddy, Varada Rajulu, & Madhukar, 2017; Qi, Cai, Zhang, & Kuga, 2009). Additional peaks in synthesized Silver nanoparticles paper at 2θ = 32.2° and 77.3° were attributed to (111) and (311) crystal planes of face centered cubic structure of silver (Sadanand, Rajini, Satyanarayana, & Rajulu, 2016). The intensity of peaks of blank paper were also observed to be higher than those of synthesized Silver nanoparticles paper, indicating a lowering of crystallinity by the presence of Ag nanoparticles (Sadanand et al., 2016). This confirms the physical interaction of synthesized Silver nanoparticles with component compound of cellulose paper.

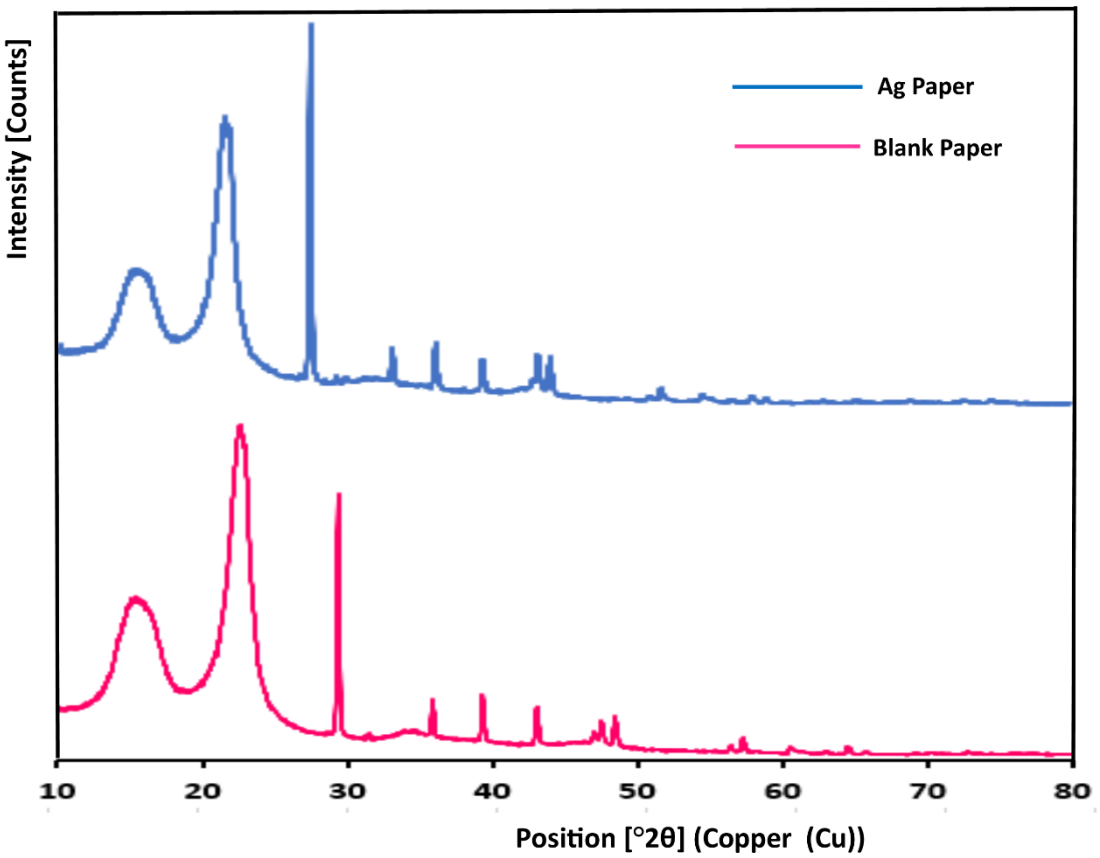

Figure 35. XRD spectra of the Silver nanoparticles and blank control paper indicating the absence of silver peaks due to the low concentration of Ag lower than the 2% dictation limit.

3. UV-Visible Spectra of Recycled Silver Nanoparticles Paper

The absorbance and reflectance spectra of synthesized silver nanoparticles and blank paper were recorded at wavelengths between 200–2000 nm (Figure 36). The absorbance spectra of synthesized silver nanoparticles paper showed a peak at 427 nm resulting in a downward trough in the reflectance spectra. This represents the plasmon resonance band of synthesized silver nanoparticles. The narrow width of the peak suggests a narrow size distribution of synthesized silver nanoparticles present in the paper. At the wavelength range tested, blank paper consistently presented a higher reflectance, whereas synthesized silver nanoparticles paper showed higher absorbance. This indicates the colour alteration witnessed with synthesized silver nanoparticles paper. The blank paper reflected all light wavelength whereas the deep brown colour of synthesized silver nanoparticles absorbed the light. Previous researchers have reported reduced light reflectance of paper after incorporation of silver nanoparticles (Dankovich, 2014; Swensson, Ek, & Gray, 2018). Silver nanoparticles have also been reported to exert a UV blocking activity (Jafari, Karimi, Mirjalili, & Derakhshan, 2016), and capable of absorbing a wide wavelength range of lights (Fahmy et al., 2019). This unique property of silver nanoparticles defines its optical application in various fields.

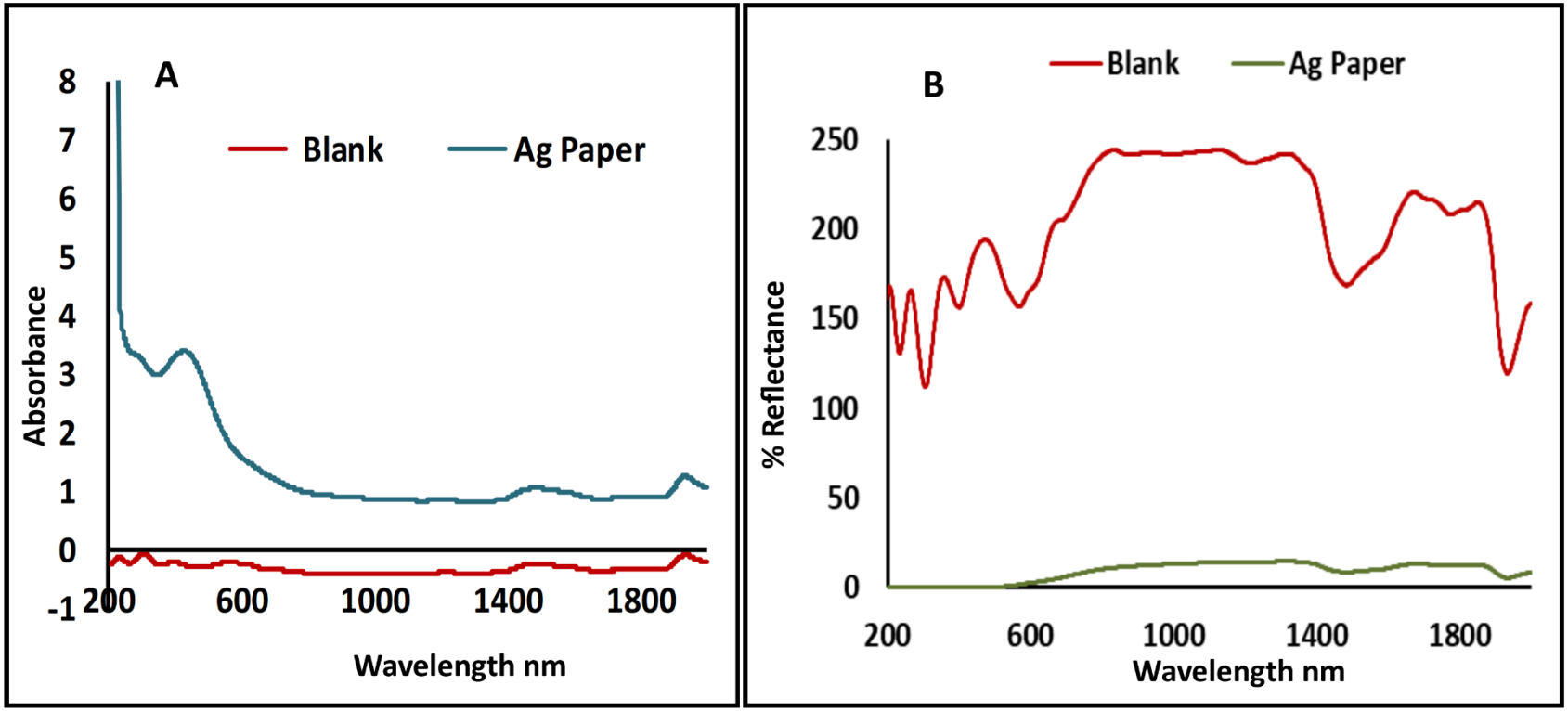

Figure 36. Absorbance and reflectance spectra of the antimicrobial silver nanoparticles and blank control paper, showing the surface plasmon resonance peak of silver nanoparticles at 427 nm and the poor reflectance of light by the silver nanoparticles paper.

4. Physicochemical Parameters of Recycled Paper

The physicochemical and mechanical properties of recycled paper are presented in (Table 16). The tensile strength of a material reflects the ability to resist breaking under stress and is dependent on the strength of the base material, surface area, length, and the bonding strength between them. Whereas the elongation at break shows the ability of a material to stretch before breaking. The results obtained reveals that synthesized silver nanoparticles paper showed significant increase in tensile strength ($p<0.05$) compared to blank control. However, the percent elongation at break was significantly higher for blank paper. The increased tensile strength might be due to the formation of strong bonding between the paper base material and synthesized silver nanoparticles. Similar results were obtained following reinforcement of active nanocomposite pouches with *in situ* generated silver nanoparticles (Mathew, Snigdha, Mathew, & Radhakrishnan, 2019). The thickness of the recycled paper ranged between 0.18–0.19 mm. No significant difference ($p<0.05$) was observed in the physicochemical parameters (water absorption, grammage, and bulk density of the samples) of synthesized silver nanoparticles paper and the blank.

Table 16. Mechanical and physicochemical characteristics of the biogenic silver nanoparticles composite and blank control paper

Samples	T_{max} MPa	EAB %	Thickness mm	Water absorption (g/m^2)	Grammage (g/m^2)	Bulk density (g/cm^3)
Ag Paper	5.82 ± 0.708^a	0.74 ± 0.336^a	0.179 ± 0.008^b	57.70 ± 2.29^b	87.400 ± 0.850^b	0.490 ± 0.017^b
Blank	3.66 ± 0.670^a	1.60 ± 0.362^a	0.187 ± 0.010^b	60.14 ± 1.99^b	90.405 ± 1.365^b	0.483 ± 0.026^b

[a] indicates significant difference, and [b] not-significantly different at ($p<0.05$). EAB- Elongation at break

5. Scanning Electron Micrograph of Recycled Silver Nanoparticles Paper

The morphology of the recycled silver nanoparticles paper and blank control is shown in (Figure 37). The surface micrograph of the samples as shown by SEM revealed a cellulose base fibrous net-like structure (Amini, Azadfallah, Layeghi, & Talaei-Hassanloui, 2016; Li et al., 2017). However, unlike the image previously reported, incorporation of silver nanoparticles into the paper did not affect the surface pore size of the paper. The difference might have resulted from the coating method employed by the previous researchers. At higher magnifications, synthesized silver nanoparticles paper reveals spherical nanosized particles distributed on the surface. These particles are believed to be silver nanoparticles embedded on the surface of the paper (Figure 37A). On the contrary, blank papers at same magnification revealed a smooth surface, showing the absence of particles. To confirm the presence of synthesized silver nanoparticles on the paper, EDS elemental analysis was performed on synthesized silver nanoparticles functionalized paper (Figure 38). The EDS quantitative revealed Ag concentration of 0.1 %Wt on the paper. Mapping of the paper surface further showed uniform distribution of synthesized silver nanoparticles on the surface of the paper. Other elemental components of the paper included carbon and oxygen from the cellulose base and starch added as binder and calcium probably from $CaCO_3$ serving as filling material in the paper production.

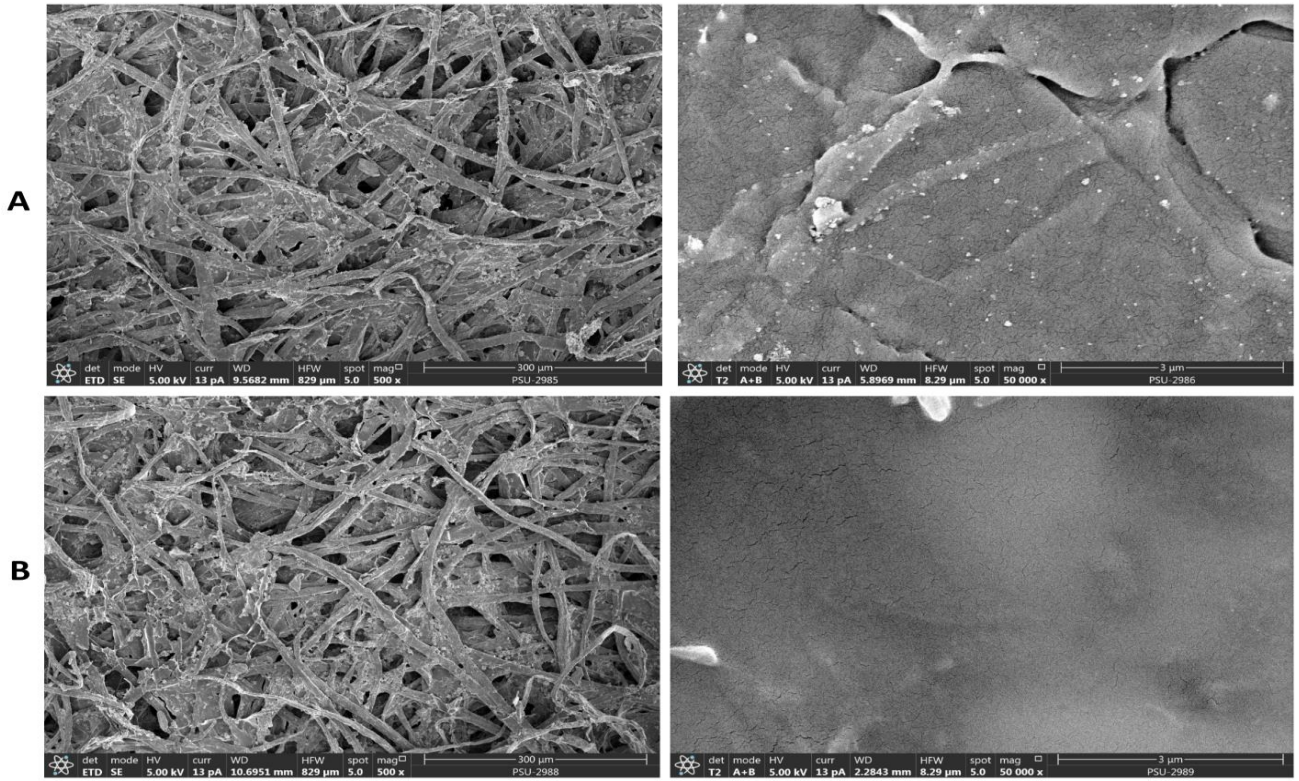

Figure 37. Scanning electron micrograph of the silver nanoparticles paper (A), and blank control paper (B) showing the cellulose fibre structure of the recycled paper and the deposition of particles believed to be silver nanoparticles on the surface of the silver nanoparticles paper.

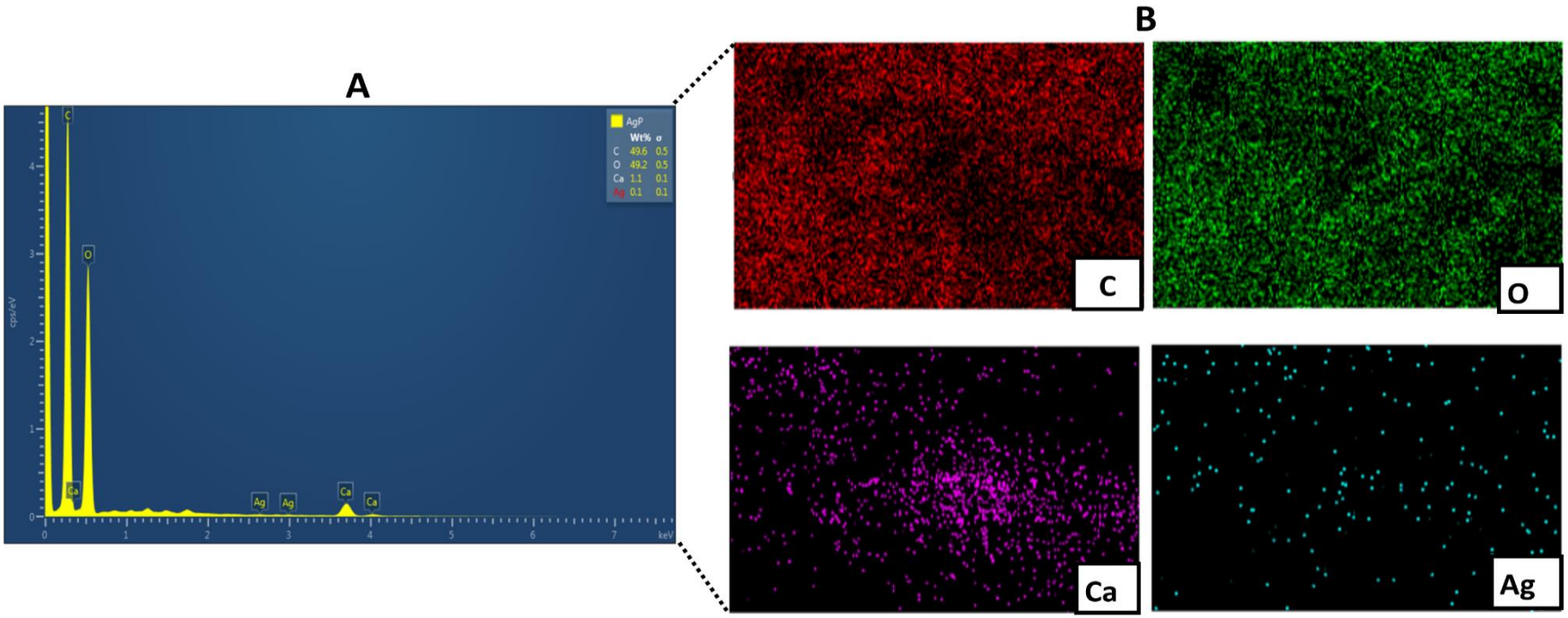

Figure 38. SEM-EDS elemental mapping of components of the silver nanoparticles paper showing the presence and distribution of carbon, oxygen, calcium, and a 0.1%Wt of Ag. EDX spectra (A), Elemental mapping (B).

6. Release and Migration of Ag from Synthesized Silver Nanoparticles Paper

To investigate the release profile of Ag from synthesized silver nanoparticles packaging paper and migration into wrapped food, a food model-based method was developed using minced beef. The initial concentration of Ag and Ag release at various intervals was evaluated using ICP-OES (Figure 39). The results obtained revealed an initial Ag concentration of 0.22 µg/mL. After 12 h, 41.8% of the Ag content was reduced, indicating migration from the packing paper into the minced meat product. Approximately 75.9% of the Ag was migrated into the meat at 48 h. The result demonstrates an unregulated release of silver. Similar result was observed by (Wu et al., 2014) who reported a high Ag^{+} release from bacterial cellulose/silver nanoparticles composite within 72 h. The antimicrobial activity of silver nanoparticles has been demonstrated by various researchers, however the easily leakage of silver from composite materials restricts its application in the design of packaging materials (Wu et al., 2019). Cytotoxicity of silver nanoparticles to cells has also been attributed to this uncontrolled release, regulating the release of Ag from composite material reduces the cytotoxicity to cells (Wu et al., 2019).

The release kinetics of Ag from the recycle silver nanoparticles paper showed "r" value of (0.978) for first order kinetics indicating a concentration dependent *in vitro* release. The interpretation of release exponent values (n) was studied to understand release mechanism of silver nanoparticles from the recycle silver nanoparticles paper. Higuchi and Korsmeyer-Peppa's model presented a linearity of 0.996 and 0.986 for

silver nanoparticles, whereas Peppa's model suggests classic Fickian diffusion with n values of 0.434.

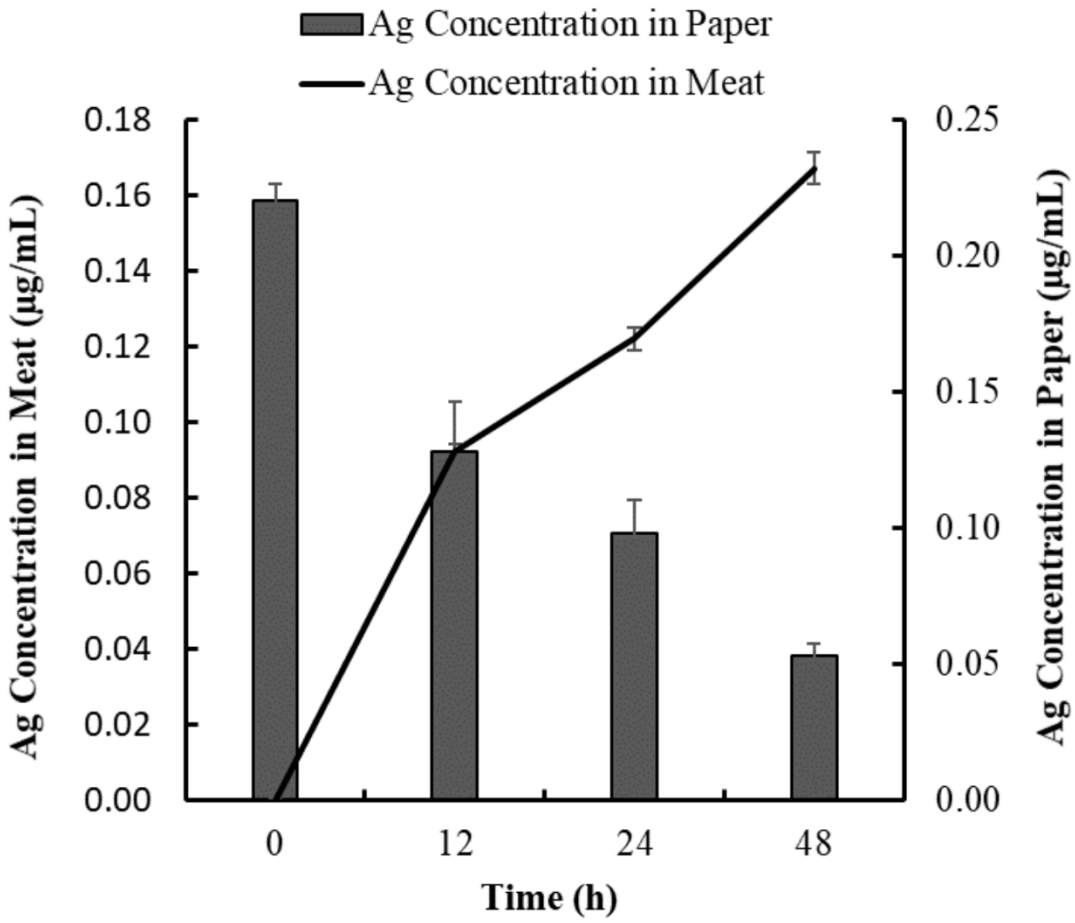

Figure 39. Release of silver from the silver nanoparticles paper and migration into wrapped minced meat at time intervals. Values represents means of triplicate measurements evaluated using ICP-OES.

7. Antibacterial Potency of Synthesized Silver Nanoparticles Paper

The antibacterial effects of synthesized silver nanoparticles and blank control paper were demonstrated against foodborne pathogenic bacterial isolates including *B. cereus*, *E. coli* O157:H7, *L. monocytogenes* F2365, and *S. aureus* ATCC 25923 in a broth culture base method (Figure 40). The results showed pronounced bactericidal effects on *B. cereus* and *E. coli* with >3log reduction after 3 h of treatment. Against *L. monocytogenes* and *S. aureus*, the paper showed bacteriostatic effects with approximately 1log reduction after 12 h treatment. The antimicrobial effects of the blank control paper were similar to that of bacterial culture without a test paper. This indicates that the antimicrobial observed with synthesized silver nanoparticles paper was due to the Ag released from synthesized silver nanoparticles paper into the broth culture. The antimicrobial effects of silver nanoparticles coated cellulose paper has been previously demonstrated (Praveena, Karuppiah, & Than, 2018; Tsai et al., 2017).

To further confirm the antimicrobial efficacy of the recycled papers against the test bacterial isolates, a modified method from ISO 20743 was used to mimic the dry state condition experienced with food wraps (Figure 41). The result confirmed the antimicrobial effects of synthesized silver nanoparticles paper against Gram–positive *B. cereus* and *L. monocytogenes* and Gram–negative *E. coli* with 2–3 log reduction after 24 h contact with synthesized silver nanoparticles paper. However, antimicrobial activity of synthesized silver nanoparticles paper only should an inhibitory effect on *S. aureus*. For all Gram–positive bacteria tested, an increase in CFU/mL was observed, indicating growth of the bacteria on the blank control paper.

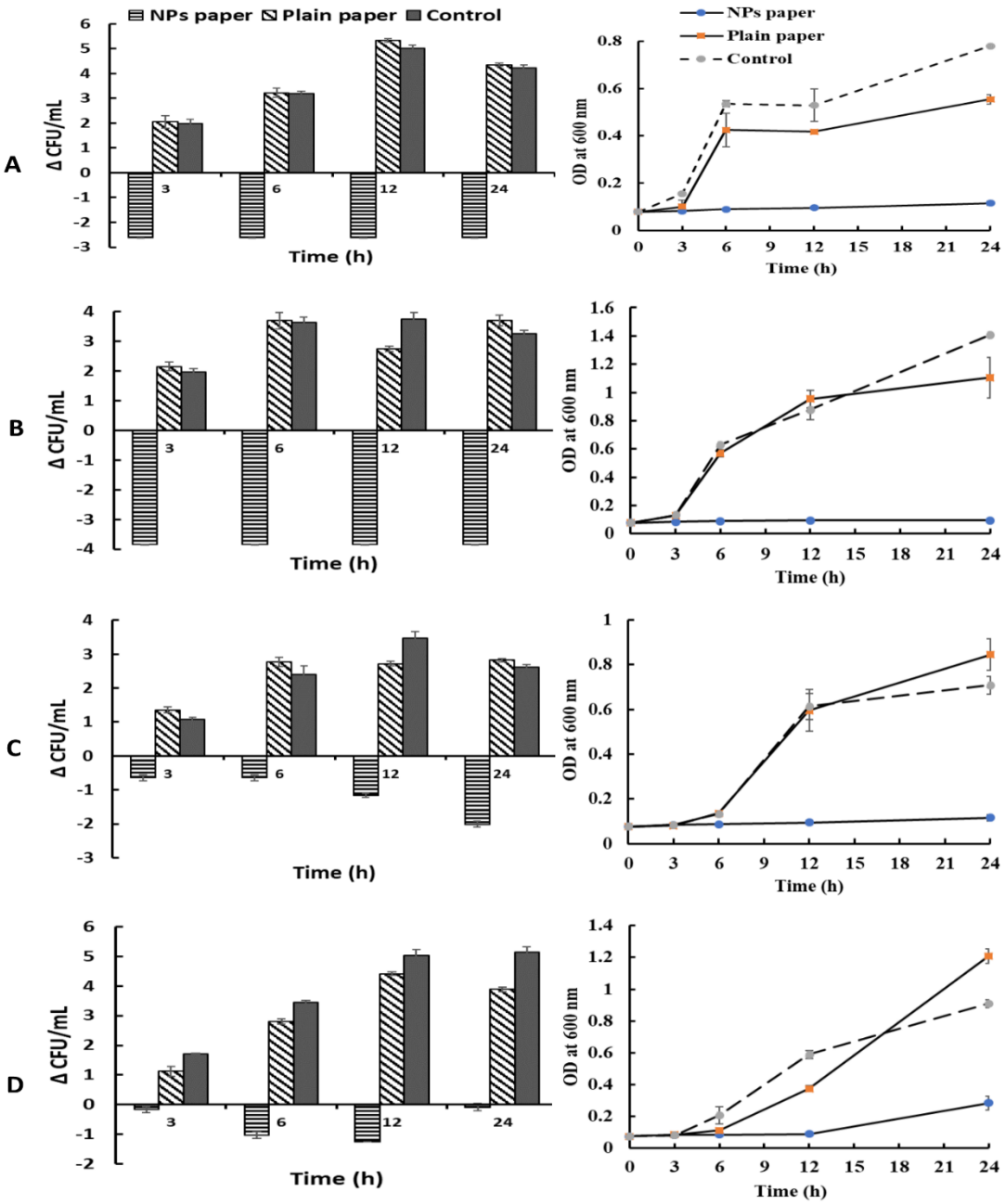

Figure 40. Bactericidal and growth inhibitory effects of the silver nanoparticles paper and blank control paper on foodborne pathogenic bacteria including; *B. cereus* (A), *E. coli* O157:H7 (B), *L. monocytogenes* F2365 (C), and *S. aureus* ATCC 25923 (D), evaluated using plate count technique and OD measurement.

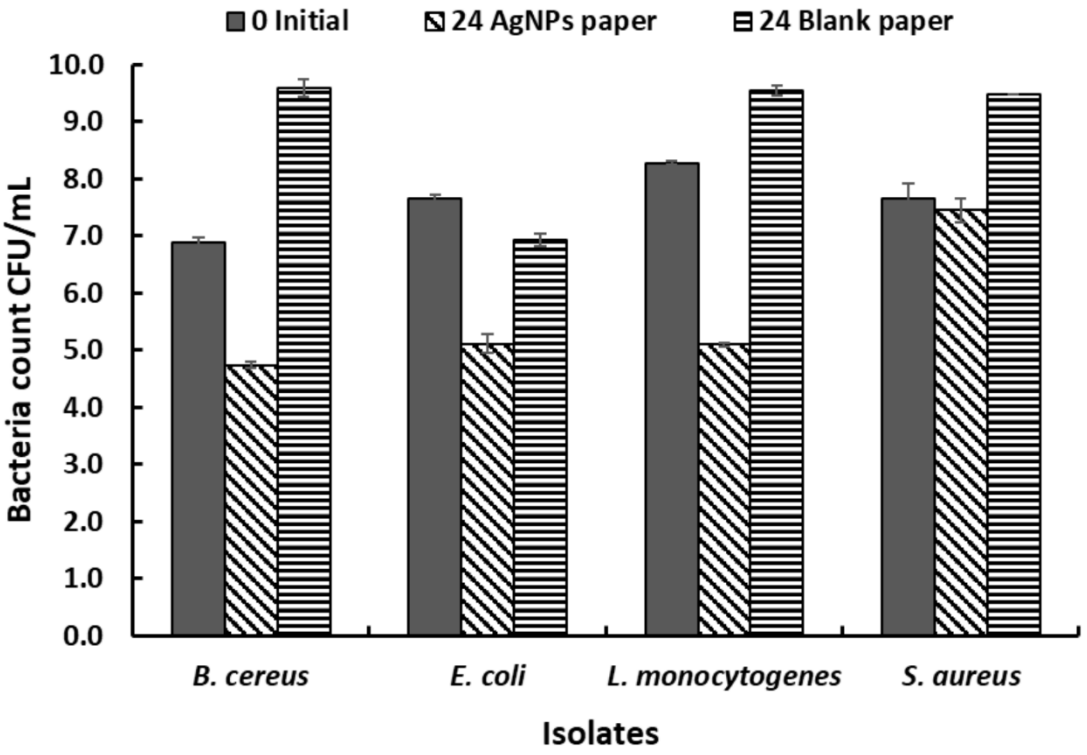

Figure 41. Antibacterial effects of the silver nanoparticles paper on selected bacteria isolates after 24 h contact with the paper in a dry state, evaluated by ISO 20743. Values indicate means of triplicate reading, of three independent experiments.

8. Cytotoxicity of Silver Nanoparticles Paper

The effects of silver nanoparticles and its toxicity on the environment and humans has attracted great attention due to the growing interest in silver nanoparticles and its applications in various area including consumer goods. Thus, to validate the use of silver nanoparticles as active agents in the design of food packaging materials, antimicrobial silver nanoparticles paper and blank control paper were evaluated for toxicity against human renal cell HEK293T and human colon cell line Caco-2 (Figure 42). The result showed that silver nanoparticles at the concentrations released after 12, 24, and 48 h showed no toxicity against both cell-lines. The human renal cell HEK 293T showed approximately ≥ 80% viability, whereas Caco-2 cells showed > 90% viability at all the tested time. Silver nanoparticles has been previously reported to exhibit a mild toxic effect on HEK 293T at a high concentration of 20 µg/mL (Jiang et al., 2018). On Caco-2 cells, silver nanoparticles has been reported to exert a non-toxic effect on differentiated Caco-2 cells at concentrations ≤ 50 µg/mL (Vila, García-Rodríguez, Cortés, Marcos, & Hernández, 2018). The effects of silver nanoparticles is dependent of various factors such as the size of the nanoparticles, concentration, time of exposure (Böhmert, Niemann, Thünemann, & Lampen, 2012). The non-toxic effect of silver nanoparticles observed in this research could be as a result of the low concentration of Ag and incomplete release of all the silver content of the paper. At all tested time, the blank paper also showed no toxic effects on HEK293T, and in addition tends to show stimulatory effects on Caco-2 cells.

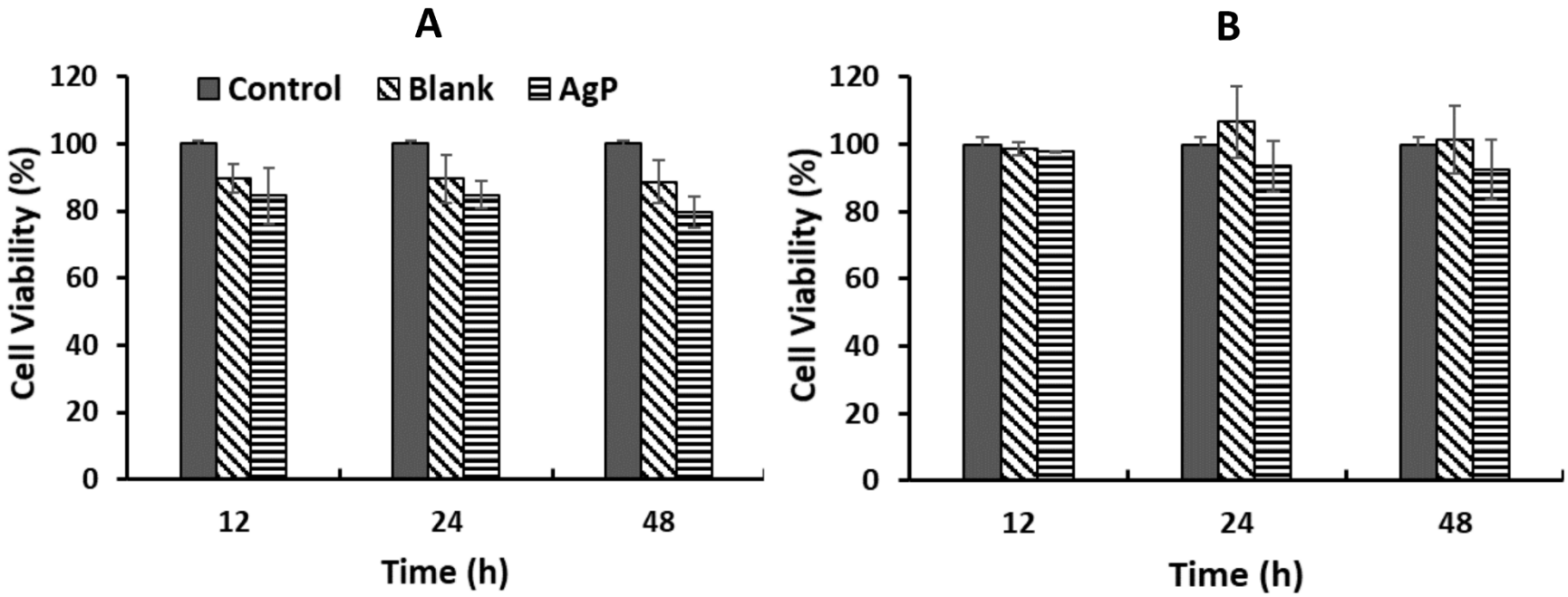

Figure 42. *In vitro* cytotoxicity of release Ag from the silver nanoparticles paper and blank control paper on human embryonic renal cell HEK293T (A) and human colon cells Caco-2 (B), showing > 80% cell viability after analysis using MTT assay at $p<0.05$. Control was maintained as cells grown in DMEM without elute, and Blank was cells treated with elutes from recycled paper without silver nanoparticles.

CHAPTER 4

CONCLUSIONS

Food contamintion and microbial proliferation has remained the major cause of foodborne diseases, intoxication and spoilage. The addition of antimicrobial and antioxidant agents in food serves to preserve sensory, organoleptic, nutritional and compositional qualities by inhibition of microbial proliferation and oxidative processes. However, as consumers awareness and the demand for green consumerism increases, the use of conventional preservatives seems obsolete. The search for alternative efficient, cost effective and bio-friendly agents has created a surge in natural products research, with various plants phytochemicals and bioactive compounds isolated and used for various applications. *E. camaldulensis*, a plant native to Australia and the Asia continent is a known source of commercially available essential oil with medical and cosmetic applications. Leaf extract of the plant demonstrated good antibacterial activity against the pathogenic foodborne pathogen *L. monocytogenes.* At sub-inhibitory concentrations, the extract demonstrated anti-adherence, antibiofilm and anti-virulence properties. In addition, the extract showed cell membrane disruptive and antioxidant properties. Encapsulation of the extract in sodium alginate and sodium CMC co-polymer matrix yielded micro-sized particles that displayed antioxidant and antibacterial properties resulting from the release of bioactive core material.

In recent times, the development of nanomaterial has gained tremendous attention in medical related fields, due to the excellent antimicrobial properties of these particles

and the need to replace or enhance available antimicrobial agents in the face of rising incidence of antimicrobial resistance. Silver nanoparticles synthesized with the extract as capping and reducing agent showed excellent antibacterial properties. Biodegradable active polymer based packaging material functionalized with the synthesized nanoparticles showed good antimicrobial and antioxidant properties, and in addition prolonged the shelf life of chiken suasage. Similarly, cellulose based active packaging fabricated from recycling of paper and functionalized with synthesized silver nanoparticles showed good qualities as packaging material. Evaluation of fabricated food packaging material demonstrated that both were not toxic to human cell.

This study demonstrated that the plant *E. camaldulensis* can be potential source of antibacterial and antioxidant bioactive compound that could be used in food preservation and/or antibacterial food-grade sanitizers.

In addition encapsulation using polymers could be explored as a possible means of preserving the stability and activity of the bioactive extract for application in food system. The extract could serve as a reducing agent and capping agent for synthesis of biogenic metal based nanopaticles. Incorporation of silver nanoparticles into composite material could be developed as a cost effective and efficient active packaging for the inhibition of food spoilage and pathogenic bacteria isolates.

Suggestion for Further Research

E. camaldulensis leaf contains bioactive compounds with great potentials for food applications. However, analytical procedures such as Liquid Chromatography is required for identification and isolation of these compounds in pure forms. In addition,

the removal of colour from the plant material should be explored. Microencapsulation using food grade polymers should be further developed.

Additional work on the mechanisms and correlations between the results reported and alterations in genetic composition of the foodborne isolates is also required. Moreover, the acute toxicity and bioaccumulation of silver ion and silver nanoparticles should be investigated.

REFERENCES

Abbaszadegan, A., Ghahramani, Y., Gholami, A., Hemmateenejad, B., Dorostkar, S., Nabavizadeh, M., & Sharghi, H. (2015). The effect of charge at the surface of silver nanoparticles on antimicrobial activity against gram-positive and gram-negative bacteria: a preliminary study. *Journal of Nanomaterials, 16*(1), 53.

Abdelrazek, E., Elashmawi, I., & Labeeb, S. (2010). Chitosan filler effects on the experimental characterization, spectroscopic investigation and thermal studies of PVA/PVP blend films. *Physica B: Condensed Matter, 405*(8), 2021-2027.

Abu-Saied, M., Wycisk, R., Abbassy, M. M., El-Naim, G. A., El-Demerdash, F., Youssef, M., Pintauro, P. N. (2017). Sulfated chitosan/PVA absorbent membrane for removal of copper and nickel ions from aqueous solutions—fabrication and sorption studies. *Carbohydrate Polymers, 165*, 149-158.

Adebayo-Tayo, B. C., Inem, S. A., & Olaniyi, O. A. (2019). Rapid synthesis and characterization of Gold and Silver nanoparticles using exopolysaccharides and metabolites of *Wesiella confusa* as an antibacterial agent against *Esherichia coli*. *International Journal of Nano Dimension, 10*(1), 37-47.

Adeniyi, B., Lawal, T., & Olaleye, S. (2006). Antimicrobial and gastroprotective activities of *Eucalyptus camaldulensis* (Myrtaceae) crude extracts. *Journal of Biological Sciences, 6*(6), 1141-1145.

Akalin, G. O., & Pulat, M. (2018). Preparation and characterization of nanoporous sodium carboxymethyl cellulose hydrogel beads. *Journal of Nanomaterials, 2018*, Article ID 9676949.

Akin, M., Aktumsek, A., & Nostro, A. (2010). Antibacterial activity and composition of the essential oils of *Eucalyptus camaldulensis* Dehn. and Myrtus communis L. growing in Northern Cyprus. *African Journal of Biotechnology, 9*(4).

Alehosseini, A., Gómez-Mascaraque, L. G., Martínez-Sanz, M., & López-Rubio, A. (2019). Electrospun curcumin-loaded protein nanofiber mats as active/bioactive coatings for food packaging applications. *Food Hydrocolloids, 87*, 758-771.

Alghamdi, A. I., & Ababutain, I. M. (2019). Phytochemical Screening and Antibacterial Activity of *Eucalyptus camaldulensis*'s Leaves and Bark Extracts. *Asian Journal of Scientific Research, 12*, 202-210.

Alghoraibia, I., Soukkarieh, C., Zein, R., Alahmad, A., Walter, J. G., & Daghestani, M. (2019). Aqueous extract of *Eucalyptus Camaldulensis* leaves as reducing and capping agent in green synthesis of silver nanoparticles. *Current Nanomaterials, 04*. doi:10.2174/2405461504666190625121807

Alvarez-Ordóñez, A., Coughlan, L. M., Briandet, R., & Cotter, P. D. (2019). Biofilms in food processing environments: challenges and opportunities. *Annual Review of Food Science and Technology, 10*, 173-195.

Amini, E., Azadfallah, M., Layeghi, M., & Talaei-Hassanloui, R. (2016). Silver-nanoparticle-impregnated cellulose nanofiber coating for packaging paper. *Cellulose, 23*(1), 557-570.

Arriola, N. D. A., De Medeiros, P. M., Prudencio, E. S., Muller, C. M. O., Amboni Castanho, R. D. M. (2016) Encapsulation of aqueous leaf extract of *Stevia rebaudiana* Bertoni with sodium alginate and its impact on phenolic content. *Food Biosciences* 13, 32-40.

Ashraf, A., Sarfraz, R. A., Mahmood, A., & ud Din, M. (2015). Chemical composition and in vitro antioxidant and antitumor activities of *Eucalyptus camaldulensis* Dehn. leaves. *Industrial Crops and Products, 74*, 241-248.

Avelelas, F., Horta, A., Pinto, L. F., Cotrim Marques, S., Marques Nunes, P., Pedrosa, R., & Leandro, S. M. (2019). Antifungal and Antioxidant Properties of Chitosan Polymers Obtained from Nontraditional *Polybius henslowii* Sources. *Marine Drugs, 17*(4), 239.

Azizi, S., Ahmad, M. B., Ibrahim, N. A., Hussein, M. Z., & Namvar, F. (2014). Cellulose nanocrystals/ZnO as a bifunctional reinforcing nanocomposite for poly (vinyl alcohol)/chitosan blend films: fabrication, characterization and properties. *International Journal of Molecular Sciences, 15*(6), 11040-11053.

Bardhan, S., Pal, K., Roy, S., Das, S., Chakraborty, A., Karmakar, P., . . . Das, S. (2019). Nanoparticle Size-Dependent Antibacterial Activities in Natural Minerals. *Journal of Nanoscience and Nanotechnology, 19*(11), 7112-7122.

Basak, S. S., & Candan, F. (2010). Chemical composition and in vitro antioxidant and antidiabetic activities of *Eucalyptus camaldulensis* Dehnh. essential oil. *Journal of the Iranian Chemical Society, 7*(1), 216-226.

Battisti, R., Fronza, N., Júnior, Á. V., da Silveira, S. M., Damas, M. S. P., & Quadri, M. G. N. (2017). Gelatin-coated paper with antimicrobial and antioxidant effect for beef packaging. *Food Packaging and Shelf Life, 11*, 115-124.

Benzie, I. F., & Strain, J. (1999). [2] Ferric reducing/antioxidant power assay: Direct measure of total antioxidant activity of biological fluids and modified version for simultaneous measurement of total antioxidant power and ascorbic acid concentration *Methods in Enzymology* (Vol. 299, pp. 15-27): Elsevier.

Bevilacqua, A., Corbo, M. R., & Sinigaglia, M. (2016). *The Microbiological Quality of Food: Foodborne Spoilers*: Woodhead Publishing.

Binsi, P., Nayak, N., Sarkar, P., Jeyakumari, A., Ashraf, P. M., Ninan, G., & Ravishankar, C. (2017). Structural and oxidative stabilization of spray dried fish oil microencapsulates with gum arabic and sage polyphenols: Characterization and release kinetics. *Food Chemistry, 219*, 158-168.

Biswas, M. C., Tiimob, B. J., Abdela, W., Jeelani, S., & Rangari, V. K. (2019). Nano silica-carbon-silver ternary hybrid induced antimicrobial composite films for food packaging application. *Food Packaging and Shelf Life, 19*, 104-113.

Böhmert, L., Niemann, B., Thünemann, A. F., & Lampen, A. (2012). Cytotoxicity of peptide-coated silver nanoparticles on the human intestinal cell line Caco-2. *Archives of Toxicology, 86*(7), 1107-1115.

Bondarenko, O. M., Sihtmäe, M., Kuzmičiova, J., Ragelienė, L., Kahru, A., & Daugelavičius, R. (2018). Plasma membrane is the target of rapid antibacterial action of silver nanoparticles in Escherichia coli and Pseudomonas aeruginosa. *International Journal of Nanomedicine, 13*, 6779.

Bondi, M., Messi, P., Halami, P. M., Papadopoulou, C., & de Niederhausern, S. (2014). Emerging microbial concerns in food safety and new control measures. *BioMed Research International, 2014*.

Borges, A., Saavedra, M. J., & Simões, M. (2012). The activity of ferulic and gallic acids in biofilm prevention and control of pathogenic bacteria. *Biofouling, 28*(7), 755-767.

Briandet, R., Leriche, V., Carpentier, B., & Bellon-Fontaine, M.-N. (1999). Effects of the growth procedure on the surface hydrophobicity of *Listeria monocytogenes* cells and their adhesion to stainless steel. *Journal of Food Protection, 62*(9), 994-998.

Cabrita, P., Trigo, M. J., Ferreira, R. B., & Brito, L. (2015). Differences in the expression of cold stress–related genes and in the swarming motility among persistent and sporadic strains of *Listeria monocytogenes*. *Foodborne Pathogens and Disease, 12*(7), 576-584.

Caetano, L., Almeida, A., & Gonçalves, L. (2016). Effect of experimental parameters on alginate/chitosan microparticles for BCG encapsulation. *Marine Drugs, 14*(5), 90.

Capanema, N. S., Mansur, A. A., de Jesus, A. C., Carvalho, S. M., de Oliveira, L. C., & Mansur, H. S. (2018). Superabsorbent crosslinked carboxymethyl cellulose-PEG hydrogels for potential wound dressing applications. *International Journal of Biological Macromolecules, 106*, 1218-1234.

Chaves, T. P., Pinheiro, R. E. E., Melo, E. S., Soares, M. J. d. S., Souza, J. S. N., de Andrade, T. B., . . . Coutinho, H. D. (2018). Essential oil of *Eucalyptus camaldulensis* Dehn potentiates β-lactam activity against *Staphylococcus aureus* and *Escherichia coli* resistant strains. *Industrial Crops and Products, 112*, 70-74.

Cheng, P. I., Hong, P. D., Lee, K. R., Lai, J. Y., & Tsai, Y. L. (2018). High permselectivity of networked PVA/GA/CS-Ag+-membrane for dehydration of Isopropanol. *Journal of Membrane Science, 564*, 926-934.

Choi, Y. R., & Chang, Y. H. (2018). Microencapsulation of gallic acid through the complex of whey protein concentrate-pectic polysaccharide extracted from Ulmus Davidiana. *Food Hydrocolloids, 85*, 222-228.

Choo, K., Ching, Y. C., Chuah, C. H., Julai, S., & Liou, N. S. (2016). Preparation and characterization of polyvinyl alcohol-chitosan composite films reinforced with cellulose nanofiber. *Materials, 9*(8), 644.

Cichello, S. A. (2015). Oxygen absorbers in food preservation: a review. *Journal of Food Science and Technology, 52*(4), 1889-1895.

CLSI. (2006). Methods for Antimicrobial Dilution and Disk Susceptibility Testing of Infrequently Isolated or Fastidious Bacteria: Approved Guideline M45-A. *Clinical and Laboratory Standards Institute, 26*.

CLSI. (2015). Methods for Antimicrobial Dilution and Disk Susceptibility Testing of Infrequently Isolated or Fastidious Bacteria ; Proposed Guideline. *35*, 64- 69.

CLSI. (2018). M100 performance standards for antimicrobial susceptibility testing: Clinical and Laboratory Standards Institute.

Condurache, N. N., Aprodu, I., Crăciunescu, O., Tatia, R., Horincar, G., Barbu, V., . . . Oancea, A. (2019). Probing the Functionality of Bioactives from Eggplant Peel Extracts Through Extraction and Microencapsulation in Different Polymers and Whey Protein Hydrolysates. *Food and Bioprocess Technology*, 1-14.

Dai, H., Ou, S., Huang, Y., Liu, Z., & Huang, H. (2018). Enhanced swelling and multiple-responsive properties of gelatin/sodium alginate hydrogels by the addition of carboxymethyl cellulose isolated from pineapple peel. *Cellulose, 25*(1), 593-606.

Dairi, N., Ferfera-Harrar, H., Ramos, M., & Garrigós, M. C. (2019). Cellulose acetate/agnps-organoclay and/or thymol nano-biocomposite films with combined antimicrobial/antioxidant properties for active food packaging use. *International Journal of Biological Macromolecules, 121*, 508-523.

Danaei, M., Dehghankhold, M., Ataei, S., Hasanzadeh Davarani, F., Javanmard, R., Dokhani, A., Mozafari, M. (2018). Impact of particle size and polydispersity index on the clinical applications of lipidic nanocarrier systems. *Pharmaceutics, 10*(2), 57.

Dankovich, T. A. (2014). Microwave-assisted incorporation of silver nanoparticles in paper for point-of-use water purification. *Environmental Science: Nano, 1*(4), 367-378.

Del Nobile, M. A., Lucera, A., Costa, C., & Conte, A. (2012). Food applications of natural antimicrobial compounds. *Frontiers in Microbiology, 3*, 287.

Devi, K. P., Nisha, S. A., Sakthivel, R., & Pandian, S. K. (2010). Eugenol (an essential oil of clove) acts as an antibacterial agent against *Salmonella typhi* by disrupting the cellular membrane. *Journal of Ethnopharmacology, 130*(1), 107-115.

Djerahov, L., Vasileva, P., Karadjova, I., Kurakalva, R. M., & Aradhi, K. K. (2016). Chitosan film loaded with silver nanoparticles—sorbent for solid phase extraction of Al (III), Cd (II), Cu (II), Co (II), Fe (III), Ni (II), Pb (II) and Zn (II). *Carbohydrate Polymers, 147*, 45-52.

Du, W., Zhou, M., Liu, Z., Chen, Y., & Li, R. (2018). Inhibition effects of low concentrations of epigallocatechin gallate on the biofilm formation and hemolytic activity of *Listeria monocytogenes*. *Food Control, 85*, 119-126.

Dykes, G. A., Amarowicz, R., & Pegg, R. B. (2003). An antioxidant bearberry (*Arctostaphylos uva-ursi*) extract modulates surface hydrophobicity of a wide range of food-related bacteria: implications for functional food safety. *Food Control, 14*(7), 515-518.

El-Hag Ali, A., Abd El-Rehim, H. A., Kamal, H., & Hegazy, D. E. S. A. (2008). Synthesis of carboxymethyl cellulose based drug carrier hydrogel using ionizing radiation for possible use as site specific delivery system. *Journal of*

Macromolecular Science®, Part A: Pure and Applied Chemistry, 45(8), 628-634.

Elansary, H. O., Salem, M. Z., Ashmawy, N. A., Yessoufou, K., & El-Settawy, A. A. (2017). In vitro antibacterial, antifungal and antioxidant activities of *Eucalyptus* spp. leaf extracts related to phenolic composition. *Natural Product Research, 31*(24), 2927-2930.

Espitia, P. J. P., Soares, N. d. F. F., Teófilo, R. F., dos Reis Coimbra, J. S., Vitor, D. M., Batista, R. A., Medeiros, E. A. A. (2013). Physical–mechanical and antimicrobial properties of nanocomposite films with pediocin and ZnO nanoparticles. *Carbohydrate Polymers, 94*(1), 199-208.

European Commission (2009). Commission Regulation (EC) No. 450/2009 of 29 May 2009 on active and intelligent materials and articles intended to come into contact with food. *Official Journal of the European Union, 135*.

Fahmy, H. M., Mosleh, A. M., Elghany, A. A., Shams-Eldin, E., Serea, E. S. A., Ali, S. A., & Shalan, A. E. (2019). Coated silver nanoparticles: synthesis, cytotoxicity, and optical properties. *RSC Advances, 9*(35), 20118-20136.

Falahati, M., Omidi Tabrizib, N., & Jahaniani, F. (2005). Anti dermatophyte activities of *Eucalyptus camaldulensis* in comparison with Griseofulvin. *Iranian Journal of Pharmacology and Therapeutics, 4*(2), 80-80.

Fasihi, H., Noshirvani, N., Hashemi, M., Fazilati, M., Salavati, H., & Coma, V. (2019). Antioxidant and antimicrobial properties of carbohydrate-based films enriched with cinnamon essential oil by Pickering emulsion method. *Food Packaging and Shelf Life, 19*, 147-154.

FDA. (2012). Bad bug book: handbook of foodborne pathogenic microorganisms and natural toxins. *Center for Food Safety and Applied Nutrition*.

Feng, G., Cheng, Y., Wang, S.-Y., Borca-Tasciuc, D. A., Worobo, R. W., & Moraru, C. I. (2015). Bacterial attachment and biofilm formation on surfaces are reduced by small-diameter nanoscale pores: how small is small enough? *Nature Biofilms and Microbiomes, 1*, 15022.

Floegel, A., Kim, D. O., Chung, S. J., Koo, S. I., & Chun, O. K. (2011). Comparison of ABTS/DPPH assays to measure antioxidant capacity in popular antioxidant-rich US foods. *Journal of Food Composition and Analysis, 24*(7), 1043-1048.

FSANZ. (2018). Food recall statistics. https://www.foodstandards.gov.au/industry/foodrecalls/recallstats/Pages/default.aspx

Gakuubi, M. M., Maina, A. W., & Wagacha, J. M. (2017). Antifungal Activity of Essential Oil of *Eucalyptus camaldulensis* Dehnh. against Selected *Fusarium* spp. *International Journal of Microbiology, 2017,* Article ID 8761610.

Ghaffar, A., Yameen, M., Kiran, S., Kamal, S., Jalal, F., Munir, B., . . . Saba, I. (2015). Chemical composition and in-vitro evaluation of the antimicrobial and antioxidant activities of essential oils extracted from seven *Eucalyptus* species. *Molecules, 20*(11), 20487-20498.

Ghalem, B. R., & Mohamed, B. (2008). Antibacterial activity of leaf essential oils of *Eucalyptus globulus* and *Eucalyptus camaldulensis*. *African Journal of Pharmacy and Pharmacology, 2*(10), 211-215.

Ghareeb, M. A., Habib, M. R., Mossalem, H. S., & Abdel-Aziz, M. S. (2018). Phytochemical analysis of *Eucalyptus camaldulensis* leaves extracts and testing its antimicrobial and schistosomicidal activities. *Bulletin of the National Research Centre, 42*(1), 16.

Gorski, L., Duhé, J. M., & Flaherty, D. (2009). The use of flagella and motility for plant colonization and fitness by different strains of the foodborne pathogen *Listeria monocytogenes*. *PLoS One, 4*(4), e5142.

Griffiths, M., & Schraft, H. (2017). *Bacillus cereus* food poisoning *Foodborne Diseases (Third Edition)* (pp. 395-405): Elsevier.

Hajji, S., Salem, R. B. S.-B., Hamdi, M., Jellouli, K., Ayadi, W., Nasri, M., & Boufi, S. (2017). Nanocomposite films based on chitosan–poly (vinyl alcohol) and silver nanoparticles with high antibacterial and antioxidant activities. *Process Safety and Environmental Protection, 111*, 112-121.

Hanani, Z. N., Yee, F. C., & Nor-Khaizura, M. (2019). Effect of pomegranate (*Punica granatum* L.) peel powder on the antioxidant and antimicrobial properties of fish gelatin films as active packaging. *Food Hydrocolloids, 89*, 253-259.

Hidalgo, G., Chan, M., & Tufenkji, N. (2011). Inhibition of *Escherichia coli* CFT073 fliC expression and motility by cranberry materials. *Applied and Environmental Microbiology, 77*(19), 6852-6857.

Hintz, T., Matthews, K. K., & Di, R. (2015). The use of plant antimicrobial compounds for food preservation. *BioMed Research International, 2015,* Article ID 246264.

Hiranrat, A., Chitbankluoi, W., Mahabusarakam, W., Limsuwan, S., & Voravuthikunchai, S. (2012). A new flavellagic acid derivative and phloroglucinol from *Rhodomyrtus tomentosa*. *Natural Product Research, 26*(20), 1904-1909.

Hoffmann, S. A., Maculloch, B., & Batz, M. (2015). *Economic burden of major foodborne illnesses acquired in the United States.* Retrieved from, https://www.who.int/activities/estimating-the-burden-of-foodborne-diseases

Hussain, S., Hameed, A., Nazir, Y., Naz, T., Wu, Y., Suleria, H., & Song, Y. (2018). Microencapsulation and the characterization of Polyherbal Formulation (PHF) rich in natural polyphenolic compounds. *Nutrients, 10*(7), 843.

Ishag, O. A. O., Erwa, I. Y., Diriye, M. A., Lawane, A. A. M., Ahmed, H. M., Ahmed, F. A., Omer, A. B. (2018). Antimicrobial Potential and Phytochemical Screening of *Eucalyptus camaldulensis* and *Eucalyptus microtheca* Leaves Extracts. *South Asian Research Journal of Natural Products*, 1-6.

Ishnava, K. B., Chauhan, J. B., & Barad, M. B. (2013). Anticariogenic and phytochemical evaluation of *Eucalyptus globules* Labill. *Saudi Journal of Biological Sciences, 20*(1), 69-74.

Jafari, N., Karimi, L., Mirjalili, M., & Derakhshan, S. J. (2016). Effect of silver particle size on color and antibacterial properties of silk and cotton Fabrics. *Fibers and Polymers, 17*(6), 888-895.

Jayakumar, A., Heera, K., Sumi, T., Joseph, M., Mathew, S., Praveen, G., . . . Radhakrishnan, E. (2019). Starch-PVA composite films with zinc-oxide nanoparticles and phytochemicals as intelligent pH sensing wraps for food package application. *International Journal of Biological Macromolecules*.

Jeong, Y., Lim, D. W., & Choi, J. (2014). Assessment of size-dependent antimicrobial and cytotoxic properties of silver nanoparticles. *Advances in Materials Science and Engineering, 2014*.

Jiang, X., Lu, C., Tang, M., Yang, Z., Jia, W., Ma, Y., . . . Wang, H. (2018). Nanotoxicity of silver nanoparticles on HEK293T cells: A combined study using biomechanical and biological techniques. *ACS Omega, 3*(6), 6770-6778.

Johani, K., Abualsaud, D., Costa, D. M., Hu, H., Whiteley, G., Deva, A., & Vickery, K. (2018). Characterization of microbial community composition, antimicrobial resistance and biofilm on intensive care surfaces. *Journal of Infection and Public Health, 11*(3), 418-424.

Jung, S. H., Song, Y. M., Lee, J.-h., Lee, Y.-p., Shim, W.-g., Park, K. H., & Lee, J.-w. (2019). Electrospun Chitosan/PVA Films with Anthocyanines from *Brassica oleraceae* (Red Cabbage) for Smart Food Packaging. *Journal of Chitin and Chitosan, 24*(1), 55-60.

Kasai, D., Chougale, R., Masti, S., Chalannavar, R., Malabadi, R. B., & Gani, R. (2018). Influence of *Syzygium cumini* leaves extract on morphological, thermal, mechanical, and antimicrobial properties of PVA and PVA/chitosan blend films. *Journal of Applied Polymer Science, 135*(17), 46188.

Katas, H., Lim, C. S., Azlan, A. Y. H. N., Buang, F., & Busra, M. F. M. (2019). Antibacterial activity of biosynthesized gold nanoparticles using biomolecules from *Lignosus rhinocerotis* and chitosan. *Saudi Pharmaceutical Journal, 27*(2), 283-292.

Kaur, C., & Kapoor, H. C. (2002). Anti-oxidant activity and total phenolic content of some Asian vegetables. *International Journal of Food Science & Technology, 37*(2), 153-161.

Kaya, M., Khadem, S., Cakmak, Y. S., Mujtaba, M., Ilk, S., Akyuz, L., . . . Deligöz, E. (2018). Antioxidative and antimicrobial edible chitosan films blended with stem, leaf and seed extracts of *Pistacia terebinthus* for active food packaging. *RSC Advances, 8*(8), 3941-3950.

Kedare, S. B., & Singh, R. (2011). Genesis and development of DPPH method of antioxidant assay. *Journal of Food Science and Technology, 48*(4), 412-422.

Khalaf, A. I., El Nashar, D. E., Helaly, F. M., & Soliman, A. (2019). Evaluation of controlled release PVC/PEG polymeric films containing 5-fluorouracil for long-term antitumor. *Polymer Bulletin, 76:3555–3568*.

Kharat, S. N., & Mendhulkar, V. D. (2016). Synthesis, characterization and studies on antioxidant activity of silver nanoparticles using *Elephantopus scaber* leaf extract. *Materials Science and Engineering: C, 62*, 719-724.

Kim, H., Chung, D., Kim, S. A., & Rhee, M.-S. (2019). Synergistic cranberry juice combinations with natural-borne antimicrobials for the eradication of uropathogenic *Escherichia coli* biofilm within a short time. *Letters in Applied Microbiology, 68*(4), 321-328.

Kim, Y. G., Lee, J. H., Gwon, G., Kim, S. I., Park, J. G., & Lee, J. (2016). Essential oils and eugenols inhibit biofilm formation and the virulence of *Escherichia coli* O157: H7. *Scientific Reports, 6*, 36377.

Kishanji, M., Mamatha, G., Obi Reddy, K., Varada Rajulu, A., & Madhukar, K. (2017). In situ generation of silver nanoparticles in cellulose matrix using *Azadirachta indica* leaf extract as a reducing agent. *International Journal of Polymer Analysis and Characterization, 22*(8), 734-740.

Klančnik, A., Gobin, I., Vučković, D., Smole Možina, S., Abram, M., & Jeršek, B. (2018). Reduced contamination and infection via inhibition of adhesion of foodborne bacteria to abiotic polystyrene and biotic amoeba surfaces. *International Journal of Food Science & Technology, 53*(4), 1013-1020.

Knezevic, P., Aleksic, V., Simin, N., Svircev, E., Petrovic, A., & Mimica-Dukic, N. (2016). Antimicrobial activity of *Eucalyptus camaldulensis* essential oils and their interactions with conventional antimicrobial agents against multi-drug resistant Acinetobacter baumannii. *Journal of Ethnopharmacology, 178*, 125-136.

Kuck, L. S., & Noreña, C. P. Z. (2016). Microencapsulation of grape (*Vitis labrusca* var. Bordo) skin phenolic extract using gum Arabic, polydextrose, and partially hydrolyzed guar gum as encapsulating agents. *Food Chemistry, 194*, 569-576.

Kumar, S., Krishnakumar, B., Sobral, A. J., & Koh, J. (2019). Bio-based (chitosan/PVA/ZnO) nanocomposites film: Thermally stable and photoluminescence material for removal of organic dye. *Carbohydrate Polymers, 205*, 559-564.

Labbé, R. G., & García, S. (2013). *Guide to foodborne pathogens*: John Wiley & Sons.

Lamari, F., Khouadja, S., & Rtimi, S. (2018). Interaction of Vibrio to biotic and abiotic surfaces: Relationship between hydrophobicity, cell adherence, biofilm production, and cytotoxic activity. *Surfaces, 1*(1), 187-201.

Lee, B. H., Hébraud, M., & Bernardi, T. (2017). Increased adhesion of *Listeria monocytogenes* strains to abiotic surfaces under cold stress. *Frontiers in Microbiology, 8*, 2221.

Lekbach, Y., Li, Z., Xu, D., El Abed, S., Dong, Y., Liu, D., . . . Wang, F. (2019). *Salvia officinalis* extract mitigates the microbiologically influenced corrosion of 304L stainless steel by *Pseudomonas aeruginosa* biofilm. *Bioelectrochemistry, 128*, 193-203.

Lemon, K. P., Higgins, D. E., & Kolter, R. (2007). Flagellar motility is critical for *Listeria monocytogenes* biofilm formation. *Journal of bacteriology, 189*(12), 4418-4424.

Li, H., Cui, R., Peng, L., Cai, S., Li, P., & Lan, T. (2017). Preparation of antibacterial cellulose paper using layer-by-layer assembly for cooked beef preservation at ambient temperature. *Polymers, 10*(1), 15.

Li, W. J., Cheng, X. L., Liu, J., Lin, R. C., Wang, G. L., Du, S. S., & Liu, Z. L. (2012). Phenolic compounds and antioxidant activities of *Liriope muscari*. *Molecules, 17*(2), 1797-1808.

Liao, S., Zhang, Y., Pan, X., Zhu, F., Jiang, C., Liu, Q., Wang, L. (2019). Antibacterial activity and mechanism of silver nanoparticles against multidrug-resistant *Pseudomonas aeruginosa*. *International Journal of Nanomedicine, 14*, 1469.

Limsuwan, S., Trip, E. N., Kouwen, T. R., Piersma, S., Hiranrat, A., Mahabusarakam, W., Kayser, O. (2009). Rhodomyrtone: a new candidate as natural antibacterial drug from *Rhodomyrtus tomentosa*. *Phytomedicine, 16*(6-7), 645-651.

Liu, Y., McKeever, L. C., & Malik, N. S. (2017). Assessment of the antimicrobial activity of olive leaf extract against foodborne bacterial pathogens. *Frontiers in Microbiology, 8*, 113.

Liu, Y., Wang, S., & Lan, W. (2018). Fabrication of antibacterial chitosan-PVA blended film using electrospray technique for food packaging applications. *International Journal of Biological Macromolecules, 107*, 848-854.

Liu, Z., Meng, R., Zhao, X., Shi, C., Zhang, X., Zhang, Y., & Guo, N. (2016). Inhibition effect of tea tree oil on *Listeria monocytogenes* growth and exotoxin proteins listeriolysin O and p60 secretion. *Letters in Applied Microbiology, 63*(6), 450-457.

Logan, N. (2012). *Bacillus* and relatives in foodborne illness. *Journal of Applied Microbiology, 112*(3), 417-429.

Loo, Y. Y., Rukayadi, Y., Mahmud-Ab-Rashid Nor-Khaizura, C., Kuan, H., Chieng, B. W., Nishibuchi, M., & Radu, S. (2018). *In Vitro* antimicrobial activity of green synthesized silver nanoparticles against selected Gram-negative foodborne pathogens. *Frontiers in Microbiology, 9*, doi: 10.3389/fmicb.2018.01555.

López-Carballo, G., Higueras, L., Gavara, R., & Hernández-Muñoz, P. (2012). Silver ions release from antibacterial chitosan films containing in situ generated silver nanoparticles. *Journal of Agricultural and Food Chemistry, 61*(1), 260-267.

López de Dicastillo, C., Nerin, C., Alfaro, P., Catalá, R., Gavara, R., & Hernández-Munoz, P. (2011). Development of new antioxidant active packaging films

based on ethylene vinyl alcohol copolymer (EVOH) and green tea extract. *Journal of Agricultural and Food Chemistry, 59*(14), 7832-7840.

Mah, T. F. C., & O'Toole, G. A. (2001). Mechanisms of biofilm resistance to antimicrobial agents. *Trends in Microbiology, 9*(1), 34-39.

Mahyudin, N. A., Mat Daud, N. I. H., Ab Rashid, N. K. M., Muhialdin, B. J., Saari, N., & Noordin, W. N. (2018). Bacterial attachment and biofilm formation on stainless steel surface and their in vitro inhibition by marine fungal extracts. *Journal of Food Safety, 38*(3), e12456.

Mao, B.-H., Chen, Z.-Y., Wang, Y.-J., & Yan, S.-J. (2018). Silver nanoparticles have lethal and sublethal adverse effects on development and longevity by inducing ROS-mediated stress responses. *Scientific Reports, 8*(1), 2445.

Marrez, D. A., Abdelhamid, A. E., & Darwesh, O. M. (2019). Eco-friendly cellulose acetate green synthesized silver nano-composite as antibacterial packaging system for food safety. *Food Packaging and Shelf Life, 20*, 100302.

Mathew, S., Snigdha, S., Mathew, J., & Radhakrishnan, E. (2019). Biodegradable and active nanocomposite pouches reinforced with silver nanoparticles for improved packaging of chicken sausages. *Food Packaging and Shelf Life, 19*, 155-166.

Mauricio-Sánchez, R. A., Salazar, R., Luna-Bárcenas, J. G., & Mendoza-Galván, A. (2018). FTIR spectroscopy studies on the spontaneous neutralization of chitosan acetate films by moisture conditioning. *Vibrational Spectroscopy, 94*, 1-6.

Medhi, S. M., Reza, S., Mahnaz, K., Reza, A. M., Abbas, H., Fatemeh, M., & Hassan, V. (2010). Phytochemistry and larvicidal activity of *Eucalyptus camaldulensis* against malaria vector, Anopheles stephensi. *Asian Pacific Journal of Tropical Medicine, 3*(11), 841-845.

Merlusca, I. P., Matiut, D. S., Lisa, G., Silion, M., Gradinaru, L., Oprea, S., & Popa, I. M. (2018). Preparation and characterization of chitosan–poly (vinyl alcohol)–neomycin sulfate films. *Polymer Bulletin, 75*(9), 3971-3986.

Metak, A., & Ajaal, T. (2013). Investigation on polymer based nano-silver as food packaging materials. *International Journal of Biological, Food, Veterinary and Agricultural Engineering, 7*(12), 772-778.

Miao, X., Liu, H., Zheng, Y., Guo, D., Shi, C., Xu, Y., & Xia, X. (2019). Inhibitory effect of TQ on *Listeria monocytogenes* ATCC 19115 biofilm formation and virulence attributes critical for human infection. *Frontiers in Cellular and Infection Microbiology, 9*, 304.

Mitsuwan, W., Olaya-Abril, A., Calderón-Santiago, M., Jiménez-Munguía, I., González-Reyes, J. A., Priego-Capote, F., Rodríguez-Ortega, M. J. (2017). Integrated proteomic and metabolomic analysis reveals that rhodomyrtone reduces the capsule in *Streptococcus pneumoniae*. *Scientific reports*, *7*(1), 2715.

Mohammed, A. E. (2015). Green synthesis, antimicrobial and cytotoxic effects of silver nanoparticles mediated by *Eucalyptus camaldulensis* leaf extract. *Asian Pacific Journal of Tropical Biomedicine*, *5*(5), 382-386.

Mohammed, H. A., Al-Omar, M. S., El-Readi, M. Z., Alhowail, A. H., Aldubayan, M. A., & Abdellatif, A. A. (2019). Formulation of ethyl cellulose microparticles incorporated pheophytin a isolated from *Suaeda vermiculata* for antioxidant and cytotoxic activities. *Molecules*, *24*(8), 1501.

Mohanapriya, M., Deshmukh, K., Chidambaram, K., Ahamed, M. B., Sadasivuni, K. K., Ponnamma, D., Pasha, S. K. (2017). Polyvinyl alcohol (PVA)/polystyrene sulfonic acid (PSSA)/carbon black nanocomposite for flexible energy storage device applications. *Journal of Materials Science: Materials in Electronics*, *28*(8), 6099-6111.

Momin, B., Rahman, S., Jha, N., & Annapure, U. S. (2019). Valorization of mutant *Bacillus licheniformis* M09 supernatant for green synthesis of silver nanoparticles: photocatalytic dye degradation, antibacterial activity, and cytotoxicity. *Bioprocess and Biosystems Engineering*, *42*(4), 541-553.

Monte, J., Abreu, A. C., Borges, A., Simões, L. C., & Simões, M. (2014). Antimicrobial activity of selected phytochemicals against *Escherichia coli* and *Staphylococcus aureus* and their biofilms. *Pathogens*, *3*(2), 473-498.

Nasr, A., Saleem Khan, T., & Zhu, G.-P. (2019). Phenolic compounds and antioxidants from *Eucalyptus camaldulensis* as affected by some extraction conditions, a preparative optimization for GC-MS analysis. *Preparative Biochemistry and Biotechnology*, 1-13.

Nasr, A., Zhou, X., Huang, S.-P., Wang, Y., Li, X., & Zhu, G.-P. (2018). Comparative effects of some extraction solvents on the antimicrobial activity of *Eucalyptus camaldulensis* leaf, bud, capsule and seed crude extracts. *Natural product research*, 1-6.

Nasr, A., Zhou, X., Huang, S.-P., Wang, Y., Li, X., & Zhu, G.-P. (2019). Comparative effects of some extraction solvents on the antimicrobial activity of *Eucalyptus camaldulensis* leaf, bud, capsule and seed crude extracts. *Natural Product Research*, *33*(17), 2560-2565.

Nightingale, K., Milillo, S., Ivy, R., Ho, A., Oliver, H., & Wiedmann, M. (2007). *Listeria monocytogenes* F2365 carries several authentic mutations potentially leading to truncated gene products, including inlB, and demonstrates atypical phenotypic characteristics. *Journal of Food Protection, 70*(2), 482-488.

Nilsuwan, K., Benjakul, S., & Prodpran, T. (2018). Properties and antioxidative activity of fish gelatin-based film incorporated with epigallocatechin gallate. *Food Hydrocolloids, 80*, 212-221.

Nwabor, O. F., Vongkamjan, K., & Voravuthikunchai, S. P. (2019). Antioxidant properties and antibacterial effects of *Eucalyptus camaldulensis* ethanolic leaf extract on biofilm formation, motility, hemolysin production, and cell membrane of the foodborne Pathogen *Listeria monocytogenes*. *Foodborne Pathogens and Disease*. *16*, 581–589.

O'Neil, H. S., & Marquis, H. (2006). *Listeria monocytogenes* flagella are used for motility, not as adhesins, to increase host cell invasion. *Infection and Immunity, 74*(12), 6675-6681.

Ortega, F., Giannuzzi, L., Arce, V. B., & García, M. A. (2017). Active composite starch films containing green synthetized silver nanoparticles. *Food Hydrocolloids, 70*, 152-162.

Oudjedi, K., Manso, S., Nerin, C., Hassissen, N., & Zaidi, F. (2019). New active antioxidant multilayer food packaging films containing Algerian Sage and Bay leaves extracts and their application for oxidative stability of fried potatoes. *Food Control, 98*, 216-226.

Paosen, S., Saising, J., Septama, A. W., & Voravuthikunchai, S. P. (2017). Green synthesis of silver nanoparticles using plants from Myrtaceae family and characterization of their antibacterial activity. *Materials Letters, 209*, 201-206.

Parsa, P., Paydayesh, A., & Davachi, S. M. (2019). Investigating the effect of tetracycline addition on nanocomposite hydrogels based on polyvinyl alcohol and chitosan nanoparticles for specific medical applications. *International Journal of Biological Macromolecules, 121*, 1061-1069.

Pasukamonset, P., Kwon, O., & Adisakwattana, S. (2016). Alginate-based encapsulation of polyphenols from *Clitoria ternatea* petal flower extract enhances stability and biological activity under simulated gastrointestinal conditions. *Food Hydrocolloids, 61*, 772-779.

Patel, N., Lalwani, D., Gollmer, S., Injeti, E., Sari, Y., & Nesamony, J. (2016). Development and evaluation of a calcium alginate based oral ceftriaxone sodium formulation. *Progress in Biomaterials, 5*(2), 117-133.

Pervez, M., & Stylios, G. (2018). Investigating the synthesis and characterization of a novel "green" h2o2-assisted, water-soluble chitosan/polyvinyl alcohol nanofiber for environmental end uses. *Nanomaterials, 8*(6), 395.

Petruzzi, L., Corbo, M. R., Sinigaglia, M., & Bevilacqua, A. (2017). Microbial spoilage of foods: Fundamentals *The Microbiological Quality of Food* (pp. 1-21): Elsevier.

Pizarro-Cerdá, J., Kühbacher, A., & Cossart, P. (2012). Entry of *Listeria monocytogenes* in mammalian epithelial cells: an updated view. *Cold Spring Harbor perspectives in medicine, 2*(11), a010009.

Praveena, S. M., Karuppiah, K., & Than, L. T. L. (2018). Potential of cellulose paper coated with silver nanoparticles: a benign option for emergency drinking water filter. *Cellulose, 25*(4), 2647-2658.

Qasim, M., Udomluck, N., Chang, J., Park, H., & Kim, K. (2018). Antimicrobial activity of silver nanoparticles encapsulated in poly-N-isopropylacrylamide-based polymeric nanoparticles. *International Journal of Nanomedicine, 13*, 235.

Qi, H., Cai, J., Zhang, L., & Kuga, S. (2009). Properties of films composed of cellulose nanowhiskers and a cellulose matrix regenerated from alkali/urea solution. *Biomacromolecules, 10*(6), 1597-1602.

Qiao, Z., Yao, Y., Song, S., Yin, M., & Luo, J. (2019). Silver nanoparticles with pH induced surface charge switchable properties for antibacterial and antibiofilm applications. *Journal of Materials Chemistry B, 7*(5), 830-840.

Rezaei, M., Khaghani, R., & Moharramipour, S. (2019). Insecticidal activity of *Artemisia sieberi, Eucalyptus camaldulensis, Thymus persicus* and *Eruca sativa* oils against German cockroach, *Blattella germanica* (L.). *Journal of Asia-Pacific Entomology, 22*(4), 1090-1097.

Rezende, Y. R. R. S., Nogueira, J. P., & Narain, N. (2018). Microencapsulation of extracts of bioactive compounds obtained from acerola (*Malpighia emarginata* DC) pulp and residue by spray and freeze drying: Chemical, morphological and chemometric characterization. *Food Chemistry, 254*, 281-291.

Rigon, R. T., & Noreña, C. P. Z. (2016). Microencapsulation by spray-drying of bioactive compounds extracted from blackberry (*Rubus fruticosus*). *Journal of Food Science and Technology, 53*(3), 1515-1524.

Rodriguez-Lopez, P., Rodríguez-Herrera, J. J., Vazquez-Sanchez, D., & Lopez Cabo, M. (2018). Current knowledge on *Listeria monocytogenes* biofilms in food-related environments: incidence, resistance to biocides, ecology and biocontrol. *Foods, 7*(6), 85.

Rojo-Molinero, E., Macià, M. D., & Oliver, A. (2019). Social behavior of antibiotic resistant mutants within *Pseudomonas aeruginosa* biofilm communities. *Frontiers in Microbiology, 10*, 570.

Roy, S., Shankar, S., & Rhim, J.-W. (2019). Melanin-mediated synthesis of silver nanoparticle and its use for the preparation of carrageenan-based antibacterial films. *Food Hydrocolloids, 88*, 237-246.

Ruiz-Montañez, G., Calderón-Santoyo, M., Chevalier-Lucia, D., Picart-Palmade, L., Jimenez-Sánchez, D. E., & Ragazzo-Sánchez, J. A. (2019). Ultrasound-assisted microencapsulation of jackfruit extract in eco-friendly powder particles: characterization and antiproliferative activity. *Journal of Dispersion Science and Technology*, 1-9.

Rutherford, S. T., & Bassler, B. L. (2012). Bacterial quorum sensing: its role in virulence and possibilities for its control. *Cold Spring Harbor Perspectives in Medicine, 2*(11), a012427.

Sadanand, V., Rajini, N., Satyanarayana, B., & Rajulu, A. V. (2016). Preparation and properties of cellulose/silver nanoparticle composites with in situ-generated silver nanoparticles using *Ocimum sanctum* leaf extract. *International Journal of Polymer Analysis and Characterization, 21*(5), 408-416.

Saikia, S., Mahnot, N. K., & Mahanta, C. L. (2015). Optimisation of phenolic extraction from *Averrhoa carambola* pomace by response surface methodology and its microencapsulation by spray and freeze drying. *Food Chemistry, 171*, 144-152.

Salvucci, E., Rossi, M., Colombo, A., Pérez, G., Borneo, R., & Aguirre, A. (2019). Triticale flour films added with bacteriocin-like substance (BLIS) for active food packaging applications. *Food Packaging and Shelf Life, 19*, 193-199.

Sansano, S., Rivas, A., Pina-Pérez, M. C., Martinez, A., & Rodrigo, D. (2017). *Stevia rebaudiana* Bertoni effect on the hemolytic potential of *Listeria monocytogenes*. *International Journal of Food Microbiology, 250*, 7-11.

Schirm, M., Kalmokoff, M., Aubry, A., Thibault, P., Sandoz, M., & Logan, S. (2004). Flagellin from *Listeria monocytogenes* is glycosylated with β-O-linked N-acetylglucosamine. *Journal of Bacteriology, 186*(20), 6721-6727.

Sebei, K., Sakouhi, F., Herchi, W., Khouja, M. L., & Boukhchina, S. (2015). Chemical composition and antibacterial activities of seven *Eucalyptus* species essential oils leaves. *Biological Research, 48*(1), 7.

Sezgin-Bayindir, Z., Antep, M. N., & Yuksel, N. (2015). Development and characterization of mixed niosomes for oral delivery using candesartan cilexetil as a model poorly water-soluble drug. *AAPS PharmSciTech, 16*(1), 108-117.

Shankar, S., & Rhim, J.-W. (2017). Preparation and characterization of agar/lignin/silver nanoparticles composite films with ultraviolet light barrier and antibacterial properties. *Food Hydrocolloids, 71*, 76-84.

Shankar, S., & Rhim, J.-W. (2018). Preparation of sulfur nanoparticle-incorporated antimicrobial chitosan films. *Food Hydrocolloids, 82*, 116-123.

Shankar, S., Rhim, J.-W., & Won, K. (2018). Preparation of poly (lactide)/lignin/silver nanoparticles composite films with UV light barrier and antibacterial properties. *International Journal of Biological Macromolecules, 107*, 1724-1731.

Singab, A.-N., Ayoub, N., Al-Sayed, E., Martiskainen, O., Sinkkonen, J., & Pihlaja, K. (2011). Phenolic constituents of *Eucalyptus camaldulensis* Dehnh, with potential antioxidant and cytotoxic activities. *Records of Natural Products, 5*(4).

Singh, M., Mallick, A., Banerjee, M., & Kumar, R. (2016). Loss of outer membrane integrity in Gram-negative bacteria by silver nanoparticles loaded with *Camellia sinensis* leaf phytochemicals: plausible mechanism of bacterial cell disintegration. *Bulletin of Materials Science, 39*(7), 1871-1878.

Singh, P., Garg, A., Pandit, S., Mokkapati, V., & Mijakovic, I. (2018). Antimicrobial effects of biogenic nanoparticles. *Nanomaterials, 8*(12), 1009.

Singh, T., Shukla, S., Kumar, P., Wahla, V., Bajpai, V. K., & Rather, I. A. (2017). Application of nanotechnology in food science: perception and overview. *Frontiers in Microbiology, 8*, 1501.

Siramon, P., & Ohtani, Y. (2007). Antioxidative and antiradical activities of *Eucalyptus camaldulensis* leaf oils from Thailand. *Journal of Wood Science, 53*(6), 498-504.

Siripatrawan, U., & Vitchayakitti, W. (2016). Improving functional properties of chitosan films as active food packaging by incorporating with propolis. *Food Hydrocolloids, 61*, 695-702.

Soković, M., Glamočlija, J., Marin, P. D., Brkić, D., & van Griensven, L. J. (2010). Antibacterial effects of the essential oils of commonly consumed medicinal herbs using an in vitro model. *Molecules, 15*(11), 7532-7546.

Song, Z., Wu, Y., Wang, H., & Han, H. (2019). Synergistic antibacterial effects of curcumin modified silver nanoparticles through ROS-mediated pathways. *Materials Science and Engineering: C, 99*, 255-263.

Surini, S., Nursatyani, K., & Ramadon, D. (2018). Gel formulation containing microcapsules of Grape seed oil (*Vitis vinifera* L.) for skin moisturizer. *Journal of Young Pharmacists, 10*(1), 41.

Swensson, B., Ek, M., & Gray, D. G. (2018). In Situ Preparation of Silver Nanoparticles in Paper by Reduction with Alkaline Glucose Solutions. *ACS Omega, 3*(8), 9449-9452.

Takahashi, H., Suda, T., Tanaka, Y., & Kimura, B. (2010). Cellular hydrophobicity of *Listeria monocytogenes* involves initial attachment and biofilm formation on the surface of polyvinyl chloride. *Letters in Applied Microbiology, 50*(6), 618-625.

Tewari, A., & Abdullah, S. (2015). *Bacillus cereus* food poisoning: international and Indian perspective. *Journal of Food Science and Technology, 52*(5), 2500-2511.

Thiagamani, S. M. K., Rajini, N., Siengchin, S., Rajulu, A. V., Hariram, N., & Ayrilmis, N. (2019). Influence of silver nanoparticles on the mechanical, thermal and antimicrobial properties of cellulose-based hybrid nanocomposites. *Composites Part B: Engineering, 165*, 516-525.

Tohidi, B., Rahimmalek, M., & Arzani, A. (2017). Essential oil composition, total phenolic, flavonoid contents, and antioxidant activity of *Thymus* species collected from different regions of Iran. *Food Chemistry, 220*, 153-161.

Tsai, T. T., Huang, T. H., Chang, C. J., Ho, N. Y. J., Tseng, Y. T., & Chen, C.-F. (2017). Antibacterial cellulose paper made with silver-coated gold nanoparticles. *Scientific Reports, 7*(1), 3155.

Upadhyay, A., Johny, A. K., Amalaradjou, M. A. R., Baskaran, S. A., Kim, K. S., & Venkitanarayanan, K. (2012). Plant-derived antimicrobials reduce *Listeria monocytogenes* virulence factors in vitro, and down-regulate expression of virulence genes. *International Journal of Food Microbiology, 157*(1), 88-94.

Upreti, A., Byanju, B., Fuyal, M., Chhetri, A., Pandey, P., Ranjitkar, R., . . . Pandey, B. P. (2018). Evaluation of α-amylase, lipase inhibition and in-vivo pharmacological activities of *Eucalyptus camaladulensis* Dehnh leaf extract. *Journal of Traditional and Complementary Medicine*.

Üstüner, T., Kordali, Ş., Bozhüyük, A. U., & Kesdek, M. (2018). Investigation of Pesticidal Activities of Essential Oil of *Eucalyptus camaldulensis* Dehn tamer üstüner, şaban kordali, ayşe usanmaz bozhüyük and memiş kesdek. *Records of Natural Products, 12*(6), 557.

Vazquez-Armenta, F., Bernal-Mercado, A., Lizardi-Mendoza, J., Silva-Espinoza, B., Cruz-Valenzuela, M., Gonzalez-Aguilar, G., . . . Ayala-Zavala, J. (2018). Phenolic extracts from grape stems inhibit *Listeria monocytogenes* motility and adhesion to food contact surfaces. *Journal of Adhesion Science and Technology, 32*(8), 889-907.

Vega-Cázarez, C. A., López-Cervantes, J., Sánchez-Machado, D. I., Madera-Santana, T. J., Soto-Cota, A., & Ramírez-Wong, B. (2018). Preparation and properties of chitosan–pva fibers produced by wet spinning. *Journal of Polymers and the Environment, 26*(3), 946-958.

Vikram, A., Jayaprakasha, G., Jesudhasan, P., Pillai, S., & Patil, B. (2010). Suppression of bacterial cell–cell signalling, biofilm formation and type III secretion system by citrus flavonoids. *Journal of Applied Microbiology, 109*(2), 515-527.

Vila, L., García-Rodríguez, A., Cortés, C., Marcos, R., & Hernández, A. (2018). Assessing the effects of silver nanoparticles on monolayers of differentiated Caco-2 cells, as a model of intestinal barrier. *Food and Chemical Toxicology, 116*, 1-10.

Vimala, K., Mohan, Y. M., Sivudu, K. S., Varaprasad, K., Ravindra, S., Reddy, N. N., . . . MohanaRaju, K. (2010). Fabrication of porous chitosan films impregnated with silver nanoparticles: a facile approach for superior antibacterial application. *Colloids and Surfaces B: Biointerfaces, 76*(1), 248-258.

Vishnuvarthanan, M., & Rajeswari, N. (2019). Preparation and characterization of carrageenan/silver nanoparticles/Laponite nanocomposite coating on oxygen plasma surface modified polypropylene for food packaging. *Journal of Food Science and Technology, 56*(5), 2545-2552.

Vongkamjan, K., Fuangpaiboon, J., Jirachotrapee, S., & Turner, M. P. (2015). Occurrence and diversity of *Listeria* spp. in seafood processing plant environments. *Food Control, 50*, 265-272.

Wang, J., Qiu, J., Tan, W., Zhang, Y., Wang, H., Zhou, X., . . . Niu, X. (2014). Fisetin inhibits *Listeria monocytogenes* virulence by interfering with the oligomerization of listeriolysin O. *The Journal of Infectious Diseases, 211*(9), 1376-1387.

Wang, L., Gao, Y., Li, J., Subirade, M., Song, Y., & Liang, L. (2016). Effect of resveratrol or ascorbic acid on the stability of α-tocopherol in O/W emulsions stabilized by whey protein isolate: Simultaneous encapsulation of the vitamin and the protective antioxidant. *Food Chemistry, 196*, 466-474.

Wang, W., Zhao, Y., Bai, H., Zhang, T., Ibarra-Galvan, V., & Song, S. (2018). Methylene blue removal from water using the hydrogel beads of poly (vinyl alcohol)-sodium alginate-chitosan-montmorillonite. *Carbohydrate Polymers, 198*, 518-528.

Wintachai, P., Paosen, S., Yupanqui, C. T., & Voravuthikunchai, S. P. (2019). Silver nanoparticles synthesized with *Eucalyptus critriodora* ethanol leaf extract stimulate antibacterial activity against clinically multidrug-resistant *Acinetobacter baumannii* isolated from pneumonia patients. *Microbial Pathogenesis, 126*, 245-257.

Wu, C., Li, Y., Du, Y., Wang, L., Tong, C., Hu, Y., . . . Yan, Z. (2019). Preparation and characterization of konjac glucomannan-based bionanocomposite film for active food packaging. *Food Hydrocolloids, 89*, 682-690.

Wu, C., Li, Y., Sun, J., Lu, Y., Tong, C., Wang, L., . . . Pang, J. (2020). Novel konjac glucomannan films with oxidized chitin nanocrystals immobilized red cabbage anthocyanins for intelligent food packaging. *Food Hydrocolloids, 98*, 105245.

Wu, J., Sun, X., Guo, X., Ji, M., Wang, J., Cheng, C., . . . Zhang, Q. (2018). Physicochemical, antioxidant, in vitro release, and heat sealing properties of fish gelatin films incorporated with β-cyclodextrin/curcumin complexes for apple juice preservation. *Food and Bioprocess Technology, 11*(2), 447-461.

Wu, J., Zheng, Y., Song, W., Luan, J., Wen, X., Wu, Z., . . . Guo, S. (2014). In situ synthesis of silver-nanoparticles/bacterial cellulose composites for slow-released antimicrobial wound dressing. *Carbohydrate Polymers, 102*, 762-771.

Wu, Y., Ying, Y., Liu, Y., Zhang, H., & Huang, J. (2018). Preparation of chitosan/poly vinyl alcohol films and their inhibition of biofilm formation against Pseudomonas aeruginosa PAO1. *International Journal of Biological Macromolecules, 118*, 2131-2137.

Wu, Z., Huang, X., Li, Y.-C., Xiao, H., & Wang, X. (2018). Novel chitosan films with laponite immobilized Ag nanoparticles for active food packaging. *Carbohydrate Polymers, 199*, 210-218.

Wu, Z., Zhou, W., Pang, C., Deng, W., Xu, C., & Wang, X. (2019). Multifunctional chitosan-based coating with liposomes containing laurel essential oils and nanosilver for pork preservation. *Food Chemistry, 295*, 16-25.

Yan, X., He, B., Liu, L., Qu, G., Shi, J., Hu, L., & Jiang, G. (2018). Antibacterial mechanism of silver nanoparticles in *Pseudomonas aeruginosa*: proteomics approach. *Metallomics, 10*(4), 557-564.

Yang, S. C., Lin, C. H., Aljuffali, I. A., & Fang, J. Y. (2017). Current pathogenic *Escherichia coli* foodborne outbreak cases and therapy development. *Arch Microbiol, 199*(6), 811-825. doi:10.1007/s00203-017-1393-y

Yang, W., Wang, L., Ban, Z., Yan, J., Lu, H., Zhang, X., . . . Li, L. (2019). Efficient microencapsulation of Syringa essential oil; the valuable potential on quality maintenance and storage behavior of peach. *Food Hydrocolloids, 95*, 177-185.

Yen, M. T., Yang, J. H., & Mau, J. L. (2008). Antioxidant properties of chitosan from crab shells. *Carbohydrate Polymers, 74*(4), 840-844.

Yeşilsu, A. F., & Özyurt, G. (2019). Oxidative stability of microencapsulated fish oil with rosemary, thyme and laurel extracts: A kinetic assessment. *Journal of Food Engineering, 240*, 171-182.

Yu, Z., Wang, W., Kong, F., Lin, M., & Mustapha, A. (2019). Cellulose nanofibril/silver nanoparticle composite as an active food packaging system and its toxicity to human colon cells. *International Journal of Biological Macromolecules, 129*, 887-894.

Yun, Y.-H., Kim, E.-S., Shim, W.-G., & Yoon, S.-D. (2018). Physical properties of mungbean starch/PVA bionanocomposites added nano-ZnS particles and its photocatalytic activity. *Journal of Industrial and Engineering Chemistry, 68*, 57-68.

Zhang, L., Wu, L., Si, Y., & Shu, K. (2018). Size-dependent cytotoxicity of silver nanoparticles to *Azotobacter vinelandii*: Growth inhibition, cell injury, oxidative stress and internalization. *PLoS One, 13*(12), e0209020.

Nwabor OF, Singh S, Ontong JC, Vongkamjan K, and Voravuthikunchai SP (2020). Valorization of wastepaper through antimicrobial functionalization with biogenic silver nanoparticles, a sustainable packaging composite. WAVE-D-20-00427 (Under review)

List of Proceedings

Nwabor OF, Vongkamjan K, and Voravuthikunchai SP. Bioactive components of *Eucalyptus camaldulensis*, a potential alternative bio-preservative against foodborne *Listeria monocytogenes*, *International Conference on Food Production and Preservation*, October 17–18, 2018, Ottawa Canada. *Journal of Food Processing & Technology*, 9: 42. 10.4172/2157-7110-C10-105

Nwabor OF, and Voravuthikunchai SP. Microencapsulation of bioactive leaf extracts of *Eucalyptus camaldulensis* by freeze drying technology using sodium alginate and sodium carboxymethyl cellulose as coating materials. *The 5th International Electronic Conference on Medicinal Chemistry session ECMC-5*, November 1–30, 2019. 10.3390/ecmc2019-06339